

Impact of distance determinations on Galactic structure. II. Old tracers

Andrea Kunder, Elena Valenti, Massimo Dall’Ora, Pawel Pietrukowicz, Chris Sneden, Giuseppe Bono

& Vittorio F. Braga, Ivan Ferraro, Giuliana Fiorentino, Giacinto Iannicola, Marcella Marconi, Clara E. Martínez-Vázquez, Matteo Monelli, Ilaria Musella, Vincenzo Ripepi, Maurizio Salaris, Peter B. Stetson

Accepted: June 18, 2018

A. Kunder, Leibniz Institut für Astrophysik, An der Sternwarte 16, D-14467 Potsdam
E-mail: amkunder@gmail.com

E. Valenti, European Southern Observatory, Karl-Schwarzschild-Str. 2, D-85748, Garching bei Munich, Germany, E-mail: evalenti@eso.org

M. Dall’Ora, INAF, Osservatorio Astronomico di Capodimonte, Via Moiarello 16, 80131 Napoli, Italy E-mail: dallora@na.astro.it

P. Pietrukowicz, Warsaw University Observatory, Al. Ujazdowskie 4, 00-478 Warszawa, Poland E-mail: pietruk@astrouw.edu.pl

C. Sneden, University of Texas Department of Astronomy, 2515 Speedway, Stop C1400, Austin, TX 78712 E-mail: chris@verdi.as.utexas.edu

G. Bono, Università di Roma Tor Vergata, Via della Ricerca Scientifica 1, 00133 Roma and INAF–Osservatorio Astronomico di Roma, Via Frascati 33, 00078 Monte Porzio Catone, Italy E-mail: bono@roma2.infn.it

V.F. Braga, Instituto Milenio de Astrofísica, Santiago, Chile and Departamento de Física, Facultad de Ciencias Exactas, Universidad Andres Bello, Av. Fernandez Concha 700, Las Condes, Santiago, Chile

I. Ferraro, INAF–Osservatorio Astronomico di Roma, Via Frascati 33, 00078 Monte Porzio Catone, Italy

G. Fiorentino, IINAF-OAS Osservatorio di Astrofisica e Scienza dello Spazio di Bologna

G. Iannicola, INAF–Osservatorio Astronomico di Roma, Via Frascati 33, 00078 Monte Porzio Catone, Italy

M. Marconi, INAF, Osservatorio Astronomico di Capodimonte, Via Moiarello 16,

Abstract Here we review the efforts of a number of recent results that use old tracers to understand the build up of the Galaxy. Details that lead directly to using these old tracers to measure distances are discussed. We concentrate on the following: (1) the structure and evolution of the Galactic bulge and inner Galaxy constrained from the dynamics of individual stars residing therein; (2) the spatial structure of the old Galactic bulge through photometric observations of RR Lyrae-type stars; (3) the three-dimensional structure, stellar density, mass, chemical composition, and age of the Milky Way bulge as traced by its old stellar populations; (4) an overview of RR Lyrae stars known in the ultra-faint dwarfs and their relation to the Galactic halo; and (5) different approaches for estimating absolute and relative cluster ages.

Keywords First keyword · Second keyword · More

Using old stars as tracers to piece together the build-up of the Milky Way (MW) allows for a glimpse of the early stages of the Milky Way Galaxy. This is because old stars have existed for several billion years – when the Galaxy was in its infancy – and are therefore a foundation of the current ensemble of stellar populations that have since begun to also populate the MW. The signatures of old stars that are discussed here involve primarily RR Lyrae stars (RRLs) and Red Clump (RC) stars as probes, arguably the most widely used old stars as stellar tracers.

RC stars are core helium-burning stars that can be considered useful distance indicators because their magnitude changes slowly and smoothly with age and metallicity. Such a change is predicted very accurately by stellar evolution models (e.g., Salaris & Girardi, 2002). They do not univocally trace old populations, but also intermediate ages. However, because being a bright and distinct feature in the color-magnitude diagram they are very numerous and

80131 Napoli, Italy

C. E. Martínez-Vázquez, Cerro Tololo Inter-American Observatory, National Optical Astronomy Observatory, Casilla 603, La Serena, Chile and IAC-Instituto de Astrofísica de Canarias, Calle Va Lactea s/n, E-38205 La Laguna, Tenerife, Spain

M. Monelli, Instituto de Astrofísica de Canarias, Calle Via Lactea, 38205, La Laguna (Tenerife), Spain

I. Musella, INAF, Osservatorio Astronomico di Capodimonte, Via Moiarello 16, 80131 Napoli, Italy

V. Ripepi, INAF, Osservatorio Astronomico di Capodimonte, Via Moiarello 16, 80131 Napoli, Italy

M. Salaris, Astrophysics Research Institute, John Moores University, IC2, Liverpool Science Park, 146 Brownlow Hill, Liverpool L3 5RF

P.B. Stetson, DAO/HIA, NRC, 5071 West Saanich Road, Victoria, BC V9E 2E7, Canada

easy to identify, they have been extensively used in the study of especially the Galactic bulge. It should be noted though that, according to the prescriptions of Salaris & Girardi (2002), when the age-metallicity relation and star formation history of a given composite stellar system are unknown the derived distance modulus by using RC can have an error up to ~ 0.3 mag. Girardi (2016) provides an overview on the advantages and caveats of using RC stars for distance determination.

RRLs, on the other hand, are unequivocally old (≥ 10 Gyr). They are low-mass ($\sim 0.6 - 0.8M_{\odot}$) horizontal branch (HB) stars that experience radial pulsations because of periodic variations of the atmosphere opacity, in partial ionized regions (H, He). This causes cyclic variations of luminosity and effective temperature, with periods ranging typically from ~ 0.3 to ~ 1 days. Their typical mean luminosity in the V -band is in the range $M_V \sim 0.5 - 1$ mag, making them moderately bright objects, while effective temperatures range from ~ 7200 K to ~ 5600 K, which transform in typical mean colors between $(B - V) \sim 0.2$ mag and $(B - V) \sim 0.4$ mag. Historically, RRLs have been used as standard candles since their mean luminosity in the V -band is almost constant, with some dependency on their metallicity and evolutionary status (e.g. Bono et al., 2003; Clementini et al., 2003). Moreover, they are moderately bright ($\sim 40L_{\odot}$), easy to detect from their light variations and practically ubiquitous. Also, the occurrence of the so-called Oosterhoff dichotomy allowed people for decades to disentangle the old component of the Galaxy in two distinct groups, putting strong constraints on the Galaxy formation mechanisms (e.g. Fiorentino et al., 2015, 2016; Martínez-Vázquez et al., 2016a). Their role as standard candles and stellar population tracers has been widely investigated also from the theoretical point of view, on the basis of extensive and detailed nonlinear convective pulsation models (see e.g. Marconi et al., 2015, and references therein).

RRLs are much less numerous and also more time-consuming to identify than the RC. Both the RC and the RRLs have their own observational and theoretical advantages and disadvantages, however, together, they have shown to be the invaluable available tracers of old population for the study of the Milky Way galaxy. In §1, Andrea Kunder discusses how RRLs and RC giants have shaped our view of the kinematics of the inner Galaxy. Similarly, Pawel Pietrukowicz focuses on using these stars to understand the spatial structure of the inner Galaxy in §2. The chemical composition and age of the inner Galaxy is then described in §3 by Elena Valenti, again utilizing RRLs and RC giants.

In §4 and §5, RRLs and RCs are also discussed within the context of the Milky Way satellites and globular clusters, to further place into context the build-up of the Milky Way. Dwarf spheroidal (dSph) satellites of the Milky Way, and the low brightness tail of the dSph, the ultra-faint dwarf (UFD) galaxies, are old, metal-poor, gas poor and dark matter-dominated systems. Comparing their RRL populations with that of the MW places allows a more complete picture of galaxy formation to emerge, as shown in §4, by Massimo

Dall’Ora, Giuseppe Bono, Giuliana Fiorentino, Marcella Marconi, Clara E. Martinez-Vazquez, Matteo Monelli, Ilaria Musella and Vincenzo Ripepi.

Similarly, globular clusters harbor some of the oldest stars in our Galaxy and their distances, distribution throughout the Galaxy, and ages have long been used to as pillars to understand the early Galaxy. In §5, new observations that have improved the accuracy and precision of stellar populations within globular clusters, as well as better stellar models, have advanced our ability to use these old tracers to understand the early formation of the components of Galaxy. This section is contributed by Giuseppe Bono, Vittorio Braga, Giuliana Fiorentino, Massimo Dall’Ora, Ivan Ferraro, Giacinto Iannicola, Matteo Monelli, Maurizio Salaris and Peter B. Stetson.

1 Kinematics of the Galactic bulge

The internal kinematics of the bulge using a statistical sample of stars was first analyzed by the Bulge Radial Velocity Assay (BRAVA) survey (Rich et al. 2007; Kunder et al. 2012). BRAVA targeted M-giants toward the Galactic bulge in a grid covering three strips of latitude, at $b = -4^\circ, -6^\circ, -8^\circ$, that span across $-10^\circ < l < 10^\circ$. From a total of $\sim 10,000$ stars, they showed that the bulge is in cylindrical rotation. Kinematic models allow at most only $\sim 10\%$ of the original model disk mass to be in the form of a “classical” spheroid formed by dissipational collapse. Subsequent kinematic bulge surveys, probing closer to the plane and/or different stellar populations, have confirmed this result. However, a more complicated kinematic view of the bulge than was first able to be disentangled by the original BRAVA results has emerged, which is reviewed here by Andrea Kunder.

The Abundances and Radial velocity Galactic Origins Survey (ARGOS; Freeman et al., 2013) probed $\sim 17,400$ red-clump giants in the bulge – fainter stars than probed by BRAVA, but having temperatures more favorable for the determination of metallicities. Probing the CaT at $R \sim 11,500$, the ARGOS stars could be separated into metallicity sub-samples, which Ness et al. (2013a) believe to represent different populations in the bulge. Sample “A” consists of stars with $[\text{Fe}/\text{H}] \sim +0.15$ dex, which are proposed to belong to a relatively thin and centrally concentrated part of the boxy/peanut bulge. Sample “B” consists of stars with $[\text{Fe}/\text{H}] \sim -0.25$ dex, belonging to a thicker boxy/peanut bulge. Compared to “A”, this sample is hotter and less compact. Sample “C” consists of stars with $[\text{Fe}/\text{H}] \sim -0.7$ dex and kinematically differs from component A and B in that it does not appear to have a latitude-independent velocity dispersion rotation. Sample “D” is the most metal-poor with $[\text{Fe}/\text{H}] \sim -1.0$ dex. It is the least understood, due to the paucity of ARGOS stars with such metallicities. For example, there are only two stars with $[\text{Fe}/\text{H}] \sim -1.0$ dex in the ARGOS field at $(l, b) = (-20^\circ, -5^\circ)$, so the velocity dispersion provided by Ness et al. (2013a) for this field is not well constrained. In all sub-samples cylindrical rotation was seen, although the most metal-poor red clump giants (sample D) rotated slower than their metal rich counterparts

(Ness et al., 2013a). But as this signature was seen at latitudes 10 degrees from the plane, they associated the slower rotation as the consequence of contamination from the halo and metal-weak thick disk populations creeping into the bulge.

The GIRAFFE Inner Bulge Survey (GIBS; Zoccali et al., 2014) is targeting red-clump giants closer to the plane than both BRAVA and ARGOS. Most of the fields are at a resolution of $R=6500$, but a handful of fields were observed at $R=22,500$. Metallicities for their ~ 5000 surveyed stars (Gonzalez et al., 2015; Zoccali et al., 2017) were derived, as well as elemental abundances for ~ 400 red clump giants. They confirmed cylindrical rotation also at latitudes $b=-2^\circ$, and found that throughout most of the bulge, a narrow metal-rich ($[\text{Fe}/\text{H}] = +0.26$) population of stars and a broad more metal-poor ($[\text{Fe}/\text{H}] = -0.31$) component appears to exist. Both components rotate cylindrically, although the metal-poor stars are kinematically hotter and less bar-like.

Lastly, the APOGEE survey has probed $\sim 19,000$ red giant stars at positive longitudes close to the plane (Zasowski et al., 2016). The high-resolution ($R=22,500$), makes it feasible to obtain elemental abundances and the near-infrared wavelength regime ($\lambda=1.51\text{-}1.70\ \mu\text{m}$) allows the plane of the bulge to be probed, where dust and reddening is severe, but minimized by longer wavelengths. They find that the transition from cylindrical to non-cylindrical rotation occurs gradually, and most notably at higher latitudes. At a longitude of $l \sim 7^\circ$ the signature of cylindrical rotation fades, which is expected, as this longitude is near the end of the boxy bulge. Despite their large chemo-dynamical sample, they are not able to find distinct and separable bulge populations, although their measures of skewness is consistent with different evolutionary histories of metal-rich ($[\text{Fe}/\text{H}] = +0.26$) and metal-poor ($[\text{Fe}/\text{H}] \sim -0.31$) bulge populations.

All of these large surveys have shown that the bulge consists of a massive bar rotating as a solid body; the internal kinematics of these stars are consistent with at least 90% of the inner Galaxy being part of a pseudobulge and lacking a pressure supported, classical-like bulge. N-body barred galaxy models (boxy peanut bulge models) can explain the global kinematics, so our bulge appears to have formed from secular evolution of a massive early disk.

However, some finely detailed behavior of stars remain unexplained. For example, it is not clear how the kinematically cooler bulge stars (which are more metal-rich) fit together with the kinematically hotter (more metal-poor) bulge stars. Also, some bulge locations have shown no evidence for a metal-rich and metal-poor population, despite being at the same latitude as other fields which do clearly separate chemically (e.g., Zoccali et al., 2017).

Figure 1 shows the distributions of the targets in the survey's mentioned above. Most survey's have focussed on the Southern bulge, where the crowding is not as extreme. The APOGEE survey, in contrast, using a telescope in the North, probes more of the Northern bulge, and has not yet been able to reach the negative longitudes. With exception of the ARGOS survey, all data has been publicly released, improving the quality and value of these surveys, and

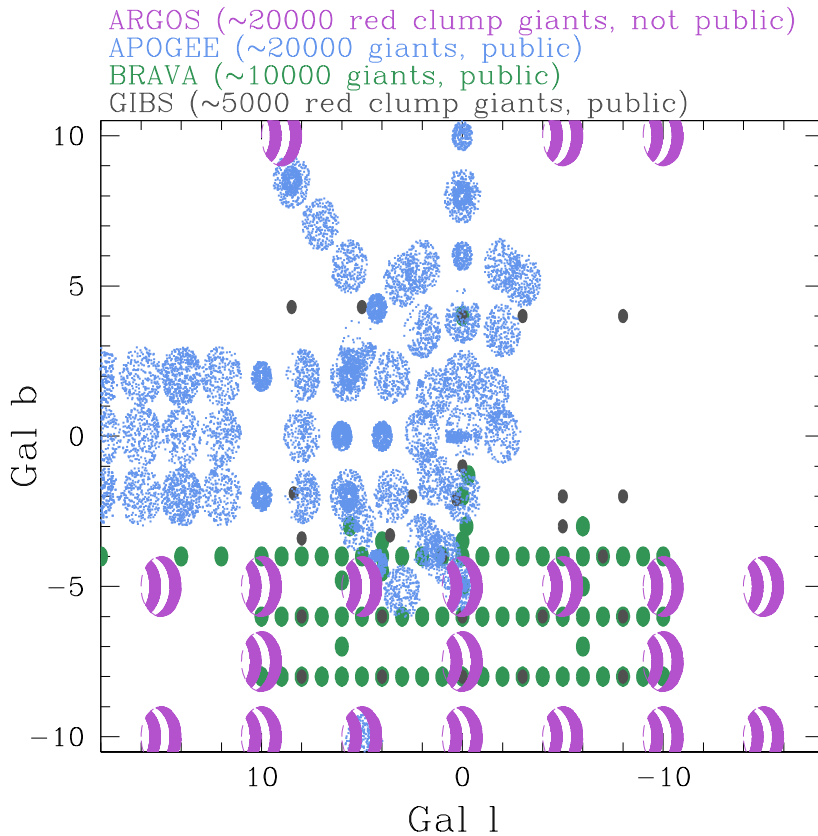


Fig. 1 The spatial location of the ARGOS, APOGEE, BRAVA and GIBS spectroscopic bulge surveys.

providing the wider scientific community the ability to productively use data for further research with the potential to advance developments.

1.1 Targeted Kinematic Studies

Notable recent high resolution studies ($R \sim 20,000-30,000$) of bulge field stars have been meticulously obtained by Johnson et al. 2011, 2012, 2013a, 2013b, 2014. In these papers, along with radial velocities, numerous individual elemental abundances, for some stars 27 elements ranging from oxygen to erbium, are derived for a sample of ~ 500 bulge giants. Therefore, not only can the kinematics, $[\text{Fe}/\text{H}]$ and $[\alpha/\text{Fe}]$ ratios of bulge stars be compared to those in the thin and thick disks, but also the light odd- Z and Fe-peak (and also neutron-capture) elements are touched on, which also provide discriminatory power between models and other stellar populations. These more detailed and

targeted observations indicate that at $[\text{Fe}/\text{H}] > -0.5$, the bulge exhibits a different chemical composition than the local thick disk in that the bulge $[\alpha/\text{Fe}]$ ratios remain enhanced to a slightly higher $[\text{Fe}/\text{H}]$ than the thick disk, and the Fe-peak elements Co, Ni, and Cu appear enhanced compared to the disk.

Further, these studies point to a bulge that formed rapidly ($<1\text{-}3$ Gyr), because of the enhanced $[\alpha/\text{Fe}]$ abundances coupled with the low $[\text{La}/\text{Eu}]$ ratios of the bulge stars (see also McWilliam et al., 2010). This confirms a very fast chemical enrichment in the bulge put forth by the very first detailed abundance studies of red giants in the Milky Way bulge (e.g., McWilliam & Rich, 1994; Zoccali et al., 2006; Fulbright et al., 2007).

Babusiaux et al. (2010, 2014) compared the velocities of metal-rich and metal-poor bulge stars and found that higher metallicity stars in the bulge show larger vertex deviations of the velocity ellipsoid than more metal-poor stars. They also found that metal-rich stars show an increase in their velocity dispersion with decreasing latitude (moving closer to the Galactic plane), while metal-poor stars show no changes in the velocity dispersion profiles. They concluded that the more metal-rich stars are consistent with a barred population and the metal-poor stars with a spheroidal component. However, other high-resolution studies of bulge stars have not confirmed such trends and instead find consistent decrease in velocity dispersion with increasing $[\text{Fe}/\text{H}]$ (e.g., Johnson et al., 2014; Uttenthaler et al., 2012; Ness et al., 2013a).

Perhaps the greatest limitation in finding possible differences between a metal-rich and a metal-poor population in the bulge is the difficulty of finding metal-poor stars in the bulge. For example, within the ARGOS survey (Ness et al., 2013a), 0.1% of the stars identified as lying in the bulge have $[\text{Fe}/\text{H}] < -2.0$ dex. The first metal-poor stars found close to the Galactic center was presented by Schultheis et al. (2015), who find 10 stars with $[\text{M}/\text{H}] \sim -1.0$ dex within ~ 200 pc from the Galactic center. García Pérez et al. (2013) used infrared spectroscopy of 2400 bulge stars to uncover five new metal-poor stars with $-2.1 < [\text{Fe}/\text{H}] < -1.6$, and using optical photometry to first select metal-poor candidates, and Schlafman & Casey (2014) uncovered three stars in the direction of the bulge with $-3.0 < [\text{Fe}/\text{H}] < -2.7$. The Extremely Metal-poor Bulge stars with AAOmega (EMBLA) survey, dedicated to search for metal-poor stars in the bulge, has uncovered ~ 40 metal-poor stars (Howes et al., 2014, 2015, 2016), including a handful with $[\text{Fe}/\text{H}] < -3.0$. Five stars in the very metal-poor regime, at $-2.7 < [\text{Fe}/\text{H}] < -2.0$ are presented in Koch et al. (2016), where they find that the metal-poor stars are a broad mix, and no single, homogeneous “metal-poor bulge” can yet be established.

Figure 2 shows the kinematics of these metal-poor stars compared to “normal” bulge giants from the BRAVA survey. Though the number statistics are still small, their velocity dispersion suggests either that the metal-poor stars in the bulge have different kinematics than the more metal-rich stars, or that the metal-poor stars discovered are a halo population.

Lacking a statistical sample of metal-poor stars in the bulge, understanding their kinematics and placing them in context within the Galaxy is nontrivial. Especially since the oldest and most metal poor stars (which may trace the

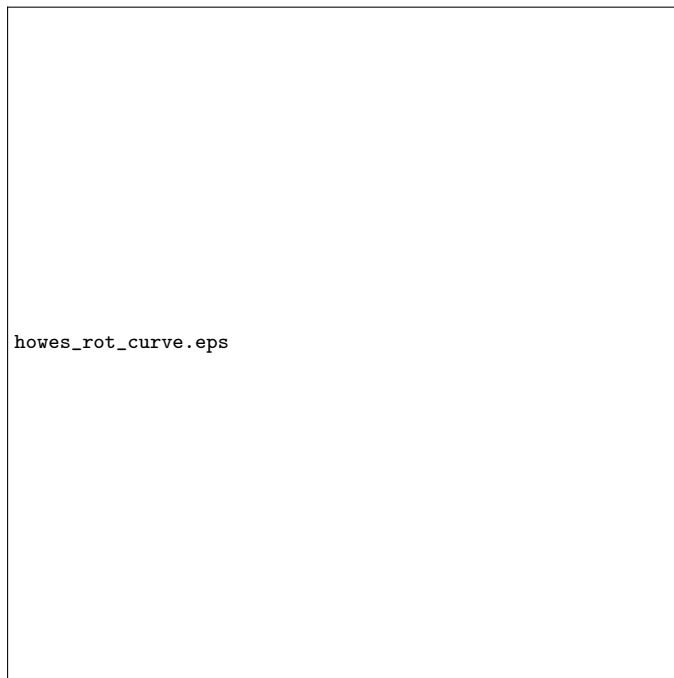


Fig. 2 The velocity dispersion profile (bottom) and rotation curve (top) for the metal-poor stars ($[\text{Fe}/\text{H}] < -2.0$) observed in the bulge compared to that of the BRAVA giants at $b = -4^\circ$, -6° , and -8° strips (Kunder et al. 2012). The individual metal-poor star measurements are given in the top panel, and the large red circles indicate the mean Galactocentric velocity (top) and velocity dispersion (bottom). The metal-poor stars have kinematics suggesting they are different from the bulge giants, although the sample size is small (~ 50). It has been put forward that these metal-poor stars are actually halo interlopers (e.g., Howes et al. 2014, Kunder et al. 2015, Koch et al. 2016).

dark matter) are thought to be found in the center of the Galaxy – in the bulge but not sharing its kinematics and abundance patterns (Tumlinson, 2010), the metal-poor “bulge” stars could provide a big piece of the puzzle in understanding the formation and subsequent evolution of the Galactic bulge.

Perhaps the easiest identifiable old, metal-poor bulge population are those horizontal branch stars that pulsate as RR Lyrae stars. Their progenitors formed long ago (~ 10 Gyr), so that the RRLs we see today tell us about conditions when the halo of the Galaxy was being formed (e.g., Lee, 1992). The bulge RRLs were shown to be on average ~ 1 dex more metal-poor than the majority of bulge stars residing in the bar (Walker & Terndrup, 1991), although some of the bulge RRLs do appear to have metallicities that overlap in abundance with the bar population.

The ongoing Bulge Radial Velocity Assay for RR Lyrae stars, BRAVA-RR survey (Kunder et al., 2016), aims to collect spectrographic information for RRLs located toward the inner Galaxy. Their sample of RRLs are selected from the Optical Gravitational Lensing Experiment (OGLE), so the periods, ampli-



Fig. 3 The velocity dispersion profile (bottom) and rotation curve (top) for the ~ 1000 RR Lyrae stars observed in the bulge compared to that of the BRAVA giants at $b = -4^\circ$, -6° , and -8° strips (Kunder et al. 2012, Kunder et al. 2016). The bulge model showing these observations are consistent with a bulge being formed from the disk is represented by the dashed lines (Shen et al. 2010). The RRLs have kinematics clearly distinct from the bulge giants, and are a non-rotating population in the inner Galaxy.

tudes and magnitudes are already precisely known. Multi-epoch spectroscopy (typically 3 epochs per star) is used to obtain center-of-mass radial velocity with uncertainties of $\sim 5\text{-}10 \text{ km s}^{-1}$. From radial velocities of about *sim*1000 RRLs surveyed by BRAVA-RR in four 2-degree fields covering approximately a Galactic latitude and longitude of $-3^\circ < b > -6^\circ$ and $-4^\circ < l > 4^\circ$, it is evident that these old and metal-poor stars are kinematically distinct from the more metal-rich red giants in the BRAVA, GIBS, ARGOS and APOGEE surveys. The RRLs show null rotation and hot (high-velocity dispersion) kinematics. In the ARGOS survey one also observes a slowly-rotating metal-poor population, but these stars are believed to be contamination from disk and halo stars (as it is only seen at high Galactic latitude). In contrast, the RRLs are at low Galactic latitudes ($|b| < 7^\circ$) and have more certain distance estimates, and the larger number statistics of the RRLs makes this result quantifiable. The RR Lyrae stars trace an older, more spheroidal component in the inner Galaxy.

The mass of this 'old' bulge is estimated to be $\sim 1\%$ of the total central mass, broadly consistent with current bulge formation models, which predict that no more than $\sim 5\%$ of a merger-generated bulge (Shen et al., 2010; Ness

et al., 2013a; Di Matteo et al., 2015). It may be that the RRL stars toward the bulge are actually an inner halo-bulge sample, as originally speculated in the early 1990s (e.g., Minniti, 1994) and as at least one RRL orbit toward the Galactic bulge seems to indicate (Kunder et al., 2015).

Prompted by the results from the RRLs, Pérez-Villegas et al. (2017) carried out N -body simulations for the Milky Way to investigate the kinematic and structural properties of the old metal-poor stellar halo in the barred inner region of the Galaxy. They showed that the RR Lyrae population in the Galactic bulge may be the inward extension of the Galactic metal-poor stellar halo, and that especially the radial velocities of RRLs in the outer Galactic longitudes constrain a bulge/halo scenario. Unfortunately, the RRLs investigated in Kunder et al. (2016) are confined to the innermost 500 pc. This is where a slow-rotating component has the smallest velocity difference compared to the metal-rich bulge giants (~ 25 km/s), and hence where population contamination from e.g., the halo or thick disk could more easily mask the effects of rotation. Observations of RRL at further longitudes in the bulge would allow us to distinguish between a bulge or halo.

1.2 Future: Gaia

Gaia has begun collecting six-dimensional space coordinates for more than 1 billion stars in the Milky Way. The bulge is a difficult target for Gaia, due to the crowding and extinction, but Gaia will still impact bulge kinematics significantly. The Radial Velocity Spectrometer (RVS), which is the spectroscopic instrument for all objects down to $G \sim 16$ mag, can cope with a crowding limit of 35,000 stars deg^{-2} (Reylé et al., 2005). In denser areas, only the brightest stars are observed and the completeness limit will be brighter than 16 mag. Therefore, we can expect the brighter giants to be surveyed throughout the bulge with RVS, but most of the red clump stars and RRLs will be lacking Gaia radial velocities.

Never-the-less, the astrometric instrument has been designed to cope with object densities up to 750,000 stars per square degree and down to $G \sim 20$ mag. Therefore, for a large area of the bulge, at least some of the horizontal branch will be reachable for useful proper-motions, although no useful (5σ) parallaxes are expected for these stars. At end of mission, Gaia will have ~ 54 Gaia transits covering the bulge (Clementini et al., 2016).

Figure 4 shows the proper motions of the giants in the direction of the bulge surveyed in APOGEE DR13 post- and pre-Gaia DR1. Before Gaia DR1 was available, the proper motions were not of the quality that allowed one to easily distinguish between a field and bulge stellar population. Color-magnitude diagrams can help in differentiating bulge stars from field stars, since bulge stars tend to be redder, but the large and variable extinction and the sheer number of field stars along the line of sight toward the bulge, makes color cuts not always reliable.

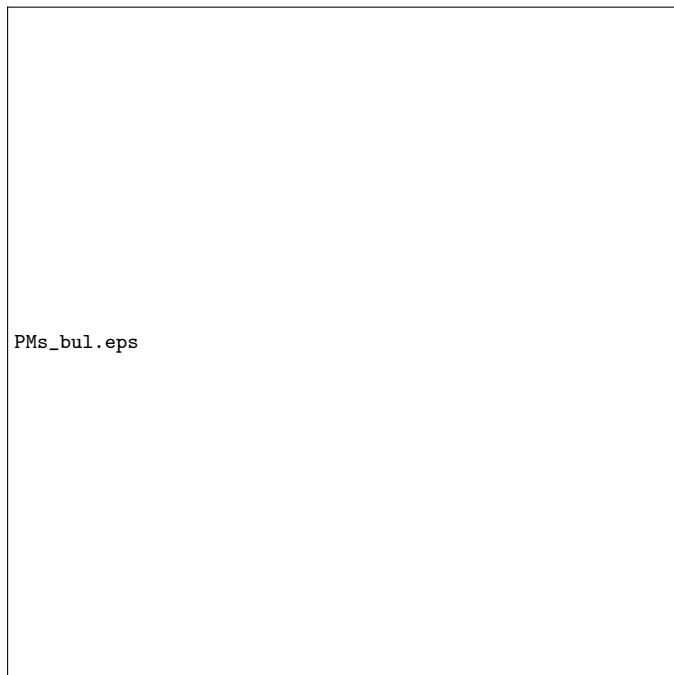


Fig. 4 *Top:* The color magnitude diagram of ~ 2500 APOGEE giants that have UCAC5 proper motions with uncertainties smaller than 2 mas/yr. *Bottom:* The UCAC5 (left) and UCAC4 (right) proper motions of the APOGEE giants with proper motion uncertainties smaller than 2 mas/yr. Already with Gaia DR1, a sharper kinematic view of the bulge than previously feasible, is possible.

With the precise positions of stars measured in Gaia DR1, significant improvements in the astrometric solutions were able to be obtained, leading to the release of UCAC5. For over 107 million stars, now proper motions with typical accuracies of 1 to 2 mas/yr ($R= 11$ to 15 mag), and about 5 mas/yr at 16th mag, exist. With Gaia, we are approaching the possibility of using proper motion information to separate the high degree of disk contamination from the bulge.

2 Spatial structure of the RR Lyrae star population toward the Galactic bulge

RR Lyrae-type variable stars can be found everywhere in the Milky Way, but they are particularly numerous in the Galactic bulge. Historically, van Gent (1932, 1933) was the first who noticed that RRLs observed close to the central regions of the Milky Way concentrate toward the Galaxy center. More than a decade later, Baade (1946) in a relatively unobscured area, today called “Baade’s Window” in his honor, found a strong predominance of RRLs indicating a presence of Population II stars in the central area of the Milky

Way. He assumed that the center of this population coincides with the Galactic center and assessed the distance to the center of the Galaxy using RRLs, obtaining a distance of 8.7 kpc (Baade, 1951).

Until the early 1990s about one thousand RRLs inhomogeneously distributed over the Galactic bulge were known. Following the advent of massive photometric surveys, particularly focused on searches for microlensing events, the number of new RRLs toward the bulge has increased. 215 such objects were discovered during the first phase of the OGLE (Udalski et al., 1992), conducted on the 1.0-m Swope telescope at Las Campanas Observatory, Chile, in years 1992–1995. About 1800 RR Lyrae pulsators were detected by the MACHO microlensing survey (Alcock et al., 1995) which used the 1.27-m Great Melbourne Telescope at the Mount Stromlo Observatory, Australia, in years 1992–1999. Alcock et al. (1998) examined mean magnitudes and colors of the new pulsators and found that the bulk of the population is not barred. Only stars located in the inner fields closer to the Galactic center ($l < 4^\circ$, $b > -4^\circ$) seem to follow the barred distribution observed for intermediate-age red clump giants (Stanek et al., 1994). Minniti et al. (1998) used this sample to show that between about 0.3 kpc and 3 kpc from the Galactic center, the spatial density distribution of RRLs can be represented by a power law of an index of -3.0 .

Analysis of the data from the second phase of the OGLE project (OGLE-II), conducted on the dedicated 1.3-m Warsaw Telescope at Las Campanas Observatory in years 1997–2000, brought a much larger set of 2713 RRLs (Miznerki, 2003). Based on the sample of 1888 fundamental-mode RRLs from OGLE-II, Collinge et al. (2006) robustly detected the signature of a barred structure in the old population within the inner $\pm 3^\circ$ of Galactic longitude. Later, about 3000 fundamental-mode RRLs from the MACHO database were used to investigate the metallicity distribution of these stars (Kunder & Chaboyer, 2008) and interstellar extinction toward the Galactic bulge (Kunder et al., 2008). It was determined that bulge variables have the average metallicity $[\text{Fe}/\text{H}] = -1.25$ dex, with a broad range from $[\text{Fe}/\text{H}] = -2.26$ to -0.15 dex, on the Zinn & West (1984) metallicity scale. Kunder & Chaboyer (2008) searched for the evidence of the Galactic bar and found a marginal signature of a bar at Galactic latitudes $|b| < 3.5^\circ$. The absence of a strong bar in the RR Lyrae population clearly indicated that they represent a different population than the metal-rich bulge. However, the shape of this population was far from being fully known. More data covering preferably the whole bulge area were needed.

In 2001, the OGLE project started its third phase with a new mosaic eight-CCD camera attached to the Warsaw Telescope. One of the OGLE-III results was the release of a collection of 16,836 RRLs found in an area of 69 deg^2 mostly south of the Galactic equator (Soszyński et al., 2011). The collection composed of 11,756 fundamental mode (RRab) stars, 4989 overtone pulsators (RRc), and 91 double-mode (RRd) stars. OGLE provided time-series photometry in two standard filters: V and I . This sample was promptly analyzed by Pietrukowicz et al. (2012) who demonstrated that the bulge RRLs form a metal-uniform population, slightly elongated in its inner part. The authors

found that the photometrically derived metallicity distribution for RRab stars is sharply peaked at $[\text{Fe}/\text{H}] = -1.02 \pm 0.18$ dex with a dispersion of 0.25 dex, on the Jurcsik (1995) metallicity scale. This result agreed very well with the one from Kunder & Chaboyer (2008), since the Jurcsik (1995) scale is shifted roughly by +0.24 dex with respect to the Zinn & West (1984) scale.

Pietrukowicz et al. (2012) also estimated the distance to the Milky Way center based on the bulge RRLs to be $R_0 = 8.54 + / - 0.42$ kpc. Here, the theoretical period-luminosity-metallicity (PLZ) relations in V and I bands published by Catelan et al. (2004) were used; the zero points of these relations were calibrated to the data obtained for the well-studied representative globular cluster M3 (Catelan, 2004). In their analysis, Pietrukowicz et al. (2012) made a simple assumption on a linear relation between I -band extinction A_I and reddening $E(V-I)$. At that time it was the only reasonable way to unreddened mean magnitudes of the RRLs. They showed that, for RRab stars as well as for RRC stars, in the inner regions ($|l| < 3^\circ$, $|b| < 4^\circ$) the old population indeed tends to follow the barred distribution of the bulge red clump giants.

A year later Dékány et al. (2013) combined optical and near-infrared data for the OGLE-III bulge RRLs to study the RRL spatial distribution. The authors used mean I -band magnitudes from OGLE and K_s -band magnitudes from the near-infrared VISTA Variables in the Vía Láctea (VVV) survey (Minniti et al., 2010). VVV was one of the ESO (European Southern Observatory) public surveys carried out on the 4.1-m Visible and Infrared Survey Telescope for Astronomy (VISTA) in years 2010–2015. Observations were taken in $ZYJHK_s$ filters and included the Milky Way bulge and an adjacent section of the Galactic plane, covering a total area of about 562 deg^2 (Saito et al., 2012). The monitoring campaign was conducted only in the K_s band.

The approach applied by Dékány et al. (2013) is expected to bring more precise results than the ones based on optical data alone. That is because PLZ relations have decreasing metallicity dependence toward longer wavelengths and measurements in near-infrared wavebands are much less sensitive to interstellar reddening than optical ones. Dékány et al. (2013) concluded that the population of RRLs does not trace a strong bar, but have a more spheroidal, centrally concentrated distribution with only a mild elongation in its very center at an angle $i = 12.5^\circ \pm 0.5^\circ$ with respect to the line of sight from the Sun to the Galactic center.

The fourth phase of the OGLE project (OGLE-IV) (Udalski et al., 2015), which was launched in 2010, covers practically the whole bulge in V and I passbands. With the installation of a 32-CCD mosaic camera of a total field of view of 1.4 deg^2 OGLE became a truly wide-field variability survey. The OGLE-IV collection of RRLs toward the Galactic bulge was released by Soszyński et al. (2014). This collection contains data on 38,257 variables detected over 182 deg^2 : 27,258 RRab, 10,825 RRC, and 174 RRd stars. The survey also includes the central part of the Sagittarius Dwarf Spheroidal Galaxy with the globular cluster M54 in its core.

Analysis of this set of data was undertaken also by the OGLE team and presented in Pietrukowicz et al. (2015). Due to some practical reasons the analysis

was based only on RRab-type pulsators, and the part closest to the Galactic plane ($|b| < 3$) was avoided. RRab stars are more numerous. On average, they are intrinsically brighter in the I -band and have higher amplitudes than RRc stars. What is extremely important, RRab variables with their characteristic saw-tooth-shaped light curves, in comparison to nearly sinusoidal light curves of RRc stars, are harder to overlook. This makes the searches for these type of variables more likely to yield better completeness ratios. Another very practical property of RRab stars is that based on the pulsation period and shape of the light curve one can assess metallicity of the star (Jurcsik, 1995; Jurcsik & Kovács, 1996; Sneden et al., 2008).

Pietrukowicz et al. (2015) found again that the spatial distribution of the inner bulge RRLs trace closely the barred structure formed of intermediate-age red clump giants. According to the most recent models of the Galactic bar, it is close to being a prolate ellipsoid. Based on OGLE-III data Cao et al. (2013) found the following axis ratios and inclination of the major axis: 1.0:0.43:0.40, $i = 29.4^\circ$. A similar result was obtained by Wegg & Gerhard (2013) using VVV red clump data: 1.0:0.63:0.26, $i = 27^\circ \pm 2^\circ$. This time in their analysis, Pietrukowicz et al. (2015) dereddened mean I -band magnitudes of RRLs using a new relation derived by Nataf et al. (2013). The relation was based on optical measurements from OGLE-III and near-infrared measurements from 2MASS and VVV for bulge red clump giants. After this correction the obtained distance distribution to the bulge RRLs turned out to be smoother in comparison with the previously used simple linear relation. They found the maximum of the distribution or distance to the Galactic center at $R_0 = 8.27 \pm 0.01(\text{stat}) \pm 0.40(\text{sys})$ kpc, which is in very good agreement with estimates from other measuring methods. Pietrukowicz et al. (2015) showed that the spatial distribution of the bulge RRLs has the shape of a triaxial ellipsoid with proportions 1:0.49:0.39 and the major axis located in the Galactic plane and inclined at an angle $i = 20^\circ \pm 3^\circ$ to the Sun-(Galactic center) line of sight (see Figure 5).

Differences between the Dékány et al. (2013) results and those from OGLE-IV are the following: (1) Dékány et al. (2013) used a smaller sample of about 7700 RRab stars from the previous phase of the OGLE survey (OGLE-III), while the OGLE-IV collection (Soszyński et al., 2014) contain nearly 27,300 pulsators of this type. (2) The Dékány et al. (2013) results are based on a lower number of collected K_s -band measurements per light curve (about 40 by 2013), which could affect the average infrared brightness of the variables and could slightly smear the observed structure. However, the amplitude variation in the K_s -band is a factor of ~ 3 smaller than that in the I - or V -band. (3) Because the Dékány et al. (2013) results uses also infrared magnitudes, the de-reddening process of the RRLs differs from that adopted in Pietrukowicz et al. (2015). Resolution of the discrepancy between the OGLE-IV RRLs presented in Pietrukowicz et al. (2015) and the VVV RRLs presented in Dékány et al. (2013) is ongoing.

The obtained sharp ellipsoidal shape does not depend on the real final distance to the studied objects. The true inclination angle as well as the axis

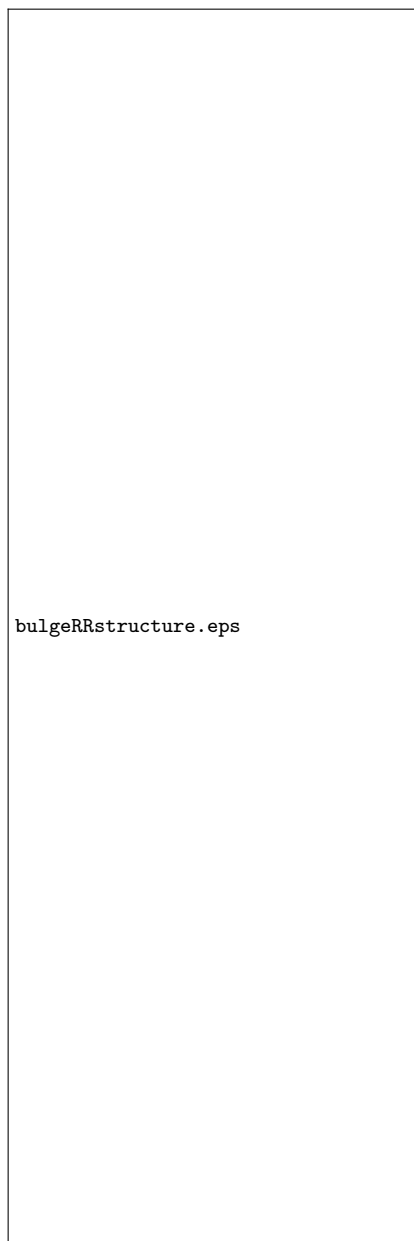


Fig. 5 Results of the analysis of density distribution of OGLE-IV bulge RRab stars (Pietrukowicz et al., 2015). Upper panel: Constant surface density lines in the sky are well represented by ellipses with a mean flattening $f = 0.33 \pm 0.03$. Middle panel: The maxima of the density distributions along four selected lines of sight clearly get closer to us with the increasing Galactic longitude. This strongly indicates the presence of a tilted axis in the plane. Lower panel: In the projection onto the Galactic plane, points of the same density level form inclined ellipses. Conclusion: the old bulge population has the shape of a triaxial ellipsoid with the major axis inclined to us at an angle $i = 20^\circ \pm 3^\circ$.

ratios may be slightly different than reported. These values may also change with the galactocentric distance. This will be known once almost all RRLs (or at least RRab-type variables) are detected from the inner bulge to the outer Galactic halo. Unfortunately, searches for RRLs in obscured Galactic plane regions are very difficult. That is because near-infrared light curves of these pulsating stars have often symmetric, nearly sinusoidal shape. If the number of data points per light curve is small and the time coverage too short, RRLs can be easily confused with other variables, particularly with contact eclipsing binaries and spotted variables. However, the first detection of RRLs in the vicinity of the Galactic center, in the so-called nuclear bulge has been made (Minniti et al., 2016; Dong et al., 2017).

A clear result from the analysis of the OGLE-IV bulge RRab variables is that their spatial density distribution in the galactocentric distance range from about 0.2 kpc to 2.8 kpc can be described as a single power law with an index of -2.96 ± 0.03 . Pietrukowicz et al. (2015) also was not able to see an X-shaped structure in the RRLs as it is observed in the case of bulge red clump giants (Nataf et al., 2010; McWilliam & Zoccali, 2010). This is expected, as it was found that only metal-rich bulge populations have this feature (Ness et al., 2012).

Another discovery by Pietrukowicz et al. (2015) is that RRab stars form two (or even more) very close sequences in the period–amplitude (or Bailey) diagram. This is interpreted as the presence of multiple old populations being likely the result of mergers in the early history of the Milky Way. So far, there are no hints that the two major old populations have different structure. They seem to be well mixed together. Lee & Jang (2016) suggest that the observed period shift between the sequences can be explained by a small difference in the helium abundance.

Recently, Pérez-Villegas et al. (2017) used N-body simulations to investigate the structural and kinematic properties of the old population in the barred inner region of the Galaxy. They showed that the RR Lyrae population in the bulge is consistent with being the inward extension of the Galactic metal-poor stellar halo, as suggested by Minniti et al. (1998) and Pietrukowicz (2016). Pérez-Villegas et al. (2017) followed the evolution of the metal-poor population through the formation and evolution of the more massive bar and boxy/peanut bulge and found the density distribution to change from oblate to triaxial. They found that at the final time of the simulations (after 5 Gyr), the axis ratios of the triaxial old stellar halo in its inner part reached $b/a \sim 0.6$ and $c/a \sim 0.5$. The ratios increase with the distance from the center to roughly 1.0 and 0.7, respectively, at a distance of 5 kpc. These results are very consistent with the observations of the bulge RRLs from OGLE-IV and also spectroscopic observations of old stars in the Milky Way halo by the SDSS survey. According to the latter studies, the Galactic halo has an oblate shape (Jurić et al., 2008; Carollo et al., 2008; Kinman et al., 2012). Ongoing photometric surveys, such as Gaia, VVV eXtended (VVVX) and OGLE-IV with extended coverage of the Galactic bulge and disk will continue in completing the picture of the old bulge population drawn by RRLs.

3 The Galactic bulge: 3D structure, chemical composition, and age traced by its old stellar population

The formation and evolution of galaxies is still a heavily debated question of modern astrophysics. As one of the major stellar components of the Milky Way, the bulge provides critical and unique insights on the formation and evolution of the Galaxy, as well as of the external galaxies. Indeed with the current observational facilities, it is the only bulge in which we are able to resolve stars down to the old main sequence turnoff, hence providing accurate studies of the stellar populations in almost every evolutionary stage. The physical, kinematics and chemical properties of the stellar populations in the bulge allow us to discriminate among various theoretical models for the formation and evolution of bulges at large, setting tight constraints on the role that different processes (i.e. dynamical instabilities, hierarchical mergers, gravitational collapse) may have taken place.

However, this advantage comes with the need of covering a large area of the sky ($\sim 500 \text{ deg}^2$). Therefore, to understand the global properties of the bulge one should look for reliable tracers of distance and age that can be easily observed in any region of the sky in the bulge direction. In this framework, Red Clump stars and RRLs play a crucial role, and indeed over the decades studies of these stars have been essential to build our current knowledge of the Galactic bulge. The present section put together by Elena Valenti is not intended to be a complete review of the Galactic bulge properties but an overview of the bulge structure, chemical composition, and age based on the observational results on RC stars and RRLs.

The age-metallicity relation and star formation history of the RCs in the bulge is not well-known, so an error of up to $\sim 0.3 \text{ mag}$ can be introduced when trying to use these stars to derive a distance. At the distance of the bulge this translates to $\sim 1 \text{ kpc}$. However, considering that overall the bulge is metal rich and old ($\gtrsim 10 \text{ Gyr}$), one could use the corresponding population effect correction and therefore reduce the error on the distance. RRLs represent, on the other hand, much more accurate distance candles. Unlike the RC stars, they trace univocally the oldest stellar population of any given complex system (see §2 above by P. Pietrukowicz).

In §3.1, a global view of the three-dimensional structure of the bulge addressing the observational evidences is presented, that leads to determination of the bar properties, the stellar density and the mass. The chemical composition and age of the bulge stellar populations are reviewed in §3.2, and 3.3, respectively. Finally, §3.4 summarizes the main stellar properties that combined define our current knowledge of the Milky Way bulge, and the pieces of evidence that are still lacking in order to improve and possibly complete the global picture are highlighted. Note that occasionally up to date versions of relevant figures obtained using state of the art observational data are presented.

Table 1 Axis scale lengths and orientation angle of the bulge main bar based on RC stars distribution.

x_0 (kpc)	y_0 (kpc)	z_0 (kpc)	Θ (deg)	Data	Area (deg ²)	Reference
1.2	0.40	0.30	24-27	OGLE-II	~11	Rattenbury et al. (2007)
1.0	0.41	0.38	29-32	OGLE-III	~90	Cao et al. (2013)
0.7	0.44	0.18	27	VVV	~300	Wegg & Gerhard (2013)

3.1 The 3D structure

3.1.1 The bar boxy/peanut/X-shaped structure

Today it is well known that the Milky Way is a barred galaxy. Although the first observational evidence of the presence of a bar in the innermost region of the Galaxy was presented by Blitz & Spergel (1991) by using the stellar density profile at $2.4\mu\text{m}$ by Matsumoto et al. (1982), its existence was hypothesized nearly 20 years earlier. Indeed, to explain the departures from circular motions seen in the HI line profile at 21 cm, de Vaucouleurs (1964) suggested for the first time that the Milky Way could host a bar in its inner regions. After then, over the decades, many different tracers - e.g. gas kinematics (Binney et al., 1991), stellar surface profile (Weiland et al., 1994; Dwek et al., 1995; Binney et al., 1997), microlensing experiments (Udalski et al., 2000; Alcock et al., 2000), and OH/IR and SiO maser kinematics (Habing et al., 2006) - have been used to confirm the presence of the bar and to constrain its properties.

Still, the strongest observational evidence for the presence of the bar comes from the use of RC stars as standard candles to deproject the stellar density distribution in the Galaxy inner region. By using the color-magnitude diagram (CMD) derived from the OGLE (Udalski et al., 1992) photometry in Baade’s Window ($l = -1^\circ, b = -3.9^\circ$) and in two additional fields at ($\pm 5^\circ, -3.5^\circ$), Stanek et al. (1994) found that the mean RC magnitude at positive longitudes was brighter than the one observed at negative longitude. Under the assumption that there is no continuous metallicity and age gradient along the longitude, the observed change in mean RC magnitude across the field was interpreted in terms of distance. Stars at positive longitudes are brighter, hence closer, than those at negative longitudes. By using a triaxial model for the bulge, Stanek et al. (1994) derived a bar pivot angle of $\Theta = 45^\circ$.

Following this pioneering work, many studies (see Stanek et al., 1997; Bisant & Gerhard, 2002; Babusiaux & Gilmore, 2005; Benjamin et al., 2005; Nishiyama et al., 2005; Rattenbury et al., 2007; Lopez-Corredoira et al., 2007; Cabrera-Lavers et al., 2008; Cao et al., 2013; Wegg & Gerhard, 2013) have used RC stars to constrain triaxial bar models. Table 1 lists the axis scale lengths and orientation angles of the bar as derived by Rattenbury et al. (2007); Cao et al. (2013); Wegg & Gerhard (2013), which among all similar studies, are those considering the largest bulge area, therefore possibly providing more accurate estimates of the bar physical properties.

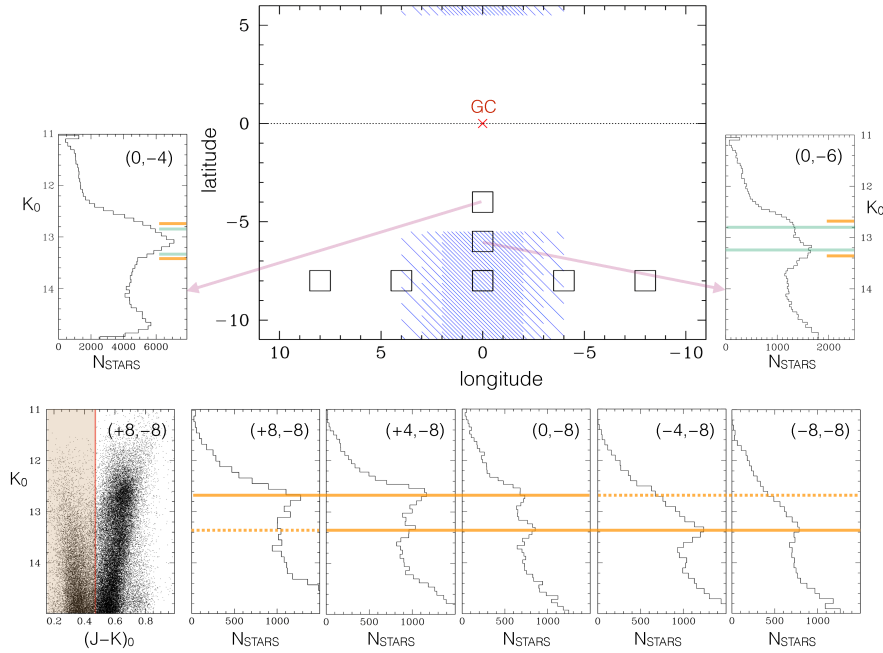


Fig. 6 Luminosity function of the bulge RGB and RC, in several fields. The large box (middle) marks the bulge area covered by the VVV survey, with the seven fields for which the RGB luminosity function is probed. The shaded blue rectangle refers to the region where the double RC is visible ($|b| > 5^\circ$, $|l| < 4^\circ$). The shading is finer where the double RC is clearly evident and becomes wider when one of the two RCs becomes significantly weaker than the other. The bottom left corner panel shows the CMD of the field at $(-8^\circ, +8^\circ)$ as an example of the colour selection applied to exclude the main sequence of the foreground disc. Orange horizontal lines mark the magnitude of the two RCs in the five fields at $b = -8^\circ$ shown in the bottom panels. Green horizontal lines mark the magnitude of the two RCs at $b = -6^\circ$, shown at the top right. Only one RC is visible at $b = -4^\circ$ (Baade’s Window), shown at the top left. Figure reproduced from Gonzalez et al. (2015, their Figure 1).

Owing to the RC stars distribution across the bulge, we now know that the bar has a boxy/peanut/X-shape structure in its outer regions: a typical characteristic of all barred galaxies when seen edge-on (Laurikainen et al., 2014; Laurikainen & Salo, 2017, for a recent review). McWilliam et al. (2010) and Zoccali et al. (2010) were the first who noticed that the distribution of the RC stars in some fields in the outer regions ($|b| > 5^\circ$) along the bulge minor axis ($l = 0^\circ$) was bimodal, suggesting the presence of a double RC. The observed split in the RC mean magnitude was then confirmed by McWilliam & Zoccali (2010) and Nataf et al. (2010) by using 2MASS and OGLE photometry, respectively. The authors explained the split in the RC as signature of two southern arms of an X-shape structure crossing the line of sight. An alternative explanation is that the double RC phenomenon is a manifestation of multiple populations observed in globular clusters (GCs) in the metal-rich regime (Lee et al., 2015; Joo et al., 2017).

Shortly after, the 2MASS-based 3D map of the RC distribution over a bulge area of 170 deg^2 by Saito et al. (2011) confirmed the presence of the X-shape and showed that the two RC over-densities were only visible in the outer bulge (i.e. $b < -5^\circ$, and $b > 5^\circ$) along the deprojected minor axis ($|l| \leq 5^\circ$, see also Figure 6). Thanks to the superior quality, in terms of photometric depth and spatial resolution, of the near-IR Vista Variable in the Via Lactea (VVV, Minniti et al., 2010; Saito et al., 2012) Wegg & Gerhard (2013) modelled the observed RC distribution across the whole bulge area ($\sim 300 \text{ deg}^2$) thus providing the first complete map of its X-shape structure. Although not specifically obtained through the study of RC stars, it is worth mentioning in this context the latest work by Ness & Lang (2016) based on WISE images, in which the X-shape nature of the Milky Way bulge revealed itself with unquestionable doubts (see their Figure 2).

There is now a general consensus that the majority of the observed Milky Way bulge structure is a natural consequence of the evolution of the bar. The bar heats the disk in the vertical direction giving rise to the typical boxy/peanut shape. Dynamical instabilities cause bending and buckling of the elongating stellar orbits within the bar, resulting in an X-shape when seen edge-on (Raha et al., 1991; Merritt & Sellwood, 1994; Patsis et al., 2002; Athanassoula, 2005; Bureau & Athanassoula, 2005; Debattista et al., 2006). However, the possible presence of a metal-poor spheroid *embedded* in the boxy/peanut bulge seems to be suggested by a number of fairly recent studies investigating the correlation between RC stars chemical and kinematics properties, as well as the spatial distribution of other stellar tracers, such as RRL, Mira and Type II Cepheids (T2C) variables. While the readers are referred to §1 above for an overview on the bulge kinematics, here it is however worth mentioning that metal-poor ($[\text{Fe}/\text{H}] \lesssim 0$) stars in the Baade’s window show negligible vertex deviation ($l_\nu \sim 0$) consistent with those of a spheroid. Conversely, metal-rich ($[\text{Fe}/\text{H}] \gtrsim 0$) stars exhibit significant ($l_\nu \sim 40$) elongated motions typical of galactic bars (Babusiaux et al., 2010). In addition, based on the spectroscopic data provided by the ARGOS survey (i.e. $\sim 14,000$ RC stars; Freeman et al., 2013), Ness et al. (2012) demonstrated that only the distribution of metal-rich stars shows the split in RC, a univocal signature of the bar X-shape. On the other hand, metal-poor stars show only a single RC peak. The scenario in which the metal-poor bulge stars, and therefore possibly the oldest population, do not trace the bar structure is also supported by the observed distribution of Mira (Catchpole et al., 2016), RRLs (Dékány et al., 2013), and T2C (Bhardwaj et al., 2017) variables. In particular, by using a combination of near-IR and optical data from VVV and OGLE-III, Bhardwaj et al. (2017) found that their sample of T2C population in the Galactic bulge shows a centrally concentrated spatial distribution, similar to OGLE-IV counterparts of metal-poor RRLs from the VVV. Mira stars are also consistent with belonging to a boxy bulge (López-Corredoira, 2017). It should be noted, however, that the spatial distribution of RRLs in the bulge is somehow still debated given that Pietrukowicz et al. (2015) by using OGLE-IV data did confirmed the presence of a bar in their spatial distribution, although the

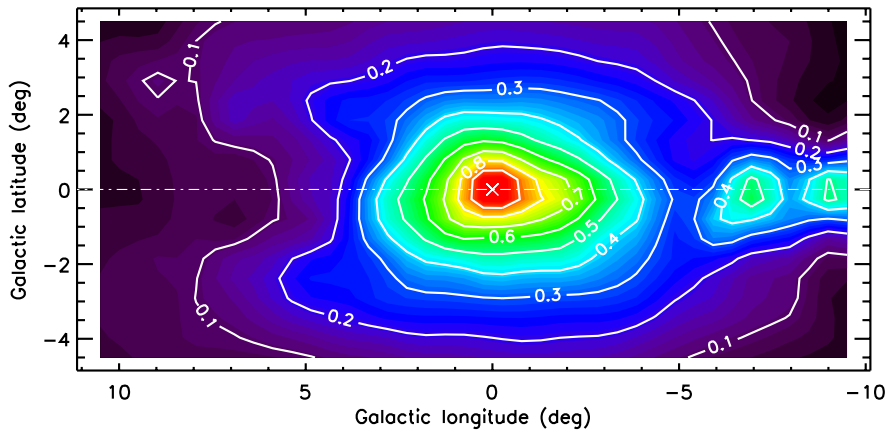


Fig. 7 Density map in the longitude-latitude plane based on VVV RC star counts from Valenti et al. (2016). Star counts are normalized to the maximum (Max). Solid contours are isodensity curves, linearly spaced by $0.1 \times Max \text{deg}^{-2}$. Figure reproduced from Zoccali & Valenti (2016, *The 3D structure of the Galactic bulge*, their Figure 4).

extension, pivot angle and ellipticity of the structure traced by the RRLs are significantly smaller than that traced by RC stars (see §2 above).

3.1.2 The stellar density map

More than two decades ago, Weiland et al. (1994) presented the first low angular resolution map at 1.25, 2.2, 3.5 and 4.9 μm of the whole Milky Way bulge based on the COBE/DIRBE data. After correction for extinction and subtraction of an empirical model for the Galactic disk, the derived surface brightness profile of the bulge was then used to study its global morphology and structure. However, more detailed investigations of the bulge innermost region (i.e. $|b| \leq 5^\circ$, $|l| \leq 10^\circ$) have been possible only recently thanks to the VVV survey. Valenti et al. (2016) presented the first stellar density profile of the bulge (see Figure 7) reaching latitude $b = 0^\circ$. Specifically, by counting RC stars within the CMD as obtained from accurate PSF-fitting photometry of VVV data and previously corrected for extinction by using the reddening map of Gonzalez et al. (2011), they derived a new stellar density map that allowed to investigate the morphology of the innermost regions with unprecedented accuracy. As seen from Figure 7, the vertical extent of the isodensity contours is larger at $l > 0^\circ$. This is an expected consequence of a bar whose closest side points towards positive longitude. The high stellar density peak in the innermost region (i.e. $|l| \leq 1^\circ$ and $|b| \leq 1^\circ$) spatially matches the σ -peak found by GIBS, the kinematics survey of RC (Zoccali et al., 2014) and by Valenti et al. (2018, *in prep*). The stellar density maximum is found in the region $|l| \leq 1^\circ$ and $|b| \leq 0.5^\circ$, and slightly asymmetric with respect to the bulge minor axis.

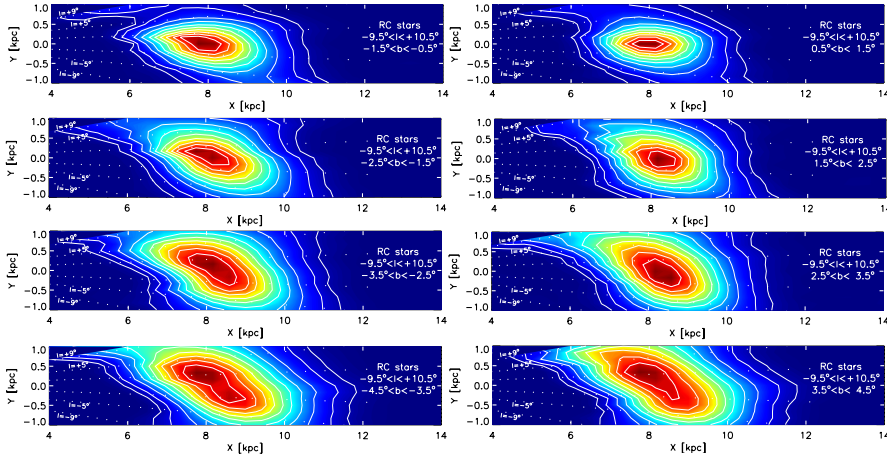


Fig. 8 Deprojection of the RC density shown in Figure 7 at different latitudes.

The observed overall elongation of the density contours towards the negative longitudes is, nevertheless, found to be progressively less pronounced when moving closer to the Galactic plane. Indeed, as shown in Figure 8 the deprojected density maps become more and more spherically concentrated when RC stars at lower latitudes are considered, hence suggesting the presence of a quasi-axisymmetric structure in the innermost region. This evidence supports the claim by Gerhard & Martinez-Valpuesta (2012) that: the variation in the RC slope at $b = \pm 1^\circ$ and $|l| \leq 10^\circ$ observed by Nishiyama et al. (2005, by using OGLE data) and by Gonzalez et al. (2011, based on VVV photometry), and interpreted by these authors as evidence for the presence of a nuclear bar in the inner bulge, is instead caused by a variation of the stellar density distribution along the line of sight.

By using a combination of UKIDSS, VVV, 2MASS and GLIMPSE data, Wegg et al. (2015) presented the so far largest (i.e. $\sim 1900 \text{ deg}^2$) density map of the Milky Way and long bar based on RC stars (see Figure 9). A particularly interesting result of this study is that the orientation angle of the long bar constrained by the best-fit model to the observed density map is consistent with that of the triaxial bulge (i.e. the main bar, $28^\circ - 33^\circ$). In other words, unlike several previous studies suggesting the presence of a long bar tilted by $\sim 45^\circ$ with respect to the Sun-Galactic centre line (i.e. in addition to the main bar; Benjamin et al., 2005; Lopez-Corredoira et al., 2007; Cabrera-Lavers et al., 2007, 2008; Vallenari et al., 2008; Churchwell et al., 2015; Amôres et al., 2013), the long bar with a semimajor axis of $\sim 4.6 \text{ kpc}$ in length as modelled by Wegg et al. (2015) appears to be the natural extension of the bulge main bar at higher longitude. This result nicely fits the scenario proposed by Martinez-Valpuesta & Gerhard (2011) and Romero-Gómez et al. (2011) based on N-body simulations, where long and main bar are parts of the

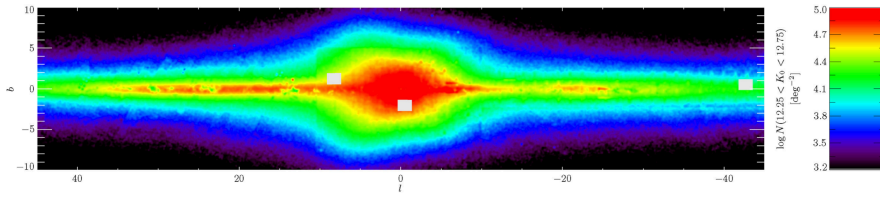


Fig. 9 Surface density map of RC stars based on VVV, UKIDSS and 2MASS K_s -band photometry. Figure reproduced from Wegg et al. (2015, *Structure of the Milky Way’s bar outside the bulge*, their Figure 1).

same structure. According to this, the boxy/peanut shape bulge would then *simply* be the central vertical extension of a longer and flatter single bar.

3.1.3 The mass

One of the fundamental question of Galactic astronomy is the determination of the mass distribution in the Milky Way because in general the mass of a given system is more likely the key element driving its evolution (see Courteau et al., 2014, for a detailed review). In this context, over the past three decades many studies addressed this specific question, deriving the dynamical mass of the Galaxy bulge either by matching the galactic rotation curve inside ~ 1 kpc, or by measuring the kinematics (i.e. velocity and velocity dispersion) of a variety of different tracers (i.e. stellar and gas). Then by using an observed luminosity profile (generally in K-band) one can derive the M/L ratio, which ultimately leads to the mass of the bulge (Sellwood & Sanders, 1988). Historically, the M/L ratio derived from fitting the rotation curve has been often found to be $\sim 2-3$, while the M/L ratio derived from stellar kinematics ~ 1 . Such discrepancy has been often explained using the argument that the mass derived from the rotation curve is overestimated because of the presence of large non-circular motions that distort the rotation curve (Sofue, 1990; Yoshino & Ichikawa, 2008). Indeed, the accuracy on the measurement of the rotation curve strongly depends on the accuracy on the distance to the Galactic centre and the solar circular velocity. In addition, the rotation curves as derived from $H\alpha$ and, in general from other gas tracers (i.e. HI, HII) are often influenced by non-circular components (i.e. inflow, outflow, streaming motions), rather than an ordered (regular) circular motion. This inevitably led to very different results for the mass of the bulge. Chemin et al. (2015) recently reviewed the uncertainties and bias affecting the determination of the Milky Way rotation curves and the consequent effects on the derived mass distribution. Table 2 lists a number of studies, together with the adopted observables/diagnostics, that over the years tackled the problem of deriving the bulge mass. Although the reader should refrain from considering Table 2 a complete compilation, it is evident that the large spread in the listed values make the mass of the bulge still poorly constrained. Most estimates cluster to $1.5 \times 10^{10} M_{\odot}$, however a few authors

Table 2 Estimates of the bulge mass over the last three decades.

Mass ($\times 10^{10} M_{\odot}$)	Diagnostics	Reference
3.0	Rotation curve & $M/L \sim 3$	Sellwood & Sanders (1988)
1.2	2.4 micron map IRT Spacelab 2 mission	Kent (1992)
2.0	Stellar kinematics & COBE brightness profile	Zhao et al. (1994)
1.3	COBE brightness profile	Dwek et al. (1995)
1.6	microlensing depth & COBE brightness profile	Han & Gould (1995)
2.8	Stellar kinematics & COBE brightness profile	Blum (1995)
2.4	Star counts DENIS near-IR (Besançon model)	Picaud & Robin (2004)
1.8	Gas rotation curve	Sofue (2009)
0.6	star counts, kinematics and metallicity (Besançon model)	Robin et al. (2012)
0.8	Unified rotation curve, CS & CO	Sofue (2013)
1.8	OGLE RC star counts	Cao et al. (2013)
1.8	M2M dynamical model & VVV RC density	Portail et al. (2015)
2.0	VVV RC star counts & observed IMF	Valenti et al. (2016)

found values as large as $3 \times 10^{10} M_{\odot}$ (Sellwood & Sanders, 1988) or as small as $0.6 \times 10^{10} M_{\odot}$ (Robin et al., 2012).

In this context, a special mention is deserved for the two most recent works by Portail et al. (2015) and Valenti et al. (2016) which, although following different methodologies, they both use the distribution of the RC stars as derived by the VVV photometry. Portail et al. (2015) used made-to-measure dynamical model of the bulge, with different dark matter halo to match the stellar kinematics from BRAVA (Rich et al., 2007; Kunder et al., 2012) and the 3D surface brightness profile derived by Wegg & Gerhard (2013). Their best-fit model is consistent with the bulge having a dynamical mass of $1.8 \pm 0.07 \times 10^{10} M_{\odot}$, with a dark matter content that varies with the adopted IMF. When the observed IMF of Zoccali et al. (2000) is considered about $0.7 \times 10^{10} M_{\odot}$ (i.e. 40%) of dark matter is required in the bulge region. In addition, they estimated that the total stellar mass involved in the peanut shape accounts for $\sim 20\%$ of the total stellar bulge mass.

On the other hands, by scaling the observed VVV RC stellar density map (see Figure 7) with the observed bulge luminosity function from Zoccali et al. (2000), and Zoccali et al. (2003), Valenti et al. (2016) provided the first empirical, hence no model-dependent, estimate of the bulge stellar mass. From the observed stellar mass profile shown in Figure 10, the authors estimated that the mass in stars and remnants of the Milky Way bulge in the region $|b| < 9.5^{\circ}$ and $|l| < 10^{\circ}$ is $2.0 \pm 0.3 \times 10^{10} M_{\odot}$.

These two latest estimates are found compatible within the quoted errors, and they might be even more close when considering that the empirical estimate by Valenti et al. (2016) refers to a larger volume that is not limited along the line of sight.

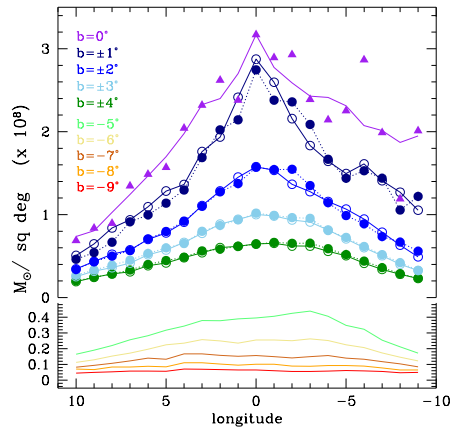


Fig. 10 Stellar mass profile across latitude in each VVV field for fixed longitudes. Filled symbols with dotted lines refer to $b < 0$, empty symbols with solid lines to $b > 0$ fields. The lower part of the plot has an expanded y-axis for a better display of the high negative longitudes, owing to the higher extinction, hence higher incompleteness in those fields. Figure reproduced from Valenti et al. (2016, *Stellar density profile and mass of the Milky Way bulge from VVV data*, their Figure 5.).

3.2 The chemical composition

Because the chemical content of any given stellar system retains crucial information to unveil its origin, formation and evolution (McWilliam, 2016), after the pioneering works of Frogel et al. (1984) and Rich (1988) several studies over the decades focussed on the determination of the bulge stars metallicity and abundances distribution to understand how the bulge formed. What follows is not meant to be a comprehensive compilation of all such studies for which one should dedicated a entire single review, but rather a summary of our current knowledge of the chemical composition of the bulge based on the latest results from RC and RRLs.

3.2.1 The metallicity distribution

As emphasized by Matteucci et al. (1999); Ferreras et al. (2003), the peak and shape of the metallicity distribution functions (MDF) provide important constraints on the IMF, star formation efficiency, as well as to the possible gas infall timescale. However, until less than a decade ago, accurate MDF based on high-resolution spectroscopy were available only for a handful number of sparse fields mainly located along the bulge minor axis (see i.e. McWilliam & Rich, 1994; Fulbright et al., 2007; Rich et al., 2007; Johnson et al., 2011; Gonzalez et al., 2011; Hill et al., 2011; Rich et al., 2012, , and reference therein). The derived MDFs were consistent across various studies, which all agreed in finding the bulge population to be on average metal-rich, although spanning a fairly broad metallicity range (e.g. $-1.5 \lesssim [\text{Fe}/\text{H}] \lesssim +0.5$). Our comprehension of the

Table 3 For each spectroscopic survey, the total number of stars, the total number of targeted fields and the region within the bulge covered by the observations are given.

Survey	Total RC stars	Number of fields	Bulge region
ARGOS	14,000	27	$-10^\circ < b < -5^\circ, l \lesssim +30^\circ$
GIBS	5,500	26	$-8^\circ < b < -1^\circ, b = +4, l \lesssim +30^\circ$
Gaia-ESO	1,200	5	$-10^\circ < b < -4^\circ, -10^\circ < l < 7^\circ$

MDF of the bulge has improved tremendously thanks to three spectroscopic surveys, namely ARGOS (Freeman et al., 2013), GIBS (Zoccali et al., 2014), and ESO-Gaia (Rojas-Arriagada et al., 2014), that all together have provided spectra for more than 20,000 RC stars across most of the inner and outer bulge regions (see Table 3 for further details). The MDF derived by these surveys confirmed previous results although extending them on a much larger area. The mean bulge population across all fields is metal-rich with a small fraction of stars with $[\text{Fe}/\text{H}] > +0.5$ dex and $[\text{Fe}/\text{H}] < -1.5$ dex. Only in the outermost fields ($b > -7^\circ, |l| > 10^\circ$) observed by ARGOS the MDF reaches metallicity as low as ~ -2.5 dex. In addition, a mild vertical gradient is found when considering the mean metallicity of each field, such as the metallicity increases moving inwards along the bulge minor axis, hence confirming what suggested previously by Minniti (1995), and Zoccali et al. (2008). However, thanks to statistically robust target samples a detailed study of the MDF shape has been possible for the first time, revealing the presence of multiple components. The observed overall metallicity gradient is therefore explained as a consequence of the presence of two (see Zoccali et al., 2017; Rojas-Arriagada et al., 2014) or more (see Ness et al., 2013b) components with different mean metallicity. As evident from Figure 11, the variations of the relative contribution of these components across the fields (i.e. metal-rich stars component becoming progressively less prominent towards the outer region) mimic the observed gradient. However, Zoccali et al. (2017) found also that at latitudes smaller than $|b| = 3^\circ$ the metal-poor component becomes important again (see first 2 top panels of Figure 11), its relative fraction increases again close to the plane. To further investigate the spatial distribution of the two components they mapped their distribution by coupling the relative fractions derived by GIBS with the bulge stellar density from Valenti et al. (2016). The result, shown in Figure 12, demonstrates that the metal-poor component has a spheroid-like spatial distribution, versus a boxy distribution of the metal-rich component. In addition, the metal-poor component shows a steeper radial density gradient.

Although as mentioned before the bulge kinematics is the subject of another paper in this volume (see §1 above by A. Kunder), here I will only briefly mention that the two components were found to have also different kinematics. Indeed, as already found by the BRAVA (Kunder et al., 2012) and ARGOS survey (Ness et al., 2013a), in the outer bulge ($|b| > 4^\circ$) the metal-poor component has a higher radial velocity dispersion compared to the metal-rich one, at all longitudes. However, Zoccali et al. (2017) showed that such behavior is re-

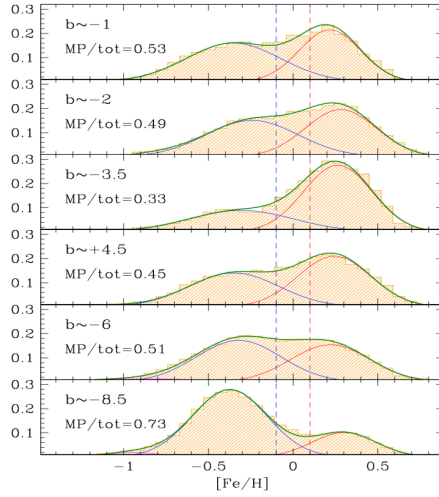


Fig. 11 MDF of RC stars at constant latitudes. The fraction of metal-poor stars, compared to the total, is given in each panel. Vertical dashed lines mark the limits of the metal-poor and metal-rich populations. Figure adapted from Zoccali et al. (2017, *GIBS-III: MDFs and kinematics for 26 fields*, their Figure 7).

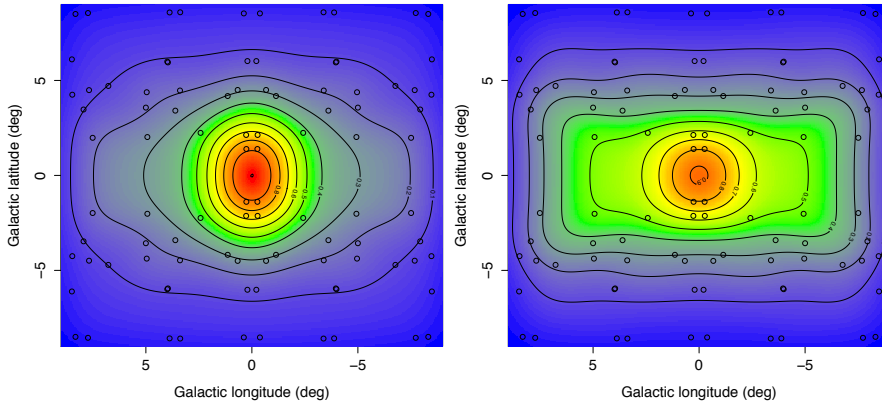


Fig. 12 Density map of metal-poor (left) and metal-rich (right) RC stars obtained using the MDF of GIBS fields and the total number of RC stars from Valenti et al. (2016). Figure adapted from Zoccali et al. (2017, *GIBS-III: MDFs and kinematics for 26 fields*, their Figure 9).

versed in the inner bulge. Specifically, the velocity dispersion of the metal-poor stars at $b = -3.5^\circ, -2^\circ$ becomes similar to that of the metal-rich counterpart, and progressively becomes smaller at $b = -1^\circ$.

While the chemical abundances of the RC stars in the bulge is one of the topics that received more attention in the recent years, the number of studies addressing the chemical content of the oldest bulge population, such the RRLs,

is still very limited. Perhaps mostly due to the observational challenges that spectroscopic observations of RRL face, as of today there is no high-medium resolution spectroscopic measurements of a sizeable sample of RRLs in the bulge. In K-band RRLs are in general about 0.5 mag fainter than RC stars, hence their brightness makes them suitable targets at high resolution only with 4 m-class telescope or above, depending on the bulge region. In addition, because they are much less numerous than RC stars, and so more sparsely distributed RRLs are not even suitable targets for the vast majority of the current multiplexing spectrograph facilities. An additional complication is the fact that the metallicity derived from the line equivalent width measurements strongly depends upon the pulsation phase at which the star was observed. This necessarily implies a good knowledge of the variables. All of these factors make their observations very telescope time consuming.

As of today the only spectroscopic study of a sizeable sample of bulge RRLs has been presented by Walker & Terndrup (1991), who derived the MDF of 59 RRLs in the Baade’s window. The individual star metallicities were derived through the ΔS method (i.e. low-resolution, see Suntzeff et al., 1991, for a detailed description of the ΔS method) and their distribution is found to cluster around $[\text{Fe}/\text{H}] = -1$ dex. Although the MDF is relatively broad, spanning a range of about 1 dex, $-1.7 \lesssim [\text{Fe}/\text{H}] \lesssim -0.5$, its very sharp peak accounts for $\approx 80\%$ of the entire sample. Based on the derived MDF, the authors concluded that the RRL are being produced by the metal-poor tail of K giants distribution (see also Figure 11).

Recently, Pietrukowicz et al. (2015) provided a photometric MDF based on more than 27,000 RRLs from the OGLE-IV catalogs and located in the bulge region between $|l| \lesssim 10^\circ$ and $-8^\circ \lesssim b \lesssim -2^\circ$, $+2^\circ \lesssim b \lesssim +5^\circ$. The photometric MDF is much broader than the spectroscopic one, as it spans mostly the range $-2.5 \lesssim [\text{Fe}/\text{H}] \lesssim +0.5$, although the peak is found at the same metallicity, $[\text{Fe}/\text{H}] = -1$ dex. The authors showed that there is no correlation between the distance and the shape of the MDF, however they find a very mild, but statistically significant, radial metallicity gradient (i.e. the metal-rich population increases towards the centre). Based on the analysis of the Bailey diagram (i.e. period-amplitude diagram) the authors argue for the existence of two different population of RRLs with likely different metallicity, similar to the bulge RC counterparts. However, it should be mentioned that unlike what is observed in the MDF of RC stars, these 2 populations of RRLs with different metallicity do not probably change in relative fraction given that the global MDF conserves its shape throughout the total covered bulge area. Moreover, because of the lack of RRLs spectroscopic measurements in the metal-rich regime, $[\text{Fe}/\text{H}] > -0.5$ dex (see Walker & Terndrup, 1991), one should refrain from drawing any firm conclusion from the available RRL MDF.

3.2.2 The α -elements abundances

The detailed study of the chemical abundances and abundance patterns in bulge stars provides a unique tool to understand the chemical evolution en-

richment of the bulge, and therefore to set tight constraints on its formation scenario. The elemental abundance distributions, and the abundance ratio of certain critical elements such as Fe-peak, CNO, and α -elements (i.e. those synthesized from α particles as O, Ne, Mg, Si, Ti, Ca and S) are particularly suitable for this purpose. Indeed, these elements are synthesized in stars of different masses, hence released into the interstellar medium on different timescales.

Because most of the chemical information on RC stars comes from the analysis of the α -elements, what follows is a summary of the picture built upon those measurements. It is not meant to be a comprehensive review of the global chemical composition of the bulge, for which the readers are instead encouraged to refer to McWilliam (2016).

As mentioned above a particularly useful abundance ratio is $[\alpha/\text{Fe}]$. Due to the time delay in the bulk of Fe and iron-peak elements production (mostly due to SNe Ia, see Nomoto et al., 1984) relative to α -elements (due to SNe II, see Woosley & Weaver, 1995), the $[\alpha/\text{Fe}]$ abundance ratio can be efficiently used as a *cosmic clock* (see e.g. McWilliam, 1997; Wyse, 2000, and references therein). For this reason many studies in the past addressed this question providing $[\alpha/\text{Fe}]$ ratios for relatively small sample of K and M giants in few bulge regions (see McWilliam & Rich, 1994; Rich et al., 2005; Cunha & Smith, 2006; Fulbright et al., 2007; Lecureur et al., 2007; Rich et al., 2007; Meléndez et al., 2008; Alves-Brito et al., 2010; Johnson et al., 2011; Gonzalez et al., 2011; Hill et al., 2011; Rich et al., 2012; Bensby et al., 2013; Johnson et al., 2014; Bensby et al., 2017, and references therein). As it has been the case for the MDF, the advent of the recent spectroscopic surveys ARGOS (Ness et al., 2013b) and GIBS (Gonzalez et al., 2015) provided α -element abundances for thousands of RC stars over a large area, hence allowing to study the $[\alpha/\text{Fe}]$ trends as a function of the position in the bulge.

All previous and very recent studies agree on finding the bulge to be α -elements enhanced with respect to the solar value, thus suggesting a fast bulge formation scenario. As shown in Figure 13, the α -element abundances of bulge stars with $[\text{Fe}/\text{H}] < -0.3$ are enhanced over iron by ~ 0.3 dex, whereas metal-rich stars show a decrease in $[\alpha/\text{Fe}]$ reaching 0 for metallicity above the solar values. However, as discussed in Gonzalez et al. (2011) the direct translation of this trend to absolute timescales is not easy because the SNe Ia delay time can depend on different production channels. This is the reason why a relative approach through the comparison of $[\alpha/\text{Fe}]$ trends observed in different Galactic components turns to be more reliable. From the comparison between bulge RC and giants in the thin and thick disk (see Figure 13, right panels), the α -elements enhancement of the bulge with respect to the thin disk is evident across most of the entire metallicity regime. At solar metallicity, the bulge and thin disk are both α -poor. On the other hands, the thick disk giants are found to be as α -enhanced as the bulge, although they never reach the high metallicity tail of bulge stars. A possible interpretation of this relative trends is that the metal-poor bulge population experienced a fast formation scenario similar to the thick disk, whereas the metal-rich bulge population underwent

a more extended (i.e. longer) star formation, on a timescale similar to that of the thin disk.

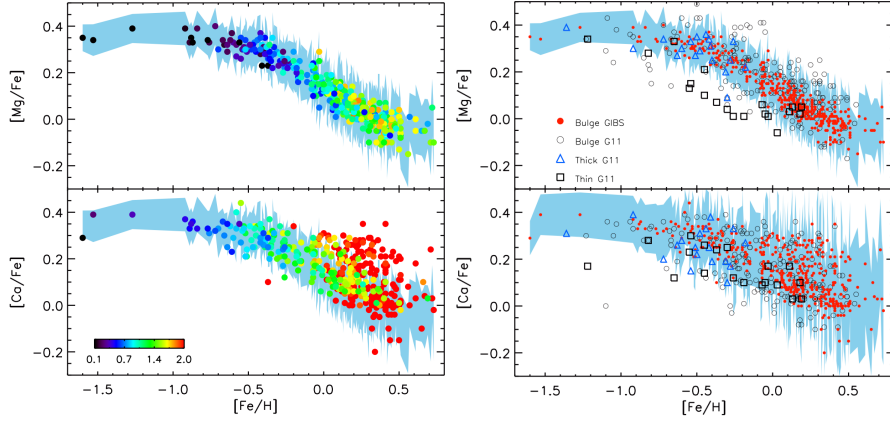


Fig. 13 Left: Distribution of $[\text{Mg}/\text{Fe}]$ (*upper panel*) and $[\text{Ca}/\text{Fe}]$ (*lower panel*) as a function of $[\text{Fe}/\text{H}]$. The abundances of $[\text{Mg}/\text{Fe}]$ and $[\text{Ca}/\text{Fe}]$ are color-coded according to their estimated uncertainty. The uncertainty contour of $[\text{Mg}/\text{Fe}]$ is also shown in the background of both panels. – Right: Distribution of $[\text{Mg}/\text{Fe}]$ (*upper panel*) and $[\text{Ca}/\text{Fe}]$ (*lower panel*) as a function of $[\text{Fe}/\text{H}]$ used as diagnostic of the formation timescale of the bulge. Red circles refers to GIBS abundances, whereas black symbols mark the abundances from Gonzalez et al. (2011). Figure adapted from Gonzalez et al. (2015, *The GIRAFFE Inner Bulge Survey (GIBS). II. Metallicity distributions and alpha element abundances at fixed Galactic latitude*, their Figures 8 and 9).

3.3 The age

An accurate dating of the bulge stellar component allows one to gauge at which lookback (i.e., at which redshift) one should look for possible analogs of the Milky Way, when their bulge formation processes were about to start, well on their way, or even already concluded. Indeed, with an age of ~ 10 Gyr or older, it is at $z \gtrsim 2$ that such analogs can be searched, or at lower redshift if significant fraction of the stellar component is found to be several Gyr younger (see Valenti et al., 2013, for detailed discussion).

However, dating bulge stars is a very complicated task, challenged by the stellar crowding, the patchy and highly variable extinction, the uncertainties in the distance modulus, the distance spread due to the spatial depth of the bulge/bar along the line of sight, the metallicity dispersion and finally the contamination by foreground disk stars. The different contribution of all these factors prevents accurate location in terms of magnitude and color of the main sequence turnoff (MSTO) of the bulge population, so far among the most reliable age diagnostics (see Renzini & Fusi Pecci, 1988, and §5 by G. Bono).

Historically, the earliest age constraint by van den Bergh & Herbst (1974) in the Plaut field along the bulge minor axis at $b = -8^\circ$ (~ 1 kpc) indicated a globular cluster (GC) like age. Terndrup (1988) fit the photometry of other bulge fields at a range of latitudes with GC isochrones of varying metallicity, but because lacking a secure distance for the bulge he derived only a weak age constraint (11-14 Gyr). Ortolani et al (1995) solved the problem of contamination and distance uncertainties by comparing the bulge population with the NGC 6528 and NGC 6553 clusters. Forcing the bulge field and cluster luminosity function to match the HB clump luminosity level, it was possible to show for the first time that the relative ages of the bulge and metal-rich cluster population could not differ by more than 5%. Feltzing & Gilmore (2000) used HST-based photometry of Baade’s window and another low extinction field known as the Sgr-I (i.e. at $l = 1.25^\circ$ and $b = 2.65^\circ$) to argue that while the density of the bulge MSTO stars increases for field closer to the centre, the foreground population does not change. They concluded that the bulk of the bulge population must therefore be old. The case for an *old bulge* has been further strengthened by later and more accurate photometric studies of different bulge fields, and by tackling the problem of contamination by foreground disk stars either kinematically by using proper motions, or statistically by considering control disk fields. Table 4 lists the location of the each observed field together with the adopted decontamination approach.

Table 4 Position of the bulge fields for which an age estimate of the stellar population has been provided through MSTO determination.

longitude	latitude	Disk decontamination	Reference
+1.13°	-3.77°	proper motions	Kuijken & Rich (1982)
+1.25°	-2.65°	proper motions	Kuijken & Rich (1982)
0°	-6°	statistical	Zoccali et al. (2003)
+1.25°	-2.65°	proper motions	Clarkson et al. (2008, 2011)
+0.25°	-2.15°	proper motions	Brown et al. (2010)
+1.26°	-2.65°	proper motions	Brown et al. (2010)
+1.06°	-3.85°	proper motions	Brown et al. (2010)
-6.75°	-3.81°	proper motions	Brown et al. (2010)
+10.3°	-4.2°	statistical	Valenti et al. (2013)
-6.8°	-4.7°	statistical	Valenti et al. (2013)

As all previous studies, Valenti et al. (2013) found that the bulk stellar population of the Milky Way bar edges is over ~ 10 Gyr old (see Figure 14), with no obvious evidence of younger population. This age is indistinguishable from the one reported for more inner bulge fields, a few degrees from the Galactic centre or lying along the bulge minor axis. From the analysis of the MSTO in the HST-based CMD kinematically decontaminated, Clarkson et al. (2011) concluded that once the blue stragglers population is taken into account a significantly younger ($\lesssim 5$ Gyr) population in the bulge must be at most 3.4%.

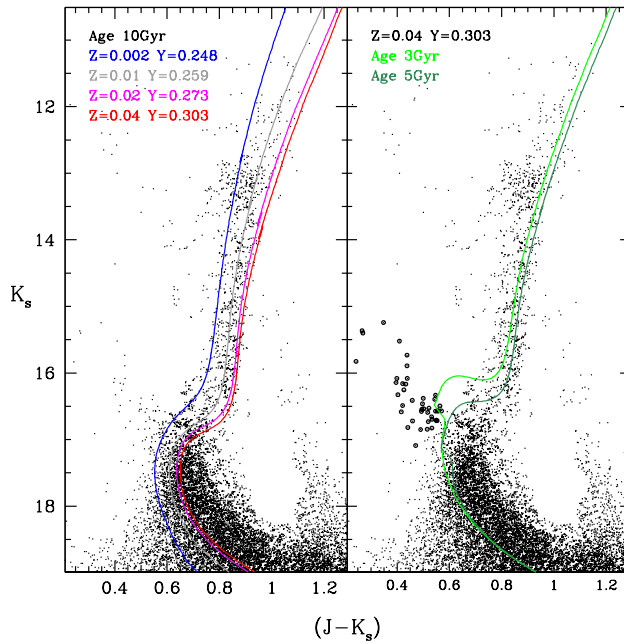


Fig. 14 Disk-decontaminated CMD of the field located at the far edge of the bar with over-plotted theoretical isochrones (Valcarce et al., 2012). Isochrones ages, metallicity and helium abundances are indicated near the top-left corner of each panel. Sub-solar isochrones are α -enhanced, and solar-scaled otherwise. The metallicity range covered by the bulk of the star in this field is $0.002 \lesssim Z \lesssim 0.060$, as derived from the observed photometric metallicity distribution. Open circles mark stars that are most likely blue stragglers. Figure adapted from Valenti et al. (2013, *Stellar ages through the corner of the boxy bulge*, their Figure 10).

However, there is a clear discrepancy between the ages inferred from the determination of the MSTO location in the observed CMDs and those derived by the microlensed project of Bensby and collaborators, which estimates single star age from its effective temperature and gravity (i.e. from isochrones in the $T_{\text{eff}}, \log g$ plane) as obtained from high resolution spectra. Indeed, based on a sample of 90 F and G dwarf, turnoff and subgiant stars in the bulge (i.e. $|l| \lesssim 6^\circ$ and $-6^\circ < b < 1^\circ$) observed during microlensing, Bensby et al. (2017) found that about 35% of the metal-rich star ($[\text{Fe}/\text{H}] > 0$) are younger than 8 Gyr, whereas the vast majority of metal-poor ($[\text{Fe}/\text{H}] \lesssim -0.5$) are 10 Gyr or older. In addition, from the derived age-metallicity and age- α elements distribution the authors concluded that the bulge must have experienced several significant star formation episodes, about 3, 6, 8 and 12 Gyr ago.

As discussed by Valenti et al. (2013), each of the two approaches has its own *pros* and *cons*. The microlensing approach depends more heavily on model atmospheres that may introduce systematics especially in the metal rich regime, and it deals with small number statistics. At the same time, it has the advantage that the metallicity of each individual stars is very well constrained.

Conversely, by dealing with a statistically significant number of stars, the traditional CMD method should in principle be able to reveal the presence of young populations. However, in this case the metallicity of individual stars are unknown, therefore one does not know if, for instance, some of the stars above the MSTO of the $Z = 0.060$ isochrones (see Figure 14) are old and have lower metallicity, or whether they are metal-rich stars younger than 10 Gyr.

The effect of the age metallicity degeneracy, specifically in terms of the color spread of the MSTO in the observed CMDs has been used by Haywood et al. (2016) to argue in favor of the scenario suggested by the microlensing results. In particular, Haywood et al. (2016) compared the MSTO color spread observed in the CMD of Clarkson et al. (2011) with that of synthetic CMDs, obtained by using two scenarios corresponding to different age-metallicity relation (AMR). In *scenario I* a simulated CMD was obtained by using the AMR presented by Bensby et al. (2013) (i.e. based on a total sample of 59 microlensed dwarf), whereas for *scenario II* an AMR that extends from $[\text{Fe}/\text{H}] = -1.35$ dex at 13.5 Gyr to $[\text{Fe}/\text{H}] = +0.5$ dex at 10 Gyr was adopted. When taking into account distance, reddening and metallicity effects, Haywood et al. (2016) showed that the MSTO color spread of a *purely* old stellar population would be wider than what observed, which in turn appears to be consistent with the simulation obtained from the *scenario I*. Unfortunately, what the Haywood et al. (2016) paper does not address is the fact that the simulation using the AMR of Bensby et al. (2013) produced a CMD that not only has a smaller MSTO color spread like the observed one but also show a remarkable number of stars just above (i.e. brighter) the MSTO, which are not matched by the observations (see their Figure 8). In this respect, the comparison between observations and simulations presented by Zoccali et al. (2003) to infer the age of the bulge population would seem more appropriate because the synthetic CMD was obtained by using the observed luminosity function, and therefore the comparison was done such as to match not only the location and spread in color of the MSTO, but also the number of stars at the MSTO level.

3.4 Summary and conclusions

Owing to the systematic and detailed study of RC star properties performed in the last decade by using wide area photometric surveys we have finally reached a good and complete comprehension of the 3D structure of the Milky Way bulge. The bulge, as referred as the region in the inner ~ 3 kpc is a bar with an orientation with respect to the Sun-Galactic centre line of sight of $\sim 27^\circ$, and whose near side points in the first Galactic quadrant. The bar has a boxy/peanut/X-shape structure in its outer regions, a characteristic morphology of bulges formed out the natural evolution of disk galaxies as the consequence of disk dynamical instabilities and vertical buckling of the bar. The observed split in the RC mean magnitude distribution in the outer regions is interpreted by the dynamical models as bar growing. In the innermost region ($|l, b| < 2^\circ$), rather than a nuclear bar, there seems to be an axisymmetric

high stellar density peak, which instead may be responsible for the observed change in the bar pivot angle. In addition, RC stars trace a thinner and longer structure with a semimajor axis of ~ 4.6 kpc, known as the long bar, which according to the latest study appears to be the natural extension of the bulge main bar at higher longitude.

The bulge is the most massive stellar component of the galaxy, with a mass ($M_B = 2 - 1.8 \times 10^{10} M_\odot$) close to 1/5 of the total stellar mass of the Milky Way, and about ten times larger than the mass of the halo.

The recent spectroscopic surveys (ARGOS, GIBS, Gaia-ESO) of RC stars, together with the ongoing that targets K and M giants (i.e. APOGEE-North) provided a comprehensive and detailed view of the chemical content of the stellar population over an area that corresponds to more than 80% of the entire bulge. The emerging picture is that the bulge MDF as traced by the RC is much more complex than previously thought, and it hosts two populations with different mean metallicity (i.e. metal-poor and metal-rich), spatial distribution and kinematics. The metal-poor population as traced by RC, RRLs and T2C is more spherically concentrated, whereas the RC metal-rich component traces the boxy/peanut bar. The observed properties of such metal-poor population possibly older (i.e. spatial distribution and kinematics) do not necessarily imply the presence of a *classical bulge* (i.e. a merger-driven structure dominated by gravitational collapse) embedded in the boxy bulge. Indeed, the recent N-body simulations model of Debattista et al. (2017) accounts for the presence of a metal-poor population spherically concentrated, as well as for other observed trends of densities, kinematics and chemistries, without invoking the need for a *composite bulge* scenario (i.e. the coexistence of two structures, one merger-driven and one boxy shaped formed out of disk and bar evolution). According to Debattista et al. (2017), the observed properties of the Milky Way bulge stellar populations are consistent with a bulge formed from a *continuum* of disk stellar populations kinematically separated by the bar.

Based on accurate abundances analysis of RC stars, the bulge show α -element enhancement typical of fast formation process. In particular, a possible interpretation of the observed relative trends of α -elements in the bulge, thin and thick disk is that the metal-poor bulge population experienced a fast formation scenario similar to the thick disk, whereas the metal-rich bulge population underwent a more extended (i.e. longer) star formation, on a timescale similar to that of the thin disk.

The innermost and still poorly unexplored regions (i.e. $|b| \lesssim 1^\circ$) will be soon probed by new IR surveys planned for the near future (i.e. APOGEE-South, Multi-Object Optical and Near-infrared Spectrograph at VLT – MOONS) hence allowing us, for the first time, to complete the puzzle with a clear understanding of the chemical properties of the bulge as a whole with unprecedented accuracy.

There is no doubt that the central regions of the Milky Way hosts an old stellar population. The strongest evidence being the presence of a prominent population of RRLs and T2C found by OGLE and VVV (Dékány et al., 2013; Pietrukowicz et al., 2015; Gran et al., 2016, and Bhardwaj et al), which are

by far the largest photometric campaigns of variable stars. Furthermore, an old age is also guaranteed by the existence of a bulge GCs system (see e.g. Valenti et al., 2010; Bica et al., 2016, and reference therein). However, what still remains to be firmly assessed is the contribution of intermediate-young (i.e. $\lesssim 5$ Gyr) stars to the global bulge stellar population. The AMR proposed by Bensby et al. (2017) should be either confirm on much statistically robust sample, or by using a methodology for the reconstruction of the star formation history more sophisticated than the approaches adopted so far. In particular, the comparison between observations and simulations should be performed by using as many as possible features of the CMDs (i.e. Gallart et al., 2005).

In the coming years, the exquisite astrometry provided by the next Gaia data releases will most probably allow us to further refine the global picture of the bulge structure. Even though a large fraction of the bulge RC population is out of GAIA reach because of the crowding and high extinction, the information derived from RC stars in the low reddening regions can be used to obtain a very accurate distances map of the bulge outer regions. This can be used then as the *reference frame* upon which, through a differential analysis with the most obscured regions, we can build the entire bulge distances and structure maps.

Finally, further efforts should be put to characterize the chemical content of the RRLs and T2C, which among all tracers are those representing *univocally* and *purely* the oldest stars in the Bulge. Indeed, accurate MDF and elemental abundances from high- or medium-resolution spectroscopy for these type of stars are still missing, or largely insufficient. The future LSST project will provide the position, magnitude and colors for thousands of variable stars, spanning a variety of ages. The spectroscopic follow up of a sizeable sample of variables would literally open new frontiers of our knowledge by allowing for the first time an accurate study of the metallicity trends as a function of the stellar ages. If such analysis would be extended also outside the bulge regions we could be in position to understand the interaction among different Galaxy structures, such for instance a clear view of the transition between disk and bulge.

4 RR Lyrae variables in the Ultra-Faint satellites of the Milky Way

In the Λ -Cold Dark Matter (Λ -CDM) scenario, large galaxies are the result of the assembling of smaller fragments, cold-dark matter dominated (e.g. Diemand et al., 2007; Lunnan et al., 2012). The baryonic component of these fragments may eventually collapse, forming small galaxies. This idea is appealing when applied to the MW, since it echoes the early scenario envisioned by Searle & Zinn (1978), in which the outer halo of the MW may have formed by a continuous infall of protogalactic fragments onto the Galaxy, for some time after that the collapse of its central part was completed. Indeed, first attempts to link the Λ -CDM cosmology with the Galactic environment foresaw the assembling of the Galactic halo starting from a number of satellites, and

producing a number of fragments and streams, which are actually observed (e.g. McConnachie, 2012; Grillmair & Carlin, 2016). For decades, the survivors of such a process have been identified with the dwarf spheroidal (dSph) satellites of the MW, since they are old, metal-poor, gas poor and dark matter-dominated systems. However, it was soon realized that the observed number of observed dSph was one or two order of magnitude smaller than that expected from theory. This mismatch, dubbed the ”missing satellites problem” (Klypin et al., 1999; Moore et al., 1999), has been for several years a major problem in the comparison between theory and observations. A second problem, pointed out in the last few years, is that the circular velocities of the known dSph are too low, when compared to the expected values from their simulated substructures. In other words, the predicted densities of the massive subhaloes are too high, to host any of the bright dSphs. This mismatch, called the ”too big to fail problem” (Boylan-Kolchin et al., 2012), has heavy implications, since it means either: i) massive dark subhaloes exist as predicted, but they host faint ($L < 10^5 L_{\odot}$) satellites; ii) massive dark subhaloes does not exist as predicted, for instance they may be less concentrated than predicted.

As a matter of fact, in the last ten years a considerable number of new and faint MW satellites has been discovered (e.g. Belokurov et al., 2007; McConnachie, 2012), most of them on the basis of the SDSS data and, more recently, thanks to the ongoing large surveys conducted with OMEGACAM@VST, DECAM@CTIO and Pan-STARRS (e.g. Koposov et al., 2015; Laevens et al., 2015). These systems, called the ultra-faint dwarfs (UFDs), have integrated luminosities similar or even lower than those of the Galactic globular clusters, and are apparently dark matter dominated (see McConnachie, 2012).

The large number of systems currently available (dSphs + UFDs), allowed to trace a statistically significant analysis of their spatial distribution, leading to the discovery that they actually populate a relatively thin ring, perpendicular to the MW plane, and possibly rotationally supported (Pawlowski & Kroupa, 2013). Moreover, several of the recently discovered candidate MW satellites also seem to be clustered around the Magellanic Clouds, hinting that they may have fallen in as a group (e.g. Sales et al., 2015), in line with the theoretical predictions (Wetzell et al., 2016). Similar aligned structures, showing a kinematic coherence, have been discovered around the Andromeda galaxy (Ibata et al., 2013) and, outside the Local Group, around NGC 5557 (Duc et al., 2014). Similar structures, but without a clear kinematic coherence, have been reported in the literature around NGC 1097, NGC 4216, NGC 4631 (Pawlowski & Kroupa, 2014, , and references therein), and possibly around the M81 and Cen A groups (Müller et al., 2016; Müller et al., 2018). The MW structure, dubbed the *Vast POLar Structure* (VPOS), opens a wide scenario of cosmological problems, since at the present time it is not clear if it is made of primordial (dark matter-dominated) systems, or tidal (dark matter-free) galaxies.

Interestingly, when the halo Galactic globular clusters are grouped in young halo (YH) and old halo (OH) on the basis of the variation of their HB morphology at constant $[\text{Fe}/\text{H}]$, which is a rough approximation of the cluster age,

they show up also a division by kinematics and spatial distribution (e.g. Zinn, 1993; Mackey & Gilmore, 2004; Lee et al., 2007). In particular, YH clusters span a wide range in ages (~ 5 Gyr Dotter et al., 2011) and are characterized by a hotter kinematics than the OH clusters. These occurrences suggest that YH clusters may be debris from accretion events. Finally, the discovery that YH clusters are part of the VPOS (Pawlowski & Kroupa, 2013; Zinn et al., 2014), strengthens the debris hypothesis. Moreover, it also suggests that a fraction of the accreted halo may have been originated in a number of moderately massive satellites that formed GCs, similar to Sagittarius, Fornax, or even the Magellanic Clouds (but see Fiorentino et al., 2016, for new insights on the contribution of Fornax-like systems).

4.0.1 The role of the RR Lyrae stars

A fraction of the problem can be settled by carefully comparing the photometric and spectroscopic properties of the stellar populations of the halo of the MW and of its companions. Moreover, since their pulsational properties such as periods and amplitudes are a function of their structural and evolutive parameters, a detailed comparison of the pulsational properties of the RR Lyrae stars can add valuable information.

In particular, the *ensemble* pulsational properties of the RR Lyrae stars can give important hints. Indeed, it is well known that cluster and field Galactic RR Lyrae stars are affected by the so-called Oosterhoff (Oo) dichotomy, where in the Oo I group the fundamental mode variables show mean periods of $\langle P_{ab} \rangle \sim 0.55$ days, while in the Oo II group they have $\langle P_{ab} \rangle \sim 0.65$ days. In fact, the bright MW companions have $\langle P_{ab} \rangle \sim 0.6$ days and are generally classified as Oo-intermediate, which is difficult to reconcile with the dichotomy of the Galactic halo. On the other side, the RRLs hosted in the UFDs suggest an Oo II classification (Dall’Ora et al., 2012), consistent with an older population of the Galactic halo, possibly produced by an early dissipative collapse or merging (e.g. Miceli et al., 2008).

4.0.2 The ultra-faint dwarfs

UFD galaxies are, at first glance, the low brightness tail of the dSph. From this point of view, there is no structural difference between the "classical" dSphs and the low luminosity UFDs. However, a careful comparison of the central surface brightness as a function of the total luminosity, shows a "knee" around $M_V \approx -8$ mag (see McConnachie, 2012, Figure 7). The galaxies brighter than $M_V \approx -8$ mag follow a linear trend, with the brightest galaxies having a higher central brightness, while galaxies weaker than this limit follow a horizontal distribution, with a constant central brightness no matter what is the total luminosity. In this work, we will therefore consider UFDs all the galaxies that follow such a horizontal distribution.

Stated in a different way, UFDs are characterized by low luminosities and projected densities. This means that it is difficult to recognize them as stellar



Fig. 15 Observed number of RRL stars as a function of the absolute magnitude. Overplotted are three specific frequencies (see text for details). The brightest galaxies have lower specific frequencies, possibly for incompleteness. UFDs are characterized by specific frequencies of in the range 20-100. Figure by Baker & Willman (2015), here reproduced by kind permission.

overdensities in the field, and the problem becomes even more severe when one wants to detect their possible tidal tails. For these reasons, RRLs become a powerful tool to study the stellar populations of the UFDs and their spatial extent. Indeed, as suggested by Baker & Willman (2015), RRLs could be the *only* method to unveil very faint satellites, with $M_V < 3.5$, especially at low Galactic latitudes when both extinction and field contamination can be important. All the UFDs searched for variability so far show at least one RRL. This is not surprising, since they are composed by (at least) old, metal-poor stellar populations, which are known to produce RRLs. The small statistics must not be misleading, since if one normalizes the observed number of RRLs by the integrated luminosity (i.e. a proxy of the baryonic mass), the fraction of RRLs is even higher than that observed in the bright dSphs. Indeed, adopting the specific frequency as parametrized by Mackey & Gilmore (2003)

$$S_{RR} = N_{RR} \times 10^{0.4(7.5+M_V)} \quad (1)$$

one finds that UFDs tend to have higher specific frequencies than dSphs, as shown in figure 3 of Baker & Willman (2015), here reproduced by kind permission. However, as suggested in Baker & Willman (2015), this could be due to incompleteness effects, being the census of the RRLs in the bright dSphs still not complete.

4.1 Our RRL sample

Table 1 collects all the positional and pulsational parameters of the RRLs discovered in the UFDs so far. For each variable, we list the position, the period, the mean magnitudes and the luminosity amplitude in the *BVI* bands (when available). In some cases, we merged the information on the same variable coming from different studies. We discuss these cases in the individual notes. Here, we point out that *B*-band photometry for the RRLs in Bootes I comes from Siegel (2006), and the *VI*-bands from Dall’Ora et al. (2006). We also explicitly note that, when a star was listed in both studies, we adopt the coordinates listed in Dall’Ora et al. (2006). This table does not include the RRLs hosted in CVn I, whose structural properties suggest a classification as a “classical” dSph instead as a UFD, and those hosted in Leo T, since it contains gas and a young stellar population, and in this sense is not a typical old, gas poor UFD. For these two galaxies, we refer the reader to the specific papers – CVn I, Kuehn et al. (2008); Leo T, Clementini et al. (2012). The galaxies are ordered by RA, and the sources of the data are: Segue II (Boettcher et al., 2013); UMa II (Dall’Ora et al., 2012; Vivas et al., 2016); UMa I (Garofalo et al., 2013); Leo IV (Moretti et al., 2009); Hyd II (Vivas et al., 2016); Coma (Musella et al., 2009); CVn II (Greco et al., 2008); Boo II (Sesar et al., 2014; Vivas et al., 2016); Boo III (Sesar et al., 2014; Vivas et al., 2016); Boo I (Siegel, 2006; Dall’Ora et al., 2006); Hercules (Musella et al., 2012).

4.1.1 Notes on individual variables

V1 UMa II: this RRL was discovered by Dall’Ora et al. (2012), where they proposed a period of $P = 0.6593$ days. Subsequently, on the basis of a more densely sampled light curve, Vivas et al. (2016) computed a new period of $P = 0.56512$ days. This period appears to be compatible with the photometry of this variable, available in our database. Therefore, we adopt the period proposed by Vivas et al. (2016).

V1 Boo II: Sesar et al. (2014) proposed a period of $P = 0.63328$ days, while Vivas et al. (2016) computed a slightly different period of $P = 0.66349$ days. We keep the Vivas et al. (2016) estimate, together with their mean magnitude and amplitude.

V1 Boo III: Sesar et al. (2014) and Vivas et al. (2016) give practically the same period. However, here we present the mean magnitude and pulsational amplitude proposed by Vivas et al. (2016).

V5 Boo I: this star was classified as a RR_c type star by Siegel (2006), with a period of $P = 0.3863158$ days, and as a RR_{ab} star by Dall’Ora et al. (2006), with $P = 0.6506$ days. We used the Siegel (2006) period estimate to phase the data of this variable available in our database, but unfortunately we were not able to achieve a satisfactorily phased light curve. Therefore, we keep the Dall’Ora et al. (2006) estimate. It is worth noting that this variable is quite peculiar, since in the Dall’Ora et al. (2006) photometry it appears redder and brighter than the HB, and it could be blended with a companion.

ID	RA (J2000.0)	Dec (J2000.0)	Period (days)	$\langle B \rangle$ (mag)	A_B (mag)	$\langle V \rangle$ (mag)	A_V (mag)	$\langle I \rangle$ (mag)	A_I (mag)	Type
V1_SegueII	02:19:00.06	+20:06:35.2	0.748	18.62	0.62	18.25	0.51			RR _{ab}
V1_UMaII	08:50:37.43	+63:10:10.0	0.56512	18.61	1.27	18.24	1.01			RR _{ab}
V1_UMaI	10:34:59.2	+51:57:07.3	0.56924	20.72	1.29	20.47	1.07			RR _{ab}
V2_UMaI	10:35:05.5	+51:55:39.8	0.584	20.85	1.09	20.37	0.78			RR _{ab}
V3_UMaI	10:34:30.8	+51:56:28.9	0.64315	20.73	0.99	20.40	0.75			RR _{ab}
V4_UMaI	10:34:18.7	+51:58:29.2	0.74516	20.62	1.15	20.24	0.90			RR _{ab}
V5_UMaI	10:35:37.5	+52:02:35.6	0.59967	20.87	1.38	20.49	0.96			RR _{ab}
V6_UMaI	10:33:07.1	+51:50:05.1	0.39673	20.73	0.72	20.42	0.63			RR _c
V7_UMaI	10:32:37.5	+51:49:55.7	0.40749	20.54	0.37	20.44	0.38			RR _c
V1_LeoIV	11:32:59.2	-00:34:03.6	0.61895	21.82	0.99	21.47	0.73			RR _{ab}
V2_LeoIV	11:32:55.8	-00:33:29.4	0.7096	21.86	0.76	21.46	0.64			RR _{ab}
V3_LeoIV	11:33:36.6	-00:38:43.3	0.635	21.81	0.82	21.52	0.65			RR _{ab}
V1_HydII	12:21:43.51	-31:59:42.8	0.645	22.00	0.77	21.56	0.62	21.30	0.38	RR _{ab}
V1_Coma	12:27:33.50	+23:54:55.7	0.66971			18.44	0.78	17.74	0.53	RR _{ab}
V2_Coma	12:26:50.89	+23:56:00.6	0.31964			18.69	0.37	18.20	0.24	RR _c
V1_CVnII	12:57:01.6	+34:19:33.4	0.358	21.74	0.83	21.49	0.68			RR _c
V2_CVnII	12:57:11.8	+34:16:52.9	0.743	21.77	0.95	21.46	0.71			RR _{ab}
V1_BooII	13:58:07.04	+12:51:22.8	0.66349			18.23	0.71			RR _{ab}
V1_BooIII	14:00:34.52	+25:55:52.7	0.63328			18.56	1.07			RR _{ab}
V1_BooI	13:59:29.36	+14:10:43.6	0.303771	19.78	0.628					RR _{ab}
V2_BooI	13:59:51.34	+14:39:06.0	0.3119	19.73	0.67	19.63	0.34	19.32	>0.13	RR _c
V3_BooI	14:00:26.86	+14:35:33.1	0.3232	19.79	0.64	19.58	0.57	19.25	>0.15	RR _c
V4_BooI	14:00:08.90	+14:34:24.1	0.3860	19.82	0.58	19.57	0.59	19.19	0.2	RR _c
V5_BooI	14:00:21.56	+14:37:28.8	0.6506	19.75	0.57	19.38	0.33	18.93		RR _{ab}
V6_BooI	13:59:45.95	+14:31:40.7	0.3919	19.86	0.61	19.58	0.53	19.13	0.22	RR _c
V7_BooI	13:59:49.37	+14:10:05.6	0.4011623	19.76	0.74					RR _c
V8_BooI	13:59:59.69	+14:27:34.0	0.4179	19.79	0.74	19.54	0.40	19.10	0.26	RR _c
V9_BooI	13:59:47.28	+14:27:56.3	0.5755	19.84	1.28	19.55	1.00	19.07	>0.41	RR _{ab}
V10_BooI	14:00:25.75	+14:33:08.4	0.628	19.78	1.32	19.47	1.09	18.98	>0.24	RR _{ab}
V11_BooI	13:58:04.38	+14:13:19.3	0.6617310	19.82	1.20					RR _{ab}
V12_BooI	13:59:56.00	+14:34:55.0	0.3948	19.90	0.54	19.59	0.53	19.13	>0.20	RR _d
V13_BooI	13:59:06.36	+14:19:00.1	0.7061108	19.77	0.82					RR _{ab}
V14_BooI	13:59:25.75	+14:23:45.3	0.7186	19.89	0.86	19.50	0.44	19.03		RR _{ab}
V15_BooI	14:00:11.09	+14:24:19.7	0.8456	19.83	0.48	19.45	0.48	18.91	0.28	RR _{ab}
V1_Her	16:31:02.17	+12:47:33.7	0.639206	21.68	1.16	21.27	1.06			RR _{ab}
V3_Her	16:30:54.93	+12:47:04.2	0.39997	21.72	0.61	21.32	0.48			RR _c
V4_Her	16:30:56.14	+12:48:29.2	0.39576	21.59	0.69	21.23	0.58			RR _c
V5_Her	16:30:52.28	+12:49:12.0	0.40183	21.64	0.61	21.30	0.47			RR _c
V6_Her	16:30:52.41	+12:49:60.0	0.69981	21.76	1.19	21.35	0.90			RR _{ab}
V7_Her	16:31:29.48	+12:47:34.9	0.67799	21.65	1.03	21.22	0.81			RR _{ab}
V8_Her	16:31:27.20	+12:44:16.7	0.66234	21.69	1.09	21.25	0.90			RR _{ab}
V9_Her	16:31:29.50	+12:40:03.1	0.72939	21.60	1.00	21.18	0.80			RR _{ab}
V10_Her	16:30:03.96	+12:52:06.3	0.6616	21.69	1.32	21.28	1.17			RR _{ab}

Table 5 Positional and pulsational parameters of the RRLs in the UFD studied so far. See text for details.

V12 Boo I: this RRL was classified as RR_{ab} by Siegel (2006), with a period of $P = 0.6797488$ days, and by a double-pulsator RR_d by Dall’Ora et al. (2006), with periods of $P_1 = 0.3948$ days and $P_0 = 0.5296$ days. since the light curve shown by Dall’Ora et al. (2006) convincingly shows a typical double-mode behavior (see their Fig. 2), here we will keep their classification.

V1 Hyd II: the photometry of this variable was presented by Vivas et al. (2016) in the *gri* system. Here, for consistency we present its pulsational properties in the *BVi* bands, where *gr* magnitudes were transformed in *B*, *V* magnitudes following Jester et al. (2005).

4.2 Discussion

A glance at the data listed in Table 5 shows that, except for a few number of galaxies (namely UMa I, Boo I, Her), UFDs host a very small number of RRLs. Of course, with such small statistics, if a distance estimate can be reliable (especially in presence of a color-magnitude diagram, to check the robustness of the measured mean magnitudes and colors), some *caveats* must be recognized when using RRLs as population tracers. Indeed, since the Oo type is an *ensemble* feature, this should be declared only when a substantial number of fundamental mode RRL is available, in order to properly put them on an amplitude-period diagram (known as Bailey’s diagram). Nevertheless, a comparison with the classic Oo I and Oo II lines in the Bailey’s diagram can give interesting insights.

4.2.1 The Oosterhoff classification and the Galactic halo

In Figure 16, we show the positions on the Bailey’s diagram of the listed RRLs. For reference, we plot the loci of the Oo I and Oo II clusters, according to Zorotovic et al. (2010). At first glance, the positions of almost all the RRLs of the UFDs are compatible with a Oo II classification. The only apparent exception is UMa I, which was classified as Oo intermediate in Garofalo et al. (2013). However, when we compare the positions of its variables with those of the Galactic globular clusters M3 (left panel) and M15 (right panel, data made available by Clement et al., 2001), we favor a Oo II classification also for this system. Indeed, from the left panel it appears that the distribution of the UMa I RR_c variables is in good agreement with those of the other UFDs and with those of the Oo II cluster M15. Also, the mean period of the fundamental pulsators of UMa I is $\langle P_{ab} \rangle = 0.628 \pm 0.063$ days, which is in agreement with the values of other Oo II systems, such as M15 ($\langle P_{ab} \rangle = 0.643 \pm 0.063$ days), M92 ($\langle P_{ab} \rangle = 0.631 \pm 0.048$ days) and M68 ($\langle P_{ab} \rangle = 0.627 \pm 0.062$ days), where the listed values are computed on the basis of the compilation published by Clement et al. (2001). However, it should also be noted that, when discarding the variable V4, significantly brighter than the others, the mean period of the fundamental pulsators lowers to $\langle P_{ab} \rangle = 0.599 \pm 0.032$ days, as discussed in Garofalo et al. (2013). This suggest that, in general, when dealing with systems with a small number of RRLs, a correct Oo classification is a risky business, and we may consider not only to compare the positions of the RR_{ab} stars with respect to the mean Oo I and Oo II loci, but to consider the whole plane instead, with the actual distributions of the RRLs belonging to some reference Oo I and Oo II clusters.

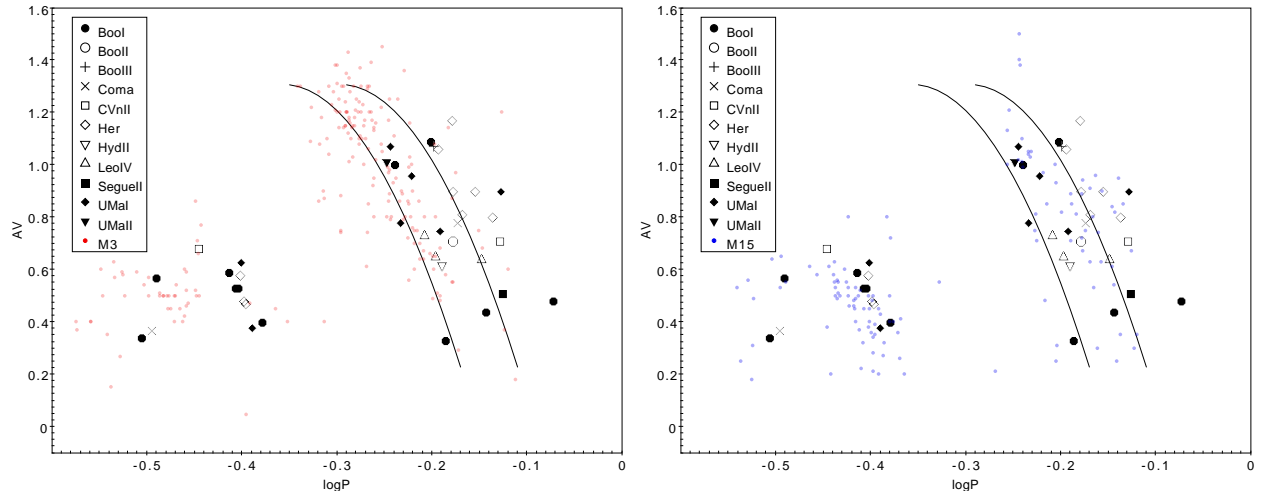


Fig. 16 Bailey’s diagram of the RRL (black symbols of the UFD satellites of the Milky Way). Left panel shows the comparison with the Oo I Galactic Globular cluster M3 (red filled circles) and with the Oo I and Oo II loci (dashed lines), according to Zorotovic et al. (2010). Right panel shows the sample comparison, but with the Oo II Galactic Globular cluster M15.

Taken at face value, the Oo II classification could suggest a major contribution of UFD-like objects in assembling the Galactic halo. However, as pointed out in Fiorentino et al. (2015), a detailed comparison of the pulsational properties of the RRLs of the Galactic halo and of the set dSphs + UFDs, shows that the latter lack the so-called high-amplitude, short-period (HASP) variables. Fiorentino et al. (2015) argue that the HASP region is filled only when RRLs are more metal-rich than $[\text{Fe}/\text{H}] = -1.5$ dex. Thus, *present-day* dSph- and UFD-like objects seem to have played a minor role, if any, in assembling the Galactic halo.

4.2.2 A homogeneous distance scale

In Table 6, we propose a homogeneous distance scale for the MW UFDs, by using the same $M_V - [Fe/H]$ relation and the same reddening calibration from Schlafly & Finkbeiner (2011). In particular, for the RRLs luminosity we adopt the absolute magnitude of $M_V = 0.54 \pm 0.03$ mag at $[\text{Fe}/\text{H}] = -1.5$ dex (based on a LMC distance of 18.52 ± 0.09 mag from Clementini et al., 2003), with a slope of $\Delta M_V [Fe/H] = 0.214 \pm 0.047$ mag dex $^{-1}$ (Clementini et al., 2003). We do not make any attempt to homogenize the metallicity scale, where all the values have been taken from the collection listed in McConnachie (2012), except of Boo III (Carlin et al., 2009), and Hyd II (Kirby et al., 2015). The uncertainties of the distance are split in intrinsic error (the standard deviation of the mean, when at least two RRLs are available, or the typical photometric error when only one variable is present), plus a contribution due to the uncertainty in the $M_V - [Fe/H]$ relation. As a matter of fact, there is also

Name	[Fe/H] (dex)	A_V (mag)	$(m - M)_0$ (mag)
SegueII	-2.00 ± 0.25	0.507	$17.31 \pm 0.03 \pm 0.06$
UMaII	-2.47 ± 0.06	0.257	$17.65 \pm 0.04 \pm 0.03$
UMaI	-2.18 ± 0.04	0.054	$19.98 \pm 0.04 \pm 0.03$
LeoIV	-2.54 ± 0.07	0.069	$21.10 \pm 0.03 \pm 0.04$
HydIII	-2.02 ± 0.08	0.167	$20.96 \pm 0.04 \pm 0.03$
Coma	-2.60 ± 0.05	0.046	$18.09 \pm 0.03 \pm 0.03$
CVnII	-2.21 ± 0.05	0.027	$21.06 \pm 0.02 \pm 0.03$
BooII	-1.79 ± 0.05	0.084	$17.67 \pm 0.04 \pm 0.03$
BooIII	-2.1 ± 0.2	0.058	$18.09 \pm 0.04 \pm 0.05$
BooI	-2.55 ± 0.11	0.047	$19.18 \pm 0.06 \pm 0.04$
Her	-2.41 ± 0.04	0.171	$20.75 \pm 0.05 \pm 0.03$

Table 6 RR Lyrae-based distances to the UFD satellites of the Milky Way. Distances have been estimated according to the $M_V - [\text{Fe}/\text{H}]$ relation provided by Clementini et al. (2003). A_V absorptions are based on the calibration by Schlafly & Finkbeiner (2011).

another source of uncertainty, that is the internal metallicity spread observed in several UFDs, but it is difficult to manage. The spread can be of the order of ~ 0.6 dex (UMa II, Kirby et al., 2008), which means an additional uncertainty up to ~ 0.15 mag. In computing the distances of the individual galaxies, we dropped the variables V1 in Coma, V4 in UMa I e V5 in Boo I, since they are significantly brighter (~ 0.2 mag) than the others and/or of the HB, and may be evolved variables not representative of the zero-age HB level.

The current radial distribution of both UFD and classical dwarf spheroidals (see Monelli contribution this book) seems to be quite similar. However, the uncertainties affecting the individual distances of UFDs are still too large. Individual distances based on the use of optical and/or near Infrared PL relations will be crucial to further constrain the similarities in radial distribution of gas poor stellar systems.

5 On the absolute and relative ages of globular clusters

The early estimates of the ages of globular clusters date back to more than half a century ago thanks to the pioneering papers from Alan Sandage (Sandage, 1958) and Halton Arp (Arp, 1962) for the observational aspects and from Fred Hoyle (Hoyle, 1959) and Martin Schwarzschild (Schwarzschild, 1970) for theoretical analyses. The reader interested in a more detailed discussion concerning the dawn of cluster age determination is referred to the seminal presentations and discussions of the 1957 Vatican Conference (O’Connell, 1958). Particularly enlightening was the empirical evidence brought forward by Walter Baade (Baade, 1958) concerning the age difference among the different stellar populations belonging to the Galactic components (Halo, Disk, Bulge).

5.1 Absolute cluster age estimates

In the following we will focus on the most reliable classical methods used to estimate absolute ages of Galactic Globular Clusters (GGCs). The first two rely on deep photometry of individual stars of a GGC down to the Main Sequence Turn Off (MSTO) and the white dwarf cooling sequence features, respectively. The second is observationally based on the detection of radioactive heavy elements in individual stellar spectra in order to use direct cosmochronometry. We will highlight strengths and weaknesses of their application.

5.1.1 The Main Sequence Turn Off

The MSTO of a cluster is identified as the bluest point along its Main Sequence. This is the most important clock to date for both open and globular stellar systems. The key advantages of this diagnostic are the following:

- i) The anti-correlation between cluster age and brightness of MSTO stars is linear over a broad range of stellar ages (see e.g., Di Cecco et al., 2015; Valle et al., 2013).
- ii) Stars in this evolutionary phase are burning hydrogen in the core. This means that they evolve on a long nuclear time scale, and therefore, the number of stars per unit magnitude tracing this evolutionary phase is quite large compared with evolved phases.
- iii) Accurate apparent optical magnitudes of MSTO stars in GGCs are within the capability of 2-4 m class telescopes equipped with CCD detectors and can be easily measured.

The main cons of the MSTO are the following:

- i) The MSTO is prone to uncertainties on cluster distance and on cluster reddening. An uncertainty of 10% in the error budget (reddening plus true distance modulus) of the MSTO, implies an uncertainty of about 1 Gyr in cluster age. The problem becomes even more severe if we are dealing with stellar systems either affected by large or by differential reddening.
- ii) The identification of the MSTO is not always trivial. In a broad range of stellar ages and chemical compositions, stars across the MSTO attain in optical bands similar colors and magnitudes. In some traditional broad-band color-magnitude systems there is nearly a vertical distribution of MSTO stars (e.g., Salaris & Cassisi, 2005). Fig. 17 shows the optical (UBVRI) CMDs of the Galactic globular M4 (Stetson et al., 2014; Braga et al., 2015). The shape of the MSTO changes from “cuspy” in the U-I,U CMD (top left panel) to “almost vertical” in the V-I,I CMD (bottom right panel).

Fortunately the variation in the color gradient of the region across the MSTO becomes more evident in the NIR and in the MIR regime. Data plotted in the top panel of Fig. 18 show that cluster stars display not only a well defined bending in the region across the MSTO, but also a sharp change in the slope of the lower main sequence across the Main Sequence Knee (MSK, see § 5.4). A glance at the data plotted in the bottom panels shows that the bending across

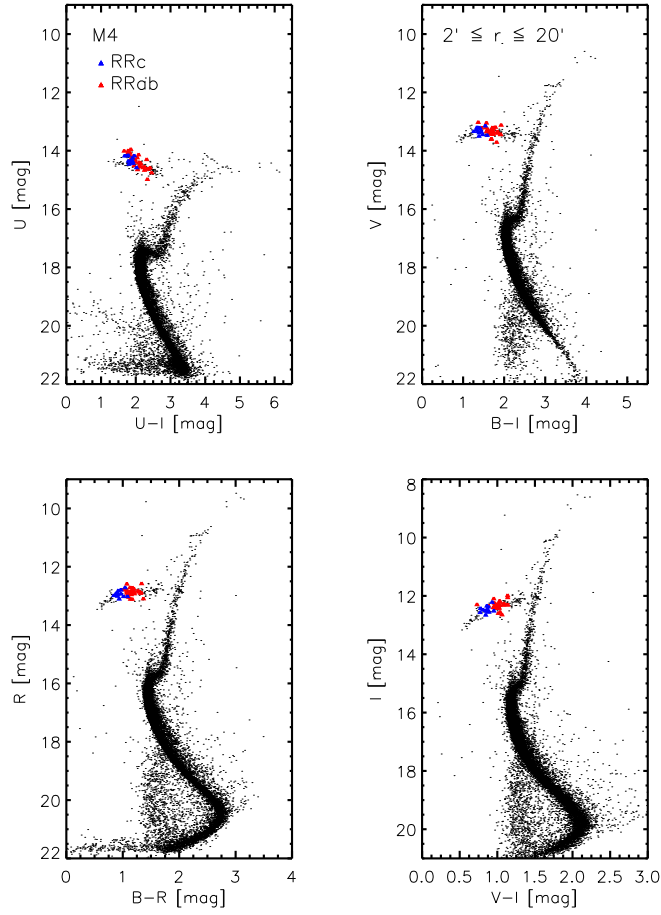


Fig. 17 Optical Color-Magnitudes Diagrams (CMDs) based on UBVRI bands of the Galactic star cluster M4. Stars plotted in the CMDs were selected according to the position. Blue and red triangles mark the position of first overtone (RRc) and fundamental (RRab) cluster RR Lyrae. Note the change in the slope of the Horizontal Branch (HB) when moving from the top left panel (U-I,U) to the bottom right panel (V-I,I). Bright red giant stars located across the tip of the red giant branch are missing due to saturation problems. The vertical plume of stars located at $B-I \sim 2.0-2.5$, $B-R \sim 1.8-2.0$ and $V-I \sim 1.2-2.5$ mag is caused by field star contamination.

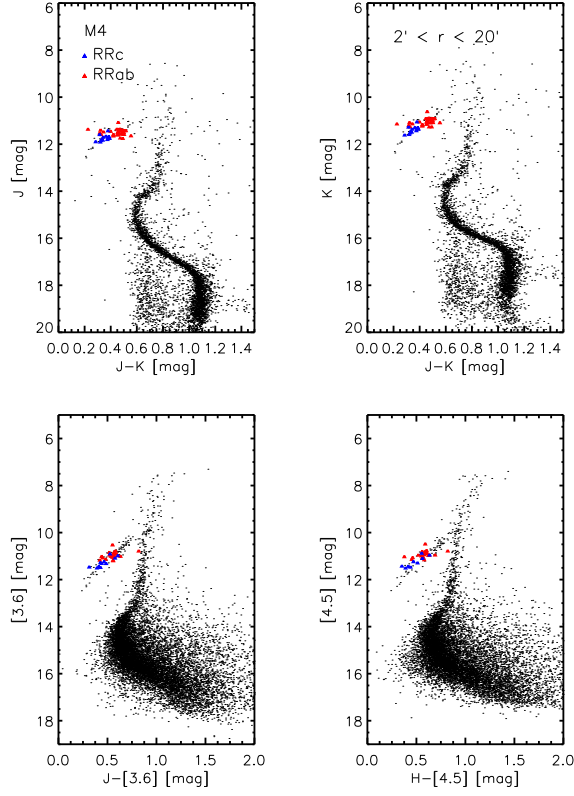


Fig. 18 Same as Fig. 17, but for NIR (JHK) and MIR ([3.6],[4.5]) bands.

the MSTO is also in NIR/MIR CMDs. However, the photometric accuracy of the MIR bands do not allow us to clearly identify the MSK.

The empirical scenario concerning the shape of both the MSTO and the MSK becomes even more interesting in dealing with optical/NIR/MIR CMDs, since they bring forward several advantages: a) They display a well defined bending across the MSTO and a sharp change in the MS slope across the MSK; b) The broad range in central wavelengths among optical and NIR/MIR bands

means also a strong sensitivity to the effective temperature. The consequence is that optical/NIR/MIR CMDs display tight stellar sequences not only along the MS, but also in advanced evolutionary phases (RGB, HB, AGB).

iii) Optical CMDs are affected in the region across the MSTO by field star contamination. This problem is less severe in optical/NIR CMDs, since the MSTO stars attain colors that are systematically bluer than typical field stars. The bottom left panel of Fig. 19 shows that field stars are typically redder ($V - K = 2.8 - 3.5$) than MSTO stars ($V - K \simeq 2.6$). However, field star contamination severely affects age and structural parameters of nearby stellar systems. Accurate and deep optical CMDs based on images collected with ACS on board of HST are less affected by the contamination of field stars. The pointing is typically located across the center of the cluster and in these regions cluster stars outnumber field stars. This rule of thumb does not apply to clusters either located or projected onto crowded Galactic regions such as the Bulge and Galactic thin disk (Zoccali et al., 2001a; Ferraro et al., 2009; Lagioia et al., 2014) or nearby dwarf galaxies (Kalirai et al., 2012). A significant step forward in dealing with this problem was provided by HST photometry. The superb image quality of HST optical images provided the opportunity to measure the proper motion using images collected on a time interval of the order of ten years. This approach provided the opportunity to split not only field and cluster stars, but also to clearly identify stellar populations belonging to Sagittarius (Anderson, 2002; King et al., 2005; Massari et al., 2013; Milone et al., 2014). The great news in this context is that similar results can also be obtained using NIR images as a second epoch collected with AO systems available at 8-10 m class telescopes (e.g., NGC 6681, Massari et al., 2016b).

The results mentioned above are based on images that only cover a few arcminutes around the center of each cluster. The separation between cluster and field stars is much more challenging away from cluster centers, since field stars outnumber cluster stars in these regions. The reason why we are interested in tracing cluster stars in external cluster regions is twofold: a) There is mounting empirical evidence that stellar populations change (chemical composition, age) as a function of radial distance – e.g., 47 Tuc, (Kalirai et al., 2012); Omega Cen, (Calamida et al., 2017); b) The estimate of structural parameters depends on the star counts in the outskirts of the clusters.

These are the reasons why new photometric approaches for the separation between field and cluster stars are required. This approach does require photometric catalogs based on at least three photometric bands. To accomplish the goal we have used either multi-dimensional ridge lines as in dealing with *griz* SDSS photometry of the metal-rich globular M71 (Di Cecco et al., 2015) or the difference in the spectral energy distribution in dealing with the *ugri* photometry of the complex globular ω Cen (Calamida et al., 2017). The latter approach was developed to deal with stellar systems characterized by multiple stellar populations (see e.g., Martínez-Vázquez et al., 2016a,b).

Initially, the ridge lines of the different sub-populations in ω Cen along the cluster evolutionary sequences (MS, SGB, RGB) were estimated. They are based on a 3D CMD (magnitude, color index, star counts) and the ridge

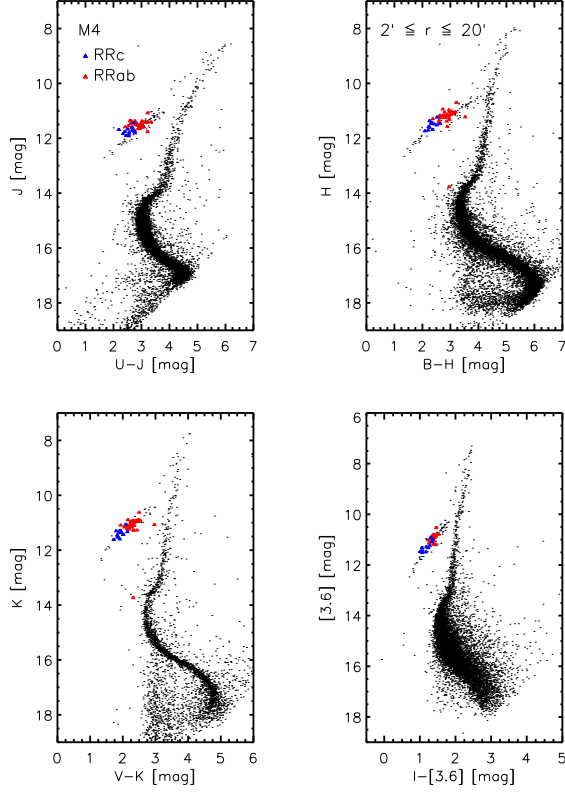


Fig. 19 Same as Fig. 17, but for optical and NIR/MIR bands.

lines trace the peaks of the stellar distribution. The horizontal branch (HB) stars are typically neglected, since they are either bluer (hot and extreme HB) or they can be easily distinguished (RR Lyrae stars, red HB) from the field stars. These ridge lines were estimated in an annulus neglecting stars located in the innermost and in the outermost cluster regions and using several cuts in radial distance and in photometric accuracy. Once the ridge lines were estimated we performed a linear interpolation among them and generated a

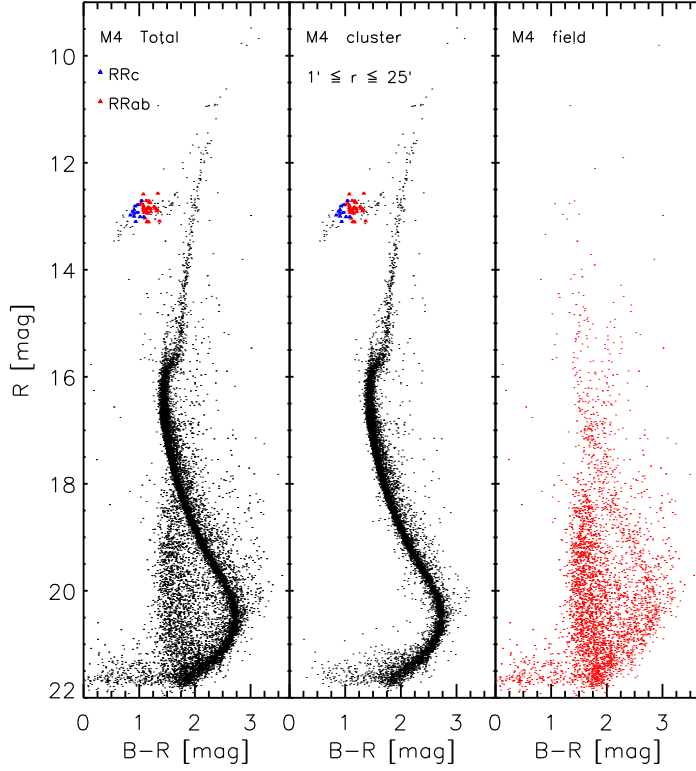


Fig. 20 Left – Optical CMD in B-R,R for stars covering a sky area of 35×35 arcmin squared around M4. Middle – Same as the left panel, but for candidate cluster stars. Right – Same as the left panel, but for candidate field stars.

continuous multi-dimensional surface. Subsequently, the separation between field and cluster stars was performed in two steps: a) We estimated the total standard deviation among the position of individual stars and the reference surface; b) We estimated the distance in magnitude and in color among the individual stars and the reference surface.

The approach discussed above relies on a conservative assumption, i.e. we do prefer to possibly lose some of the candidate cluster stars instead of including possible candidate field stars. Note that this assumption is fully supported by the fact that the age diagnostics we use for estimating cluster ages depend on the shape of MSTO and/or of the MSK. Stellar completeness mainly affects cluster ages based on cluster luminosity functions (Zoccali et al., 1998).

Fig. 20 shows the separation between field and cluster stars for the Galactic globular M4. This cluster is an acid test for the selection criteria based on photometry, since it is projected onto the Galactic Bulge and it is also affected by differential reddening. To overcome some of these problems we decided to follow the same approach we adopted for ω Cen, but the initial ridge lines were derived candidate field stars located outside the tidal radius of the cluster (Ferraro et al. 2018, in preparation). Data plotted in the left panel display stars located across the sky region covered by M4 in the B-R,R CMD. Field stars can be easily identified both along the MS and the RGB. The middle panel of the same figure shows the CMD, but for candidate cluster stars. The “cleaning” appears quite good across the cluster sequences. Note that the sequence running parallel to the cluster MS is due either to binaries or to photometric blends. The plausibility of the criteria adopted to separate field and cluster stars are further supported by the CMD of candidate field stars plotted in the right panel. Once again there is evidence that a minor fraction of candidate field stars were misidentified, but the main peak of field stars even across the MSTO was properly identified.

To further support the photometric criteria adopted to separate field and cluster stars, Fig. 21 shows a color-color-magnitude diagram of the selected candidate cluster stars. It is worth mentioning the smoothness of the cluster sequences when moving from the RGB to the MSTO and to the MSK.

5.1.2 The error budget

The global error budget of absolute ages of globular clusters based on the MSTO includes theoretical, empirical and intrinsic uncertainties.

Theoretical uncertainties – The precision of the clock adopted to date stellar systems depends on the precision of the input physics adopted to construct evolutionary models and, in turn, cluster isochrones. The main sources of uncertainties can be split into micro-physics (nuclear reactions, opacity, equation of state, astrophysical screening factors) and macro-physics (mixing length, mass loss, atomic diffusion, rotation, radiative levitation). The uncertainties affecting the nuclear reactions, such as the pp and the CNO cycle, have already been discussed by degl’Innocenti et al. (2004) and Valle et al. (2013). They suggest that the uncertainties on age range from 3% for the ${}^1\text{H}(p, \nu_e, e^+){}^2\text{H}$ nuclear reaction to roughly 10% for the ${}^{14}\text{N}(p, \gamma){}^{15}\text{O}$ reaction. The same authors also suggest an uncertainty of the order of 5% for

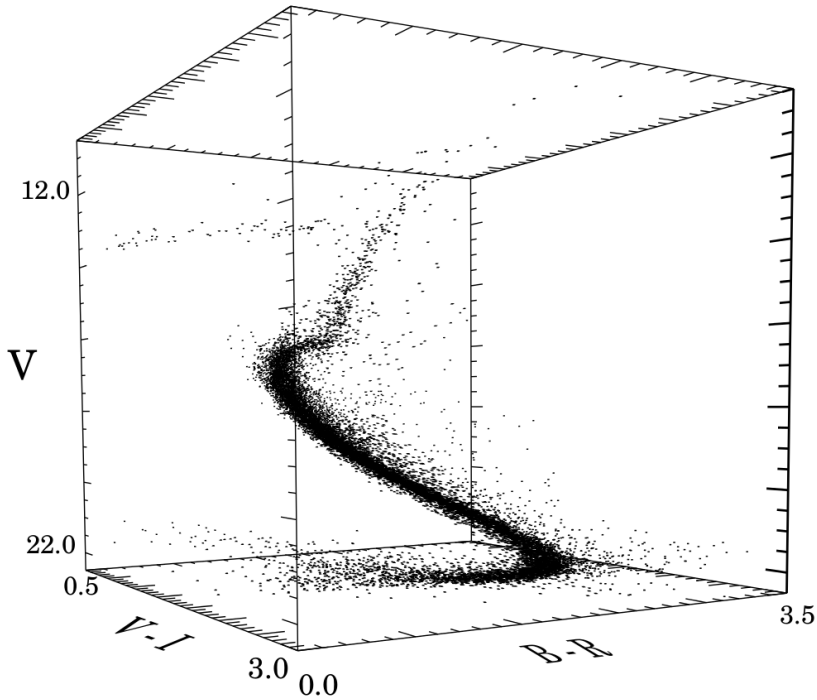


Fig. 21 Optical V, B-R, V-I color-color-magnitude diagram of candidate cluster stars for the globular M4 (see text for more details).

the radiative opacities adopted for constructing MS and HB models. Moreover, they also suggest a similar uncertainty (5%) for the conductive opacities affecting the energy transport in electron degenerate isothermal helium cores typical of RGB structures and, in turn, on the HB luminosity level (e.g., Marta et al., 2008; Chaboyer et al., 2017).

The impact of macro-physics, and in particular the treatment of the mixing in convective regions has been addressed comprehensively in the literature (e.g., Chiosi & Maeder, 1986; Castellani et al., 1999; Maeder & Meynet, 2000; Salaris & Cassisi, 2008; Bertelli et al., 2009; Rosenfield et al., 2017)). The treatment of atomic diffusion and radiative levitation has also been investigated in many studies (Proffitt & Vandenberg, 1991; Ciacio et al., 1997; Michaud et al., 2004; Vandenberg et al., 2013).

Finally, to transform theory into the observational plane, we also need predictions based on stellar atmosphere models (Gustafsson et al., 2008). We have to take account of uncertainties affecting bolometric corrections and color-

temperature transformations. The impact that the quoted ingredients have on cluster isochrones has been discussed in detail in the literature (e.g., Pietrinferni et al., 2004; Cassisi et al., 2008; Pietrinferni et al., 2009; Sbordone et al., 2011; VandenBerg et al., 2013; Salaris, 2016).

As a whole, the typical theoretical uncertainty in the adopted MSTO is of the order of 10%. In this context it is worth stressing that theoretical uncertainties mainly affect the zero point of the absolute age determinations. The relative age determinations are minimally affected by these uncertainties (see e.g., Dotter et al., 2011; VandenBerg et al., 2013; Chaboyer et al., 2017).

In this context, it is also worth mentioning that the helium to metal enrichment ratio ($\Delta Y/\Delta Z$), a fundamental ingredient in evolutionary prescriptions, is poorly known. This is used to derive the current stellar helium content through the following relation: $Y = Y_P + \Delta Y/\Delta Z \times Z$, where Y_P is the primordial helium content. However, empirical estimates range from $\Delta Y/\Delta Z = 3 \pm 2$ Pagel & Portinari (1998) to $\Delta Y/\Delta Z = 5.3 \pm 1.4$ Gennaro et al. (2010). Moreover and even more importantly, there are no solid reasons why this relation should be linear over the entire metallicity range and that the current local estimate is universal (Peimbert et al., 2010).

Empirical errors – The main uncertainties in the absolute age estimate of globulars are the cluster distances. Indeed an error of 10% in true distance modulus ($\Delta\mu_0 \sim 0.1$ mag) implies an uncertainty of ~ 1 Gyr in the absolute age. The error budget becomes even more severe once we also account for uncertainties in reddening corrections. An uncertainty of 2% in color excess implies an uncertainty of 6% in visual magnitude. The impact of this limitation becomes even more stringent if the cluster is also affected by differential reddening. In this context, it is worth mentioning that more metal-rich globular clusters are mainly distributed across the Galactic Bulge, *i.e.*, a region of the Galactic spheroid affected by large reddening and by differential reddening (Stetson et al., 2014).

The ongoing effort in trying to quantify the systematics affecting the measurements of the MSTO of a large fraction of GGCs also faces the problem of the absolute photometric calibration. In handling this thorny problem, two independent approaches have provided the opportunity to limit and/or to overcome the uncertainties associated with the zero-points of different photometric systems:

- i) Cluster photometry collected either with HST/WFPC2 or HST/ACS has provided the unique opportunity to collect accurate and deep photometry in a single well-calibrated photometric system for a sizable sample of GGCs (~ 60 out of 160, e.g., Zoccali et al., 2001b; Sarajedini et al., 2007; Marín-Franch et al., 2009; VandenBerg et al., 2013);
- ii) The major effort to provide local standard stars in GGCs also has significantly improved the accuracy of photometry and saved significant amount of telescope time (Stetson, 2000).

The age diagnostic adopted to estimate the cluster age also depends on the iron content. The massive use of multi-object fiber spectrographs paved the

way for the definition of a firm metallicity scale including a significant fraction of GGCs (e.g., Carretta et al., 2009). This translates to a systematic decrease in the uncertainties on the iron and on α -element abundance scale.

Intrinsic uncertainties – Dating back to more than forty years ago, spectroscopic investigations brought forward a significant star-to-star variation in C and in N among cluster stars (e.g., Osborn, 1971). This evidence was complemented by discoveries of variations in Na, Al, and in O (e.g., Cohen, 1978; Pilachowski et al., 1983; Leep et al., 1986) and by anti-correlations in CN–CH (e.g., Kraft, 1994) as well as in O–Na and in Mg–Al (e.g., Suntzeff et al., 1991; Gratton et al., 2012).

The light element abundance variation was further strengthened by the occurrence of multiple stellar populations in more massive clusters (Bedin et al., 2004; Piotto et al., 2005, 2007). However, detailed investigations concerning the different stellar populations indicate a difference in age that is, in canonical GGCs (i.e. the most massive globulars are not included), on average shorter than 1 Gyr (Ventura et al., 2001; Cassisi et al., 2008). The intrinsic uncertainty does not seem to be the main source in the error budget of GGCs absolute ages.

5.1.3 The cluster distance scale

Several approaches have been suggested in the literature to overcome some of the thorny problems affecting the estimate of the absolute age of GGCs. The time scale within which we can significantly reduce the theoretical uncertainties can be barely predicted. On the other hand, the empirical uncertainties are strongly correlated with technological developments either in the detectors or in the observing facilities or in both. The uncertainties affecting individual cluster distances would significantly benefit by the development of a *homogeneous cluster distance scale*.

Although Galactic globulars are at the cross-road of major theoretical and empirical efforts, we still lack a distance scale based on the same diagnostic and on homogeneous measurements. The problem we are facing is mainly caused by the intrinsic limitations in the diagnostics used to determine the distance. The difficulties of these methods can be summarized briefly.

i) The tip of the Red Giant Branch (TRGB) can only be applied to two clusters (ω Cen, 47 Tuc), due to limited stellar (Poisson) statistics when approaching the tip of the RGB.

ii) Main sequence fitting is hampered by the fact that the number of field dwarfs with accurate trigonometric parallaxes is small and covers a limited range in iron abundance (Chaboyer et al., 2017; VandenBerg et al., 2014a).

iii) Another possible approach to constrain cluster distances is to fit the white dwarf cooling sequence. However, this method can only be applied to a few clusters (Zoccali et al., 2001b; Richer et al., 2013; Bono et al., 2013) and we are still facing some discrepancies between the distances based on this diagnostic and other distance indicators (Bono et al., 2008). Furthermore,

the number of nearby White Dwarfs (WDs) for which are available accurate trigonometric parallaxes is limited.

iv) Cluster distances based on the kinematic approach appear also to be affected by systematics. This diagnostic has the potential to be a powerful geometrical method, since it is only based on the ratio between the standard deviation of proper motions and the standard deviation of radial velocities. There is mounting evidence that the current kinematic distances are slightly larger than those based on other primary distance indicators (Bono et al., 2008).

v) During the last few years, accurate distances have been provided for a few globulars using eclipsing binary stars. This is also a very promising approach, since it is based on a geometrical method (Thompson et al., 2001). The main limitation of this distance indicator as well as methods iii) and iv) is that they are challenging from the observational point of view. This means that they have only been applied to a very limited number of clusters.

vi) The Horizontal Branch (HB) luminosity level is one of the most popular distance indicator for GGCs. The typical anchor for the HB luminosity is the M_V^{RR} -metallicity relation at the mean color of the RR Lyrae instability strip. This color region was selected because it is quite flat in CMDs using the V -band magnitude. This distance indicator might be affected by two possible sources of systematic errors:

a) The HB morphology – The metallicity is the most important parameter affecting HB morphology, indeed the HB is mainly blue in the metal-poor regime and becomes mainly red in the metal-rich regime. The parameter used to trace the change in the HB morphology is $\tau_{HB}=(B-R)/(B+V+R)$, i.e. the number ratio among stars either bluer (B) or redder (R) than variable (V) RR Lyrae stars. Globulars approaching the two extrema (± 1) typically lack of RR Lyrae stars. This means that it is quite difficult from an empirical point of view to anchor the HB luminosity level. The impact of this limitation becomes even more stringent for globulars more metal-rich than 47 Tuc, since their HBs typically display a stub of red HB stars. There are two exceptions, NGC 6441 and NGC 6388, that are metal-rich but display a well populated blue and red HB, plus a good sample of RR Lyrae stars (Pritzl et al., 2003);

b) Predicted HB luminosity level – The current evolutionary prescriptions concerning the zero age HB (ZAHB) luminosity are typically 0.10–0.15 mag brighter than the observed ones. New interior conductive opacities (Cassisi et al., 2007) contribute to alleviate the problem, but the discrepancy is still present.

vii) Near-infrared and mid-infrared observations of cluster RR Lyrae stars appear to be very promising for providing a homogeneous cluster distance scale. The RR Lyrae stars do obey to well defined PL relations in these bands. These relations are very narrow (e.g., Braga et al., 2015; Marconi et al., 2015; Neeley et al., 2017) and are not affected by off-ZAHB evolution, thus reducing the systematics discussed above. NIR photometry has also the advantage of being less prone to uncertainties introduced by either large and/or by differential reddening corrections. This is a typical problem among the more metal-rich

Bulge globulars. Indeed, the uncertainties affecting NIR/MIR bands are on average one order of magnitude smaller than the optical bands. However, the number of globulars hosting a sizable sample of RR Lyrae stars is roughly half of the entire Galactic sample. Finally, we still lack a detailed knowledge on how the reddening law changes when moving across the Bulge, along the Bar and into the nuclear Bulge (e.g., Indebetouw et al., 2005; Nishiyama et al., 2006, 2008, 2009; Nataf et al., 2013; Schultheis et al., 2014).

5.1.4 *The white dwarf cooling sequence*

The white dwarf cooling sequence depends on different physics than the previously-discussed methods, and as such should be an excellent diagnostic to constrain possible systematics in absolute cluster age estimates based on the MSTO (Hansen et al., 2004; Salaris et al., 2010). This means that deep and accurate photometry of nearby globulars can provide crucial constraints on the plausibility of the physical assumptions adopted to construct either main sequence or cooling sequence models. The key advantages in using cluster WD cooling sequences is that they display a well defined blue turn off (WDBTO) in deep and accurate I,V-I CMDs. Theory and observations indicate that this change in the slope of the WD cooling sequence is due to interplay between an opacity mechanism called Collisional Induced Absorption (CIA) mainly from molecular hydrogen and/or to the cooling time of more massive WDs (Brocato et al., 1999; Hansen, 2004; Richer et al., 2006; Moehler et al., 2008; Salaris et al., 2010; O'Malley, 2013).

Recently, Bono et al. (2013) performed a detailed theoretical investigation of cluster WD cooling sequences and found new diagnostics along the WD cooling sequences and in NIR Luminosity Functions (LFs). The interplay between CIA and the cooling time of progressively more massive WDs causes a red turn-off along the WD cooling sequences (WDRTO). This feature is strongly correlated with the cluster age, and indeed the faint peak in the K-band increases by 0.2–0.25 mag/Gyr in the range 10–14 Gyr. Moreover, they also suggested to use the difference in magnitude between the MSTO and the WDRTO, since this age diagnostic is independent of distance and reddening. These predictions appear very promising in view of the unprecedented opportunity offered by JWST in the NIR/MIR regimes. This encouraging prospect also applies to ground-based extremely large telescopes equipped with state-of-the-art multi-conjugated adaptive optics systems (Bono et al., 2013).

5.1.5 *Thorium Cosmochronometry*

Elements beyond the iron-group are overwhelmingly created in neutron-capture fusion reactions by target heavy-element seed nuclei. Their syntheses mostly are either slow (β -decay timescales fast compared to neutron-capture timescales; called the *s*-process) or rapid (neutron-capture timescales much faster than β -decay ones; the *r*-process). Very heavy radioactive elements thorium ($Z = 90$) and uranium ($Z = 92$) can be created only via the *r*-process. The heaviest

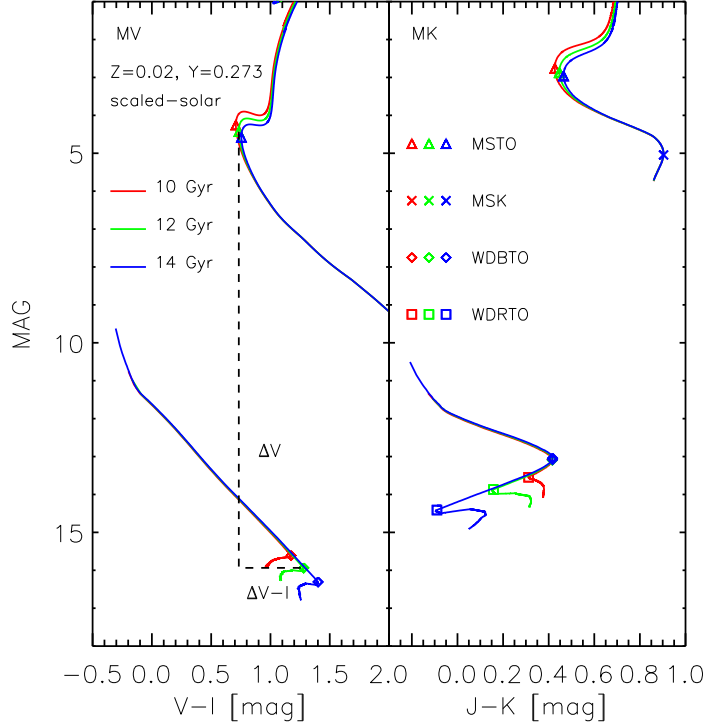


Fig. 22 Left – Predicted optical (V-I,V) CMD for cluster isochrones at solar chemical composition and at scaled solar chemical mixture. The bright solid lines show isochrones of 10 (red), 12 (green) and 14 (blue) Gyr (BaSTI data base). The triangles mark the position of the Main Sequence Turn Off (MSTO). The faint solid lines show WD isochrones of 10 (red), 12 (green) and 14 (blue) Gyr. The WD isochrones account for chemical separation (Salaris et al., 2010). The diamonds mark the position of the White Dwarf Blue Turn Off (WDBTO). The vertical and horizontal black dashed lines show the difference in magnitude and in color between the 12 Gyr MSTO and the WDBTO. Right – Same as the left, but in the NIR (K,J-K) CMD. The triangles mark the position of the MSTO, the crosses mark the MS Knee (MSK, Bono et al., 2010), the diamonds mark the WDBTO, while the squares mark the White Dwarf Red Turn Off (WDRTO).

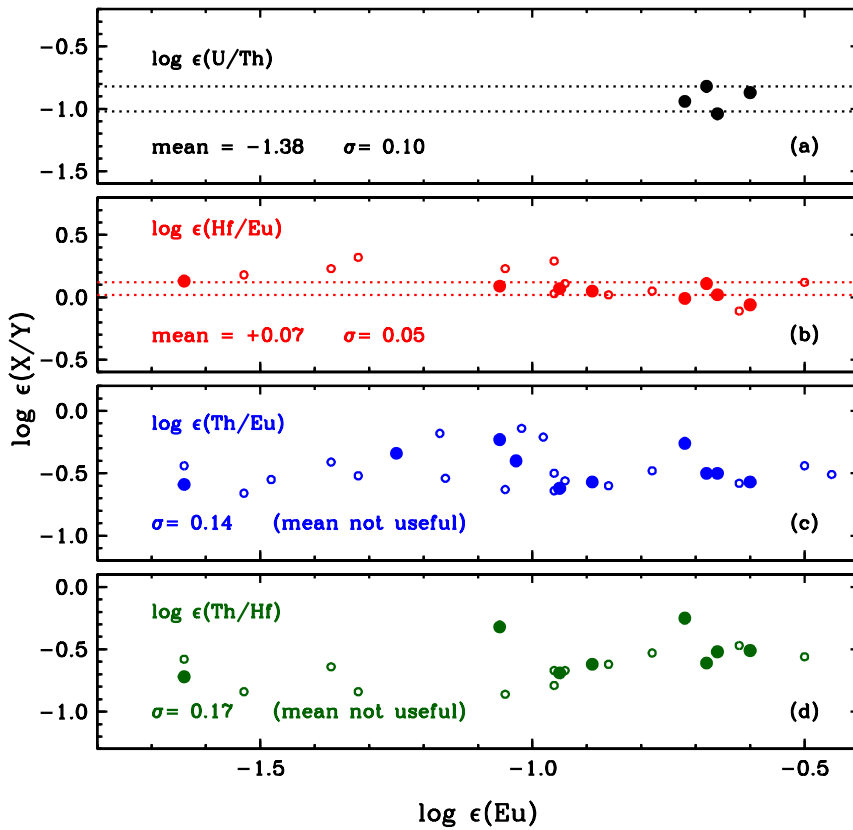


Fig. 23 Abundance ratios of elements of interest to cosmochronometry plotted as functions of the Eu abundance. The large filled circles are from individual high-resolution spectroscopic studies Westin et al. (2000); Hill et al. (2002); Cowan et al. (2002); Sneden et al. (2003); Hayek et al. (2009); Siqueira Mello et al. (2013); Mashonkina et al. (2014); Hill et al. (2016), and the small open circles are from a single survey of many r -process-rich stars Roederer et al. (2009). Means and standard deviations, computed only for the individual high-res studies, are written in each panel. Only in panels (a) and (b) are dotted lines drawn to indicate the σ widths around the means; the scatters in panels (c) and (d) are too large to be useful for cosmochronometry.

stable element is bismuth ($Z = 83$, with its sole natural isotope ^{209}Bi). All isotopes of elements with $Z = 83\text{--}89$ have very short half-lives, and therefore cannot be created in the s -process. Th and U decay on astrophysically interesting timescales: half-lives are 1.4×10^{10} yr for ^{232}Th (its only naturally-occurring isotope), 7.0×10^8 yr for ^{235}U , and 4.5×10^9 yr for ^{238}U . Therefore, derived abundances of Th and U with respect to stable r -process-dominated neutron-capture elements in low-metallicity halo stars have the potential to be translated into Galactic age estimates.

Attempts to use stellar Th abundances as chronometers began with Butcher (1987). That study included only disk stars with metallicities $[\text{Fe}/\text{H}] \geq -0.8$. As is the case for most Th abundance studies, Butcher (1987) analyzed just

the 4019.2 Å Th II transition. That line in high metallicity stars is at best a weak blending absorption in this crowded spectral region. Additionally, for a comparison stable neutron-capture element Nd was chosen in the Butcher (1987) study. Unfortunately, Nd in the solar system (and probably in most disk stars) has a *s*-process origin, accounting for $\simeq 58\%$ of its abundances; the *r*-process fraction is only $\simeq 42\%$ (e.g. Smolec (2005)). With these limitations, Butcher (1987) argued that the Th/Nd ratios were roughly constant in their sample of disk stars, irrespective of assumed stellar age.

Analyses of low-metallicity halo population *r*-process-rich stars have yielded more easily-interpreted results. The first such star, HD 115444, initially identified by Griffin et al. (1982), has $[\text{Fe}/\text{H}] \simeq -2.9$, and $[\text{Eu}/\text{Fe}] \simeq +0.9$ (e.g. Westin et al. (2000); Sneden et al. (2009)). Then CS 22892-052, a red giant from the Beers et al. (1992) low resolution Galactic halo survey, was serendipitously discovered (Sneden et al., 1994) to be very *r*-process rich: $[\text{Fe}/\text{H}] \simeq -3.0$, $[\text{Eu}/\text{Fe}] \simeq +1.7$, and an unambiguously strong 4019 Å line, yielding $[\text{Th}/\text{Fe}] \simeq +1.4$ or $[\text{Th}/\text{Eu}] \simeq -0.3$ (e.g., Sneden et al., 2003). The relatively depressed Th compared to Eu was taken to be a sign of radioactive decay from an *assumed* initial production ratio of $[\text{Th}/\text{Eu}] \equiv 0.0$. Initial application of theoretical models suggested an ancient age for the neutron-capture elements but with a large uncertainty: $11.5 \leq t \leq 18.8$ Gyr (Cowan et al., 1997).

Detailed study of another *r*-process-rich star CS 31082-001 (Cayrel et al., 2001; Hill et al., 2002) revealed the first detection of U in a low metallicity star (Hill et al., 2002). But the individual abundance ratios $[\text{Th}/\text{Eu}]$ and $[\text{U}/\text{Eu}]$ in this star turned out to be too large to be sensibly interpreted as a straightforward radioactive decay. Instead, it was necessary to postulate an “actinide boost” with initial production ratios $[\text{Th}/\text{Eu}] > 0$ and $[\text{U}/\text{Eu}] > 0$. Fortunately, the ratio between neighboring elements Th and U should have well-understood production ratios and, for example, Schatz et al. (2002) derived an age from the U-Th abundance ratio of 15.5 ± 3.2 Gyr, consistent with but not constraining the age of the Galaxy determined from other indicators.

The problems and prospects of U and Th abundances are considered well in Hill et al. (2002) and Schatz et al. (2002) and will not be repeated here. The actinide boost problem effectively forces attention on detection of both Th and U for meaningful radioactive cosmochronometry. But the problem is the rarity of U detections even in low metallicity stars with extreme *r*-process enhancements (e.g. $[\text{Eu}/\text{Fe}] > +1$). Only a single U II transition at 3539.5 Å has been detected to date, and it is at most a very weak bump among a clump of lines dominated by two strong Fe I lines as well as weaker Nd II and CN lines. This is shown, for example, in Fig. 10 of Hill et al. (2002), Fig. 9 of Cowan et al. (2002), Fig. 2 of Frebel et al. (2007).

If *r*-process production ratios $[\text{Th}/\text{Eu}]$ cannot be predicted with certainty given the large Periodic Table stretch between elements 63 and 90, can another element closer to Th serve as the stable comparison element? Kratz et al. (2007) suggested that Hf ($Z = 72$) might be a good candidate, as their computations showed that Hf is made in the *r*-process at similar neutron densities to Th (see their Fig. 3). We tested this idea by considering Eu, Hf, Th, and U

abundances reported for these kinds of stars in the literature. In Fig. 23 panel (a) we show that for radioactive elements U and Th, their “absolute” number density ratios $\log \epsilon(\text{U}/\text{Th})^1$ are essentially constant in the high-resolution studies published to date, and Hill et al. (2016) report discovery of a fifth r -rich star that has a nearly identical value of this ratio. In panel (b) we show a similarly tight correlation between the stable rare-earth elements Hf and Eu. Star-to-star scatter increases markedly in ratios $\log \epsilon(\text{Th}/\text{Eu})$ and $\log \epsilon(\text{Th}/\text{Hf})$. Observations are clearly telling us that any actinide boost of the heaviest r -process elements sets in beyond $Z = 72$. Abundance data on 3^{rd} r -process peak elements Os, Ir, Pt ($Z = 76\text{--}78$) and Pb ($Z = 82$); see individual papers cited above, (e.g., Cowan et al., 2005; Plez et al., 2004). But these elements: (i) have detectable transitions only from their neutral species, whereas all other neutron-capture elements with $Z \geq 56$ are represented only by ionized transitions, greatly increasing the derived abundance uncertainties in the comparison; (ii) all of their detectable transitions are in the near-UV or vacuum-UV. Their abundances do correlate with those of other very heavy neutron-capture elements, but do not add effective cosmochronometry information at present.

Moreover, predicted production ratios in the r -process can have significant uncertainties, as very little experimental data exist on nuclei far from the valley of β stability. The influence of these uncertainties have been discussed in several papers published after Th and U detections were announced (e.g., Goriely & Clerbaux, 1999). A good summary of the nuclear issues is in Niu et al. (2009), who considered uncertainties in astrophysical r -process fusion conditions, nuclear mass models, and β -decay rates. They suggest that “the influence from nuclear mass uncertainties on Th/U chronometer can approach 2 Gyr.”; see their Fig. 5, which shows derived ages of HE 1523-091 (Frebel et al., 2007) and CS 31082-001 (Cayrel et al., 2001; Hill et al., 2002) with variations in all of the quantities that can influence the conversion of derived observational U/Th abundance ratios into final age estimates. Their computed mean ages are 11.8 ± 3.7 Gyr for HD 1523-0901 and 13.5 ± 2.9 Gyr for CS 31082-001, consistent with current age estimates of the Galaxy, albeit with substantial error bars.

Cosmochronometry from radioactive elements U and Th is promising, but not precise enough yet to set serious age constraints. Since uncertainties abound in all phases of this exercise, one suspects that a prerequisite for further progress is simply more detections of U in very low metallicity r -process-rich stars, which should naturally have strong Th transitions. One looks forward to more discoveries of more such stars in field star surveys in the near future.

This appears as a good viaticum for future developments, since age-dating methods based on MSTO and/or on the MSK can only be applied to ensemble of stars. The key advantage of the cosmochronometric method is that it can be applied to individual cluster and field stars and it is independent of both

¹ $\log \epsilon A \equiv \log_{10}(N_A/N_H) + 12.0$

distance and reddening. The reader interested in a more detailed discussion concerning age-dating of field stars is referred to Salaris (2016).

5.2 Relative cluster age estimates

Relative cluster ages are used to address different astrophysical problems, e.g. they play a crucial role in investigating the early formation of the Galactic components dominated by old stellar populations (Halo, Bulge). In particular, the spread in relative ages of Halo and Bulge stars is tightly correlated with the timescale of the collapse of the protogalactic cloud. Classical results based on accurate and homogeneous photometry of GGCs suggested that a significant fraction of Galactic globulars are, indeed, coeval (e.g., Buonanno et al., 1998; Rosenberg et al., 1999). There are reasons, mainly kinematic, to believe that the ones that do not follow this trend are clusters that have been accreted.

Cluster ages based on a relative diagnostic (vertical, horizontal) are less prone to systematic uncertainties. The key idea in these methods is to estimate the difference in magnitude between the MSTO and a brighter point that is either independent or mildly dependent on the absolute age of the cluster. This means that they are independent of uncertainties on cluster distance and reddening. In dealing with large homogeneous photometric data sets, the relative ages are also less affected by uncertainties on the photometric zero-point. The pros are also on the theoretical side, since the clock is used, over the entire metallicity range, in relative and not in absolute sense.

The relative cluster ages of GGCs is lively debated in the recent literature due to their impact on the early formation and evolution of the Galactic halo. The new results are based on deep and accurate photometry collected with ACS at HST. On one hand, it has been found by Marín-Franch and collaborators (Marín-Franch et al., 2009) that a sample of 64 GCs, covering a broad range in metallicity, in Galactocentric distance and in kinematic properties, show a bi-modal distribution. The former group is coeval within the errors, i.e. its mean age is ~ 12.8 Gyr with a small dispersion (5%). The latter group is more metal-poor and follows an age–metallicity relation. This group might be associated to dwarf galaxies that have been accreted into the Halo as supported by their kinematic properties. The top panel of Fig. 24 summarizes the results obtained by Marín-Franch et al. (2009).

On the other hand, based on independent ages estimated by Vandenberg et al. (2013) and Leaman et al. (2013), it was found that GGCs display a clear dichotomy, since at fixed cluster age there are two groups of GCs with roughly 0.4 dex of difference in metallicity (see bottom panel of Fig. 24). These two groups seem to follow two different, and well defined, age–metallicity relations. Leaman et al. (2013) also suggested that the metal-poor group were accreted, while the metal-rich ones are the truly globulars formed *in situ*. In this context it is worth mentioning that the globulars and the optical photometry adopted by Leaman et al. (2013) significantly overlap with the sample adopted by Marín-Franch et al. (2009). We note here that data plotted in Fig. 24 are only

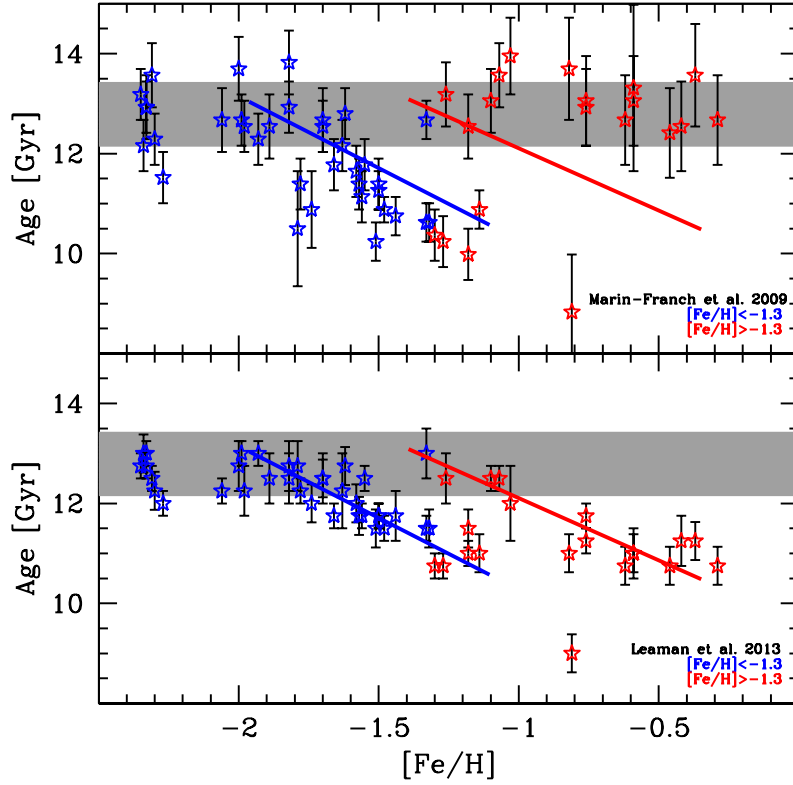


Fig. 24 Top: Relative age estimates of Galactic globular clusters according to Marín-Franch et al. (2009), these have been scaled to 12.8 Gyr, i.e. a mean age coming assuming isochrones from Dotter et al. (2007). Clusters more metal-poor than $[Fe/H]=-1.3$ were plotted as blue stars, while those that are more metal-rich as red stars. The blue and the red lines display the age–metallicity relations estimated by Vandenberg et al. (2013) and by Leaman et al. (2013). The metallicities of the GCs are in the Carretta et al. (2009) metallicity scale. The grey area shows the $\pm 1\sigma$ uncertainty in the age estimate. Bottom: Same as the top, but for the absolute age estimates by Vandenberg et al. (2013) and used in Leaman et al. (2013). This sample includes the GCs observed by Marín-Franch et al. (2009) and plotted on the top panel. However, we have plotted only GGCs in common between the two studies.

those in common between the two studies and a glance to the data indicates a significant difference in their age determination. In particular, Fig. 24 shows several interesting features worthy of discussion.

i) Absolute age estimates provided by VandenBerg et al. (2013) (VB) are, at fixed metal content, more precise than the relative age estimates provided by Marín-Franch et al. (2009) (MF). The dispersion in age in the former sample is $\sim 17\%$ smaller than the latter one over the entire metallicity range.

ii) The metal-poor globulars seem to show an age-metallicity relation independently of the approach adopted to estimate the absolute cluster ages. The relation drawn through the VB’s ages (blue solid line) is also a reasonable ‘eye’ fit to the MF’s age estimates. The quoted samples also show evidence of a flattening of the quoted age-metallicity relation when moving from metal-poor ($[\text{Fe}/\text{H}] \sim -2$) to more metal-poor GCs.

iii) The more metal-rich GCs display a different trend in the two different absolute age estimates. The more metal-rich GCs in the MF sample are within the errors coeval, while in the VB estimates they show a slope that is quite similar to the slope of the more metal-poor GCs, but shifted by 0.4 dex in metallicity.

The above findings clearly indicate that the main difference between the MF and the VB analysis is in the age estimates of metal-rich GCs. Note that to overcome possible deceptive uncertainties on the cluster iron abundance we adopted the homogeneous metallicity scale provided by Carretta et al. (2009). The current uncertainties on cluster iron abundances are on average smaller than 0.1 dex (Gratton et al., 2004). To unveil possible deceptive systematics either in age-dating globulars or in their metallicity scale the use of NIR diagnostics appears very promising. This applies not only to NIR photometry to use the MSK (see § 5.4), but also to high-resolution NIR spectroscopy to use different sets of iron and α -element lines.

5.2.1 The empirical routes for relative age estimates

The two most popular approaches adopted to estimate relative ages are the vertical and the horizontal photometric methods. The key advantages of these approaches are that they are independent of uncertainties affecting the distance modulus and the cluster reddening.

i) *Vertical Method* – The vertical method relies on the difference in magnitude between the HB luminosity level and the MSTO. The HB luminosity level is typically chosen across the RR Lyrae instability strip. The former anchor is assumed to be independent of age, while the latter is age dependent. In applying this method there are a number of caveats. The main one is that it is mainly based on visual magnitudes, since at shorter (U,B) and at longer (R,I) wavelengths the HB shows a well defined negative/positive slope when moving from red to blue HB stars. This means that the anchor to the middle of the RR Lyrae instability strip might be affected by systematic errors, due to the quoted problems with the HB morphology. Moreover, this approach is also hampered by the lack either of RR Lyrae stars or of accurate and homogeneous

multi-band photometry for cluster RR Lyrae stars. It is worth mentioning that the cluster age is considered to be one of the main culprits in the variation of the HB morphology (second parameter problem) when moving from more metal-poor to more metal-rich GCs. In case the cluster age is confirmed to be the second parameter, then the ages based on the vertical method would be affected by systematic errors. In particular, a decrease in the age of the progenitor causes a decrease in the HB luminosity level, therefore smaller vertical parameters, and in turn systematically younger ages. This effect becomes more relevant for stellar structures at the transition between forming or not forming an electron degenerate helium core. This means the young tail in the age distribution of GCs (see Fig. 8). Note that a systematic decrease in age typically means a redder HB morphology, thus suggesting once again that more metal-rich clusters are more prone to possible systematic age uncertainties.

ii) *Horizontal Method* – The horizontal method relies on the difference in color between the MSTO and the base of the red giant branch. The empirical estimate of the latter reference point is not trivial in the V,I bands. Therefore, it was suggested to use the difference in color between the MSTO and the color of the RGB at a luminosity level that is 2.5 magnitudes brighter than the MSTO (Buonanno et al., 1998; Rosenberg et al., 1999). This approach has the same advantages of the vertical method, since it is independent of uncertainties on the cluster distance and reddening. Moreover, the reference point along the RGB is less affected by age effects and the RGB morphology is well defined in GGCs. However, the use of the color (horizontal method) instead of the magnitude (vertical method) together with the dependence of predicted effective temperatures at the MSTO, and in particular along the RGB, by the adopted mixing length parameter, are a source of further concern. The color-temperature relations predicted by atmosphere models are also less accurate when compared with the bolometric corrections. Note that this limitation becomes more severe when moving from the metal-poor to the metal-rich regime (Tognelli et al., 2015). Moreover, it is worth mentioning that the ratio between the duration of the sub-giant phase (hydrogen thick shell burning) and the MSTO age is not constant when moving from metal-poor to metal-rich stellar structures (Salaris & Weiss, 1997). Furthermore, the slope of the RGB depends on the metal content, therefore, the difference in color with the MSTO steadily decreases when moving from more metal-poor to more metal-rich globulars.

5.3 A new approach for absolute age estimates

During the last few years it has been suggested a new vertical method to estimate the absolute age of stellar systems (Bono et al., 2010). It relies on the difference either in magnitude or in color between the MSTO and a well defined knee in the low-mass regime of the main sequence (MSK). The MSK has already been detected in several GCs – ω Cen (Pulone et al., 1998); M4 (Pulone et al., 1999; Milone et al., 2014; Braga et al., 2015; Correnti et al.,

2016); NGC 3201 (Bono et al., 2010); 47 Tuc (Lagioia et al., 2014; Correnti et al., 2016); NGC 2808 (Milone et al., 2012; Massari et al., 2016a); M71 (Di Cecco et al., 2015); NGC 6752 (Correnti et al., 2016)), in intermediate-age open clusters (Sarajedini et al., 2009b; An et al., 2008, 2009) and in the field of the Galactic bulge (Zoccali et al., 2000) by using either near-infrared (NIR) and/or optical–NIR photometry.

Empirical and theoretical evidence indicates that this feature is mainly caused by the collisionally induced absorption of H_2 at NIR wavelengths (Saumon et al., 1994) in the atmosphere of cool dwarfs. The shape of the bending in NIR and optical–NIR CMDs depends on the metal content, but the magnitude of the knee seems to be independent of cluster age and of metallicity (magnitude in K-band of ~ 3.5 mag). This means that the difference in magnitude between the MSTO and the MSK should be a robust diagnostic to constrain the absolute cluster age. The new diagnostic shares the same positive features than the classical vertical and horizontal methods. It is independent of uncertainties in cluster distance and reddening and minimally affected by uncertainties in photometric zero-point.

The key advantages of the MSK when compared with the classical vertical and horizontal methods are the following:

i) *The MSK is a faint but well defined feature* – The reference magnitude for the MSK is fainter than the MSTO, this implies larger photometric uncertainties for individual stars than when belonging to brighter features (RGB, HB). However, the number of faint, low mass stars ($\leq 0.5 M_{\odot}$) is intrinsically larger than that of more massive and brighter stars. Furthermore, these stars are in their slow central hydrogen burning phase, thus they are more populous than in subsequent evolved phases. As a result, old, intermediate and young stellar systems always display a well sampled faint MS, whereas: a) the HB is less populous because it is populated by stars in their central helium burning phase and, even more, this feature shows up only in old stellar systems and depends on a number of parameters, including the metallicity; b) the RGB is typical of stellar systems that are either old or of intermediate age, and again the difference in color with the MSTO depends on the metallicity.

The main consequence is that the MSK can be easily identified in all the stellar systems, provided that photometric data sets are pushed to reach very faint magnitudes, while the HB and the RGB detection/morphology strongly depend on the evolutionary properties of the underlying stellar population.

ii) *The MSK is less affected by theoretical uncertainties* – The MSK only relies on the physics of hydrogen burning phase, while the vertical and the horizontal methods are affected by uncertainties in extra-mixing (RGB, HB), in microphysics (electron degeneracy, conductive opacities, 3α and $^{12}C(\alpha, \gamma)^{16}C$ nuclear reaction rates) and in dealing with the transition from the core helium flash to the core helium burning (ZAHB, Sweigart et al., 2004).

Furthermore, the MSK together with the vertical method are independent of the theoretical uncertainties plaguing the color–temperature transformations required in the horizontal method. The same outcome applies to the

dependence on the adopted mixing length parameter. According to theory, MS stellar structures with a stellar mass of $M \sim 0.5-0.4 M_{\odot}$ are minimally affected by uncertainties in the treatment of convection, since they are almost entirely convective and the convective transport is nearly adiabatic (Saumon & Marley, 2008).

iii) *The MSK has a lower global error budget* – Recent empirical evidence indicates that the MSK provides absolute cluster ages that are a factor of two more precise when compared with the classical method of the MSTO (Bono et al., 2010; Sarajedini et al., 2009a; Di Cecco et al., 2015; Monelli et al., 2015; Massari et al., 2016a; Correnti et al., 2016). Moreover, preliminary findings suggest that the correlation between the MSK and the cluster age is linear over the age range typical of old open cluster (a few Gyrs) to GGCs. We still lack a detailed theoretical investigation to constrain the dependence of the MSK on the chemical composition (metals, helium) when moving from optical to NIR and optical/NIR CMDs.

The main cons in dealing with the MSK is that the identification of the knee requires accurate and deep photometry in crowded stellar fields. However, the advent of HST and of modern Adaptive Optics (AO) assisted NIR instrumentation overcame this problem. The MSK is a feature that can be detected and used in both optical and NIR bands, whereas the classical vertical and horizontal methods are robust age diagnostics only in optical CMDs. Accurate and deep NIR CMDs show that HB stars are far from being horizontal. They become systematically fainter when moving from cool to hot and extreme HB stars (positive slope Del Principe et al., 2006; Coppola, 2011; Milone et al., 2013; Stetson et al., 2014). The same problem shows up in CMDs based on near UV and far UV bands (negative slope, Ferraro et al., 2012). This means that the identification of the HB luminosity level needs a further anchor in color along the HB, difficult to be uniquely identified. On the other hand, the difference in color between the MSTO and the RGB, required by the horizontal method, is hampered by the fact that MSTO and RGB have almost the same color in NIR bands. This means that the difference in color is steadily decreasing (Coppola, 2011; Stetson et al., 2014) when moving from optical to NIR.

NIR photometry is going to be exploited even more in the near future when sophisticated AO will allow us to reach the diffraction limit of ground based extremely large telescopes (Diolaiti et al., 2016) and from the space with JWST. The use of new observables also means the opportunity to constrain possible systematics in evolutionary diagnostics currently adopted.

5.3.1 *The absolute age of M15*

To provide a new and independent absolute age estimate of the GC M15 (NGC 7078), (Monelli et al., 2015) have collected collected AO images of the GC M15 (NGC 7078) using the First Light AO (FLAO, Esposito et al., 2012)

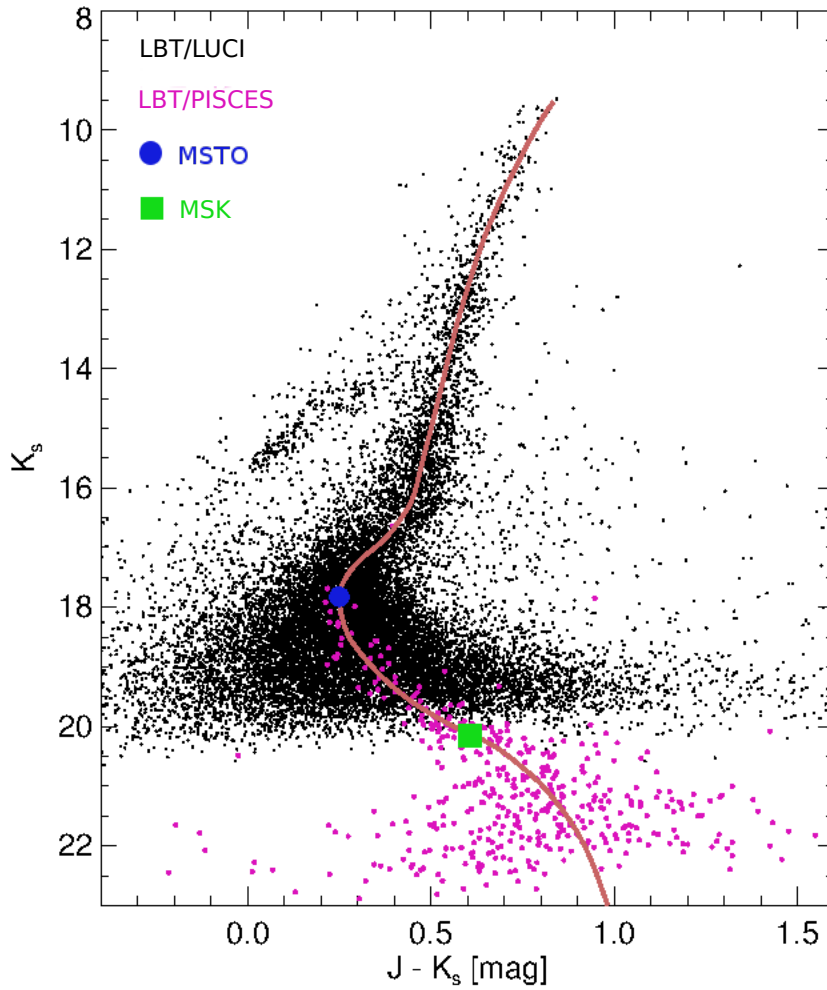


Fig. 25 Near-Infrared (K , $J - K$) CMD of the Galactic globular M15, based on images collected with LBT (black dots: LUCI; red dots: PISCES). The orange solid line shows the cluster ridge line adopted to determine the position of both MSTO (blue circle) and of the MSK (green square).

operating at the Large Binocular Telescope (LBT). We remember here that M15 is located at ~ 10 Kpc and it is affected by moderate extinction ($E(B-V)=0.08$, (Harris, 1996, updated 2010 version) thus with current AO assisted 10 m telescopes we do expect to detect the MSK. Interestingly, M15 is supposed to be one of the oldest and most metal poor ($[Fe/H] \sim -2.4$) GCs of the Milky Way Halo.

FLAO data have been taken with the NIR high resolution imager PISCES (pixel scale=0.0193"/pix) in J and K_s bands. Due to the highly structured and asymmetric PSF shape, the data reduction was successfully performed with ROMAFOT suite of programs (see details in Fiorentino et al., 2014; Monelli et al., 2015). A natural guide star (NGS) of $R=12.9$ mag has been used to close the AO loop on a field located at $\sim 3'$ from the cluster center. This field was sufficiently uncrowded to allow us to reach a very deep K_s band magnitude of ~ 22 mag, see Fig. 25. This limiting magnitude allowed us to measure the location of the MSK; see Table 3 in Monelli et al. (2015). Note that the detection of faint stars in crowded stellar fields as the center of GCs is severely hampered by the large number of bright stars. However, as it is shown in Fig. 25, given the small PISCES field of view (FoV) $\sim 20''$ and the radial distance from the cluster center, we do not have sufficient sampling of the MSTO magnitude. We have used LUCI1 data (FoV= $4' \times 4'$) to properly determine the location of the MSTO. These LUCI1 data have also been used to perform a proper calibration of PISCES data to the 2MASS photometric system.

After measuring the difference MSTO-MSK, we are ready to compute the absolute age of M15. We compare this number with theoretical relations derived using a set of evolutionary isochrones provided by Vandenberg et al. (2014b) that relate the variation of MSTO-MSK with the absolute ages. Using only NIR, we derived an absolute age for M15 of 13.7 ± 1.4 Gyr, which is compatible, but with a smaller uncertainty, to that obtained using the classical MSTO method in NIR (14.0 ± 3.1 Gyr) or in purely optical HST bands (12.8 ± 2.0 Gyr). This old age provides an upper limit to the age of the Universe and a lower limit to the Hubble constant H_0 , since the former parameter is roughly the inverse of the latter one (Gratton et al., 2003; Monelli et al., 2015).

5.4 Conclusions and final remarks

There is mounting evidence of a difference between estimates of a Hubble constant based on direct measurements (Cepheids plus supernovae: Riess et al. (2016); Freedman et al. (2010), Beaton this conference) and indirect methods (CMD, BAO, lensing, Suyu et al. (2013); Bennett et al. (2014); Calabrese et al. (2015), Planck collaboration 2015). This critical issue has been addressed in several recent papers suggesting a difference that ranges from almost 2σ (Efstathiou, 2014) to more than 3σ (Riess et al., 2011, 2016). The quoted uncertainties on the Hubble constant, once confirmed, can open the path to new physics concerning the number of relativistic species and/or the mass of neutrinos Dvorkin et al. (2014); Wyman et al. (2014); Luković et al. (2016). Moreover, the quoted range in H_0 implies an uncertainty on the age of the universe t_0 of the order of 2 Gyr. This uncertainty has a substantial impact not only on galaxy formation and evolution, but also on the age of the most

ancient stellar systems, i.e. the globular clusters can play a crucial cosmological role.

Based on the tantalizing evidence that stellar age is not an observable, the different stellar “clocks” that can be applied to date globular clusters provide the unique opportunity to constrain the micro- and the macro-physics adopted to construct evolutionary models. This comparison becomes even more rewarding when comparing main sequence stellar structures with white dwarf models. It might be possible that in the era of “precision cosmology” we could use cosmological parameters to constrain the physics of stellar interiors. In the meantime, it is clear that calibrating clusters to which we can apply different age diagnostics (MSTO, MSK, white dwarf cooling sequence, cosmochronometry) become fundamental astrophysical and cosmological laboratories.

In this investigation we reviewed the most popular methods to estimate both relative and absolute cluster ages. We focussed our attention on the error budget and critically discussed pros and cons of the different age diagnostics. In particular, we outlined the key advantages in using a new NIR age diagnostic – the main sequence knee – and its application to M15. The main limitation being the faintness of this anchor. However, there are two new observing facilities that are going to play a fundamental role in the use of the MSK.

i) *Multi-conjugated adaptive optics* – The development of multi-conjugated adaptive optics systems at the 8-10 m class telescopes is a real quantum jump. They provide NIR images that approach the diffraction limit of a field of view of the order of one arcmin. This means that they can provide accurate and deep NIR CMDs of the innermost crowded regions of GCs. Recent findings based on NIR images collected with GEMS at GEMINI indicate that the mix between NGS and lasers allow us to reach the MSK in a sizable sample of Galactic globulars Massari et al. (2016a); Turri et al. (2016). The empirical scenario becomes even more compelling if we take account for the next generation of NIR detectors AO assisted at VLT (ERIS). This instrument will simultaneously cover NIR bands and the L-band, and in turn, the unique opportunity to identify the MSK in the most crowded and most reddened regions of the Galactic Bulge.

ii) *JWST* – JWST is going to revolutionize the view of resolved stellar populations in the nearby Universe. The coupling between field of view and NIR/MIR bands would provide the unique opportunity to identify the MSK in a significant fraction of nearby dwarf galaxies. This means the opportunity to determine homogeneous ages for old stars in old stellar systems (dwarfs, globulars) to investigate whether they formed, as suggested by cosmological models, at the same epoch.

The cosmic distance scale and the age-dating of nearby stellar systems have been for more than half a century the two fundamental pillars on which quantitative astrophysics build up. At the beginning of the new millennium they are waiting for massive solidification. The near future appears quite bright not only for the next Gaia data releases, but also for the near future ground-based (LSST, ELTs) and space observing facilities (JWST, WFIRST, EUCLID). The

same outcome applies for the wide spectroscopic surveys in optical and NIR regimes (DESI, PFS, 4MOST, MOONS-GAL, APOGEE, WEAVE).

References

- Alcock, C., Allsman, R. A., Axelrod, T. S., Bennett, D. P., Cook, K. H. et al., 1995, *AJ*, 109, 1653
- Alcock, C., Allsman, R. A., Alves, D. R., Axelrod, T. S., Becker, A. C. et al., 1998, *ApJ*, 492, 190
- Alcock, C., Allsman, R. A., Alves, D. R., Axelrod, T. S., Becker, A. C., Bennett, D. P., Cook, K. H., Drake, A. J., Freeman, K. C., Geha, M., Griest, K., Lehner, M. J., Marshall, S. L., Minniti, D., Nelson, C. A., Peterson, B. A., Popowski, P., Pratt, M. R., Quinn, P. J., Stubbs, C. W., Sutherland, W., Tomaney, A. B., Vandehei, T., Welch, D. L., MACHO Collaboration, 2000, *ApJ*, 541, 734
- Alonso-García, J., Mateo, M., Sen, B., Banerjee, M., Catelan, M., Minniti, D. & von Braun, K. 2012, *AJ*, 143, 70
- An, D., Johnson, J. A., Clem, J. L. et al. 2008, *ApJS*, 179, 326
- An, D., Pinsonneault, M. H., Masseron, T. et al. 2009, *ApJS*, 700, 523
- Alves-Brito, A., Meléndez, J., Asplund, M., Ramírez, I., Yong, D. 2010, *A&A*, 513, 35
- Amôres, E. B., López-Corredoira, M., González-Fernández, C., 2013, *A&A*, 559, 11
- Arp, H., 1962, *ApJ*, 135, 971
- Anderson, J. 2002, *ASPCS*, eds: van Leeuwen, F., Hughes, J. D., Piotto, G. 265, 87
- Athanassoula, E. 2005, *MNRAS*, 358, 1477
- Baade, W., 1946, *PASP*, 58, 249
- Baade, W., 2951, *Pub. Obs. Univ. Michigan*, 10, 7
- Baade, W., 1958, *Ricerche Astronomiche, Specola Vaticana*, Proceedings of the conference sponsored by the Pontifical Academy of Science and the Vatican Observatory, 5
- Babusiaux, C. & Gilmore, G. 2005, *MNRAS*, 358, 1309
- Babusiaux, C., Gómez, A., & Hill, V. et al. 2010, *A&A*, 519, A77
- Babusiaux, C., Katz, D., & Hill, V. et al. 2014, *A&A*, 563, A15
- Baker, M., & Willman, B. 2015, *AJ*, 150, 160
- Bastian, N., Covey, K. R. & Meyer, M. R. 2010, 48, 339
- Bedin, L. R. Piotto, G. Anderson, J. Cassisi, S. King, I. R. Momany, Y. & Carraro, G. 2004, *ApJL*, 605, 125
- Beers, T. C., Preston, G. W. & Shectman, S. A. 1992, *AJ*, 103, 1987
- Belokurov, V., Zucker, D. B., Evans, N. W., et al. 2007, *ApJ*, 654, 897
- Benjamin, R. A., Churchwell, E., Babler, B. L., Indebetouw, R., Meade, M. R., Whitney, B. A., Watson, C., Wolfire, M. G., Wolff, M. J., Ignace, R., Bania, T. M., Bracker, S., Clemens, D. P., Chomiuk, L., Cohen, M., Dickey, J. M.,

- Jackson, J. M., Kobulnicky, H. A., Mercer, E. P., Mathis, J. S., Stolovy, S. R., Uzpen, B. 2005, *ApJL*, 630, 149
- Bender R., Burstein D., Faber S. M., 1993, *ApJ*, 411, 15
- Bensby, T., Feltzing, S., Lundström, I., 2003, *A&A*, 410, 527
- Bensby, T., Zenn, A. R., Oey, M. S., Feltzing, S., 2007, *ApJL*, 663, 13
- Bensby, T., Yee, J. C., Feltzing, S., et al., 2013, *A&A*, 549,147
- Bensby, T., Feltzing, S., Gould, A., et al., 2017 *arXiv:1702.02971*
- Bennett C. L., Larson D., Weiland J. L. and Hinshaw G. 2014 *ApJ* 794 135
- Bertelli, G. Nasi, E. Girardi, L.& Marigo, P. 2009, *A&A*, 508, 355
- Bhardwaj, A., Rejkuba, M., Minniti, D., Surot, F., Valenti, E., Zoccali, M., Gonzalez, O. A., Romaniello, M., Kanbur, S. M. & Singh, H. P. 2017, *A&A*, 605, 100
- Binney, J., Gerhard, O. E., Stark, A. A., Bally, J., Uchida, K. I. 1991, *MNRAS*, 252, 210
- Binney, J., Gerhard, O., Spergel, D. 1997, *MNRAS*, 288, 365
- Bica, E., Ortolani, S., Barbuy, B. 2016, *PASA*, 33, e028
- Bissantz, N., & Gerhard, O. 2002, *MNRAS*, 330, 591
- Blitz, L. & Spergel, D. N. 1991, *ApJ*, 379, 631
- Blum, R. D., 1995, *ApJL*, 444, L89
- Boettcher, E., Willman, B., Fadely, R., et al. 2013, *AJ*, 146, 94
- Bono, G., Caputo, F., Castellani, V., et al. 2003, *MNRAS*, 344, 1097
- Bono, G., Stetson, P. B., Sanna, N., et al. 2008, *ApJL*, 686, 87
- Bono, G., Stetson, P. B., Vandenberg, D., et al. 2008, *ApJL*, 708, 74
- Bono, G., Salaris, M. Gilmozzi, R. 2013, *A&A*, 549, 102
- Braga, V. F. et al. 2015, *ApJ*, 799, 165
- Brocato, E. Castellani, V. Romaniello, M., 1999, *A&A*, 345, 499
- Brown, T. M., Ferguson, H. C., Smith, E., Kimble, R. A., Sweigart, A. V., Renzini, A., Rich, R. M., Vandenberg, D. A. 2003, *ApJL*, 592, L17
- Brown, T. M., Smith, E., Ferguson, H. C., Rich, R. M., Guhathakurta, P., Renzini, A., Sweigart, A. V., Kimble, R. A. 2006, *ApJ*, 652, 323
- Brown, T. M., Sahu, K., Ferguson, J., Tumlinson, J., et al. 2010, *ApJL*, 725, L19
- Bruzual, G. & Charlot, S. 2003, *MNRAS*, 344, 1000
- Boylan-Kolchin, M., Bullock, J. S., & Kaplinghat, M. 2012, *MNRAS*, 422, 1203
- Buonanno, R., Corsi, C. E., Pulone, L., Fusi Pecci, F. & Bellazzini, M. 1998, *A&A*, 333, 505
- Bureau, M., Athanassoula, E., 2005, *ApJ*, 626, 159
- Butcher, H. R., 1987, *Nature*, 328, 127
- Cabrera-Lavers, A., Hammersley, P. L., González-Fernández, C., López-Corredoira, M., Garzón, F., Mahoney, T. J. 2007, *A&A*, 465, 825
- Cabrera-Lavers, A., González-Fernández, C., Garzón, F., Hammersley, P. L., López-Corredoira, M. 2008, *A&A*, 491, 781
- Calabrese E., Carbone C., Fabbian G. Baldi, M. & Baccigalupi, C. 2015 *JCAP* 3 49
- Calamida, A., Strampelli, G., Rest, A., et al. 2017, *AJ*, 153, 175

- Cao, L., Mao, S., Nataf, D., Rattenbury, N. J., Gould, A. 2013, *MNRAS*, 434, 595
- Castellani, V. degl'Innocenti, S. & Marconi, M. 2013, *MNRAS*, 303, 265
- Catchpole, R. M., Whitelock, P. A., Feast, M. W., Hughes, S. M. G., Irwin, M., Alard, C. 2015, *MNRAS*, 455, 2216
- Catelan, M., 2004, *ApJ*, 600, 409
- Catelan, M., Pritzl, B. J., & Smith, H. A., 2004, *ApJS*, 154, 633
- Carlin, J. L., Grillmair, C. J., Muñoz, R. R., Nidever, D. L., & Majewski, S. R. 2009, *ApJL*, 702, L9
- Carollo, D., Beers, T.C., Lee, Y.S. et al. 2008, *Natur*, 451, 216
- Carretta, E. Bragaglia, A. Gratton, R. D'Orazi, V. & Lucatello, S. 2009, *A&A*, 508, 695
- Cassisi, S., Potekhin, A. Y. Pietrinferni, A. Catelan, M. & Salaris, M. 2007, *ApJ*, 661, 1094
- Cassisi, S., Salaris, M., Pietrinferni, A., Piotto, G., Milone, A. P., Bedin, L. R., & Anderson, J. 2008, *ApJ*, 672, L115
- Cayrel, R., Hill, V., Beers, T. C., et al. 2001, *Nature*, 409, 691
- Chaboyer, B., et al. 2017, *ApJ*, 835, 152
- Chemin, L., Renaud, F., Soubiran, C. 2015, *A&A*, 578, A14
- Chiosi, C. & Maeder, A. 1986, *ARA&A*, 24, 329
- Churchwell, E., Babler, B. L., Meade, M. R., Whitney, B. A., Benjamin, R., Indebetouw, R., Cyganowski, C., Robitaille, T. P., Povich, M., Watson, C., Bracker, S. 2009, *PASP*, 121, 213
- Ciocio, F. degl'Innocenti, S. & Ricci, B. 1997 *A&AS* 123
- Clarkson, W., Sahu, K. Anderson, J. et al. 2008, *ApJ*, 684, 1110
- Clarkson, W. I., Sahu, K. C., Anderson, J., Rich, R. M., Smith, T. E., Brown, T. M., Bond, H. E., Livio, M., Minniti, D., Renzini, A., Zoccali, M., 2011, *ApJ*, 735, 37
- Clementini, G., Gratton, R., Bragaglia, A., et al. 2003, *AJ*, 125, 1309
- Clementini, G., Cignoni, M., Contreras Ramos, R., et al. 2012, *ApJ*, 756, 108
- Clementini, G. 2016, *CoKon*, 105, 3
- Clement, C. M., Muzzin, A., Dufton, Q., et al. 2001, *AJ*, 122, 2587
- Collinge, M. J., Sumi, T., & Fabrycky, D., 2006, *ApJ*, 651, 197
- Cohen, J. G., 1978, *ApJ*, 223, 487
- Coppola, G., Dall'Ora, M., Ripepi, V., et al. 2011, *MNRAS*, 416, 1056
- Correnti, M., Gennaro, M., Kalirai, J. S., Brown, T. M. & Calamida, A. 2016, *ApJ*, 823, 18
- Courteau, S., Cappellari, M., de Jong, R. S., Dutton, A. A., Emsellem, E., Hoekstra, H., Koopmans, L. V. E., Mamon, G. A., Maraston, C., Treu, T., Widrow, L. M. 2014, *Reviews of Modern Physics*, 86, 47
- Cowan, J. J., McWilliam, A., Sneden, C. Burris, D. L. 1997, *ApJ*, 480, 246
- Cowan, J. J. Sneden, C. Burles, S. et al. 2002, *ApJ*, 572, 861
- Cowan, J. J., Sneden, C. Beers, T. et al. 2002, *ApJ*, 627, 238
- Cunha, K., Smith, V. V. 2006, *ApJ*, 651, 491
- Dall'Ora, M., Clementini, G., Kinemuchi, K., et al. 2006, *ApJL*, 653, L109
- Dall'Ora, M., Kinemuchi, K., Ripepi, V., et al. 2012, *ApJ*, 752, 42

- Debattista, V. P., Mayer, L., Carollo, C. M., Moore, B., Wadsley, J., Quinn, T. 2006, *ApJ*, 645, 209
- Debattista, V. P., Ness, M., Gonzalez, O. A., Freeman, K., Zoccali, M., Minniti, D. 2017, *MNRAS*, 469, 1587
- Del Principe, M., Piersimoni, A. M., Storm, J. et al. 2006, *ApJ*, 652, 362
- Dékány, I., Minniti, D., Catelan, M., Zoccali, M., Saito, R. K., Hempel, M., Gonzalez, O. A. 2013, *ApJL*, 776, L19
- degl’Innocenti, S. Fiorentini, G. Ricci, B. & Villante, F. L. 2004, *Physics Letters B*, 590, 13
- de Vaucouleurs, G., 1964, *IAU Symposium*, 20, 195, eds Kerr, F.J.
- Di Cecco, A. et al. 2015, *AJ*, 150, 51
- Di Matteo, P. et al. 2015, *A&A*, 577, 1
- Diemand, J., Kuhlen, M., & Madau, P. 2007, *ApJ*, 667, 859
- Diolaiti, E., Ciliegi, P., Abicca, R. et al. 2016, *SPIE*, 9909, 99092D
- Djorgovski, S. & Davis, M. 1987, *ApJ*, 313, 59
- Dressler, A., Lynden-Bell, D., Burstein, D., et al. 1987, *ApJ*, 313, 42
- Dong, H., Schödel, R., Williams, B. F. et al. 2017, *MNRAS*, 471, 3617
- Dotter, A., Chaboyer, B., Jevremović, D. et al. 2007, *AJ*, 134, 376
- Dotter, A., Sarajedini, A., & Anderson, J. 2011, *ApJ*, 738, 74
- Duc, P.-A., Paudel, S., McDermid, R. M., et al. 2014, *MNRAS*, 440, 1458
- Dvorkin C., Wyman M., Rudd D. H. and Hu W. 2014 *PhRvD* 90 083503
- Dwek, E., Arendt, R. G., Hauser, M. G., Kelsall, T., Lisse, C. M., Moseley, S. H., Silverberg, R. F., Soderoski, T. J., Weiland, J. L. 1995, *ApJ*, 445, 716
- Efstathiou G. 2014, *MNRAS*, 440, 1138
- Esposito, S., Riccardi, A., Pinna, E. et al. 2014, *SPIE*, 8447, 84470U
- Feltzing, S. & Gilmore, G. 2000, *A&A*, 355, 949
- Ferraro, F.R. et al 2009, *Nature*, 462, 483
- Ferraro, F.R., Lanzoni, B., Dalessandro, E. et al 2009, *Nature*, 492, 393
- Ferreras, I., Wyse, R. F. G., Silk, J. 2003, *MNRAS*, 345, 1381
- Fiorentino, G., Ferraro, I., Bono, G., et al. 2014, *SPIE*, 9148, 3U
- Fiorentino, G., Bono, G., Monelli, M., et al. 2015, *ApJL*, 798, L12
- Fiorentino, G., Monelli, M., Stetson, P. B., et al. 2016, arXiv:1612.02991, *A&A accepted*
- Frebel A., Christlieb, N., Norris, J. E. et al., 2007, *ApJ*, 660, 117
- Freedman W. L. & Madore B. F., 2010, *ARA&A*, 48, 673
- Freeman, K., Ness, M., Wylie-de-Boer, E., Athanassoula, E., Bland-Hawthorn, J., Asplund, M., Lewis, G., Yong, D., Lane, R., Kiss, L. & Ibata, R. 2013, *MNRAS*, 428, 3660
- Frogel, J. A., Whitford, A. E., Rich, R. M. 1984, *AJ*, 89, 1536
- Fulbright, J. P., McWilliam, A., & Rich, R. M. 2007, *ApJ*, 661, 1152
- Gallart, C., Zoccali, M., Aparicio, A., 2005, *Annual review of astronomy and astrophysics*, 43, 387
- García Pérez, A. E., Cunha, K., Shetrone, M., et al. 2013, *ApJ*, 767, L9
- Garofalo, A., Cusano, F., Clementini, G., et al. 2013, *ApJ*, 767, 62
- Gennaro, M. Prada Moroni, P. G. & Degl’Innocenti, S. 2010, *A&A*, 518, 13
- Gerhard, O. & Martinez-Valpuesta, I. 2012, *ApJL*, 744, 8

- Girardi, L. 2016, *ARA&A*, 54, 95
- Gonzalez, O. A., Rejkuba, M., Zoccali, M., Valenti, E., Minniti, D. 2011, *A&A*, 534, 3
- Gonzalez, O. A., Rejkuba, M., Minniti, D., Zoccali, M., Valenti, E., Saito, R. K. 2011, *A&A*, 534, 14
- Gonzalez, O. A., Rejkuba, M., Zoccali, M., Hill, V., Battaglia, G., Babusi-
aux, C., Minniti, D., Barbuy, B., Alves-Brito, A., Renzini, A., Gomez, A.,
Ortolani, S. 2011, *A&A*, 530, 54
- Gonzalez, O.A., Zoccali, M., Vasquez, S. et al. 2015, *A&A* 584, 46
- Gran, F., Minniti, D., Saito, R. K., et al. 2016, *A&A*, 591, 145
- Gratton, R.G., et al. 2003, *A&A*, 408, 529
- Gratton, R.G., Sneden, C., Carretta, E., 2004, *ARA&A*, 42, 385
- Gratton, R. G. Carretta, E. & Bragaglia, A. 2012, *A&A Rev.*, 20, 50
- Greco, C., Dall’Ora, M., Clementini, G., et al. 2008, *ApJL*, 675, L73
- Griffin, R., Gustafsson, B., Vieira, T., & Griffin, R. 1982, *MNRAS*, 198, 637
- Grillmair, C. J., & Carlin, J. L. 2016, *Astrophysics and Space Science Library*,
420, 87
- Goriely, S. & Clerbaux, B., 1999, *A&A*, 346, 798
- Gustafsson, B. Edvardsson, B. Eriksson, K. Jørgensen, U. G. Nordlund, Å. &
Plez, B. 2008, *A&A*, 486, 951
- Habing, H. J., Sevenster, M. N., Messineo, M., van de Ven, G., Kuijken, K.
2006, *A&A*, 458, 151
- Han, C. & Gould, A. 1995, *ApJ*, 449, 521
- Hansen, B. M. S. Richer, H. B. Fahlman, G. G. et al. 2004, *ApJS*, 155, 551
- Hansen, B. M. S. 2004, *Phys. Rev.*, 399, 1
- Harris, W. E. 1996, *AJ*, 112, 1487
- Hayek, W., Wiesendahl, U., Christlieb, N. et al. 2009, *A&A*, 504, 511
- Haywood, M., Di Matteo, P., Snaith, O., Calamida, A. 2016, *A&A*, 593, 82
- Hill, V., Plez, B. Cayrel, R. et al. 2002, *A&A*, 387, 560 [archiv:1608.07463](https://arxiv.org/abs/1608.07463)
- Hill, V., Lecureur, A., Gomez, A. et al. 2011, *A&A*, 534, 80
- Hill, V., Christlieb, N., Beers, T. C. et al. 2016, *A&A*, 534, 80
- Howes, L.M., Asplund, M., Casey, A.R. et al. 2014, *MNRAS*, 445, 4241
- Howes, L.M., Casey, A.R., Asplund, M., et al. 2015, *Natur*, 527, 484
- Howes, L.M., Asplund, M., Keller, A.C. et al. 2016, *MNRAS*, 460, 884
- Hoyle, F. 1959, *MNRAS*, 119, 124
- Ibata, R. A., Lewis, G. F., Conn, A. R., et al. 2013, *Nature*, 493, 62
- Indebetouw, R. Mathis, J. S. Babler, B. L., et al. 2005, *ApJ*, 619, 931
- Jester, S., Schneider, D. P., Richards, G. T., et al. 2005, *AJ*, 130, 873
- Johnson, C.I., Rich, R.M., Fulbright, J.P., Valenti, E. & McWilliam, A. 2011,
ApJ, 732, 108
- Johnson, C.I., Rich, R.M., Kobayashi, C., Fulbright, J.P. 2011, *ApJ*, 749, 175
- Johnson, C.I., Rich, R.M., Kobayashi, C., Kunder, A., Pilachowski, C., Koch,
A. & De Propris, R. 2013a, *ApJ*, 765, 157
- Johnson, C.I., McWilliam, A, & Rich, R.M. 2013b, *ApJ*, 775, 27
- Johnson, C.I., Rich, R.M., Kobayashi, C., Kunder, A. & Koch, A. 2014, *AJ*,
148, 67

- Joo, S.-J., Lee, Y.-W., Chung, C. 2017, *ApJ*, 840, 98
- Jurcsik, J., Revision of the [Fe/H] Scales Used for Globular Clusters and RR Lyrae Variables, *Acta Astronomica*, 45, 653 (1995)
- Jurcsik, J., & Kovács, G., Determination of [Fe/H] from the light curves of RR Lyrae stars, *A&A*, 312, 111 (1996)
- Jurić, M., Ivezić, Ž., Brooks, A., Lupton, R. H., Schlegel, D. et al., 2008, *ApJ*, 673, 864
- Kalirai, J. S. et al. 2012, *ApJ*, 143, 11
- Kent, S. M. 1992, *ApJ*, 387, 181
- King, I. R., Bedin, L. R., Piotto, G., Cassisi, S., & Anderson, J. 2005, *AJ*, 130, 626
- Kinman, T. D., Cacciari, C., Bragaglia, A., Smart, R. & Spagna, A. 2012, *MNRAS*, 422, 2116
- Kirby, E. N., Simon, J. D., Geha, M., Guhathakurta, P., & Frebel, A. 2008, *ApJL*, 685, L43
- Kirby, E. N., Simon, J. D., & Cohen, J. G. 2015, *ApJ*, 810, 56
- Klypin, A., Kravtsov, A. V., Valenzuela, O., & Prada, F. 1999, *ApJ*, 522, 82
- Koch, A., McWilliam, A., Preston, G.W. & Thompson, I. B. 2016, *A&A*, 587, 124
- Koposov, S. E., Belokurov, V., Torrealba, G., & Evans, N. W. 2015, *ApJ*, 805, 130
- Kormendy, J. & Illingworth, G. 1982, *ApJ*, 256, 460
- Kraft, R. P. 1994, *PASP*, 106, 553
- Kratz, K.-L., Farouqi, K., Pfeiffer, B., et al. 2007, *ApJ*, 662, 39
- Kuehn, C., Kinemuchi, K., Ripepi, V., et al. 2008, *ApJL*, 674, L81
- Kuijken, K., Rich, R. M., 2002, *AJ*, 124, 2054
- Kunder, A., Popowski, P., Cook, K. H., Chaboyer, B., 2008, *AJ*, 135, 631
- Kunder, A., & Chaboyer, B., 2008, *AJ*, 136, 2441
- Kunder, A., Koch, A., Rich, R. M., et al. 2012, *AJ*, 143, 57
- Kunder, A., Rich, R. M., Hawkins, K. et al. 2015, *ApJ*, 808, 12
- Kunder, A., Rich, R. M., Koch, A. et al. 2016, *ApJ*, 821, 25
- Laurikainen, E., Salo, H., Athanassoula, E., Bosma, A., Herrera-Endoqui, M. 2014, *MNRAS*, 444, 80
- Laurikainen, E., Salo, H. 2017, *A&A*, 598, 10
- Laevens, B. P. M., Martin, N. F., Bernard, E. J., et al. 2015, *ApJ*, 813, 44
- Lagioia, E. P. et al. 2014, *ApJ*, 782, 50
- Leaman, R., VandenBerg, D. A. & Mendel, J. T. 2013, *MNRAS*, 436, 122
- Lecureur, A., Hill, V., Zoccali, M., Barbuy, B., Gómez, A., Minniti, D., Ortolani, S., Renzini, A. 2007, *A&A*, 465, 799
- Lee, Y.-W. 1992, *AJ*, 104, 1780
- Lee, Y.-W., Gim, H. B., & Casetti-Dinescu, D. I. 2007, *ApJL*, 661, L49
- Lee, Y.-W., Joo, S.-J. & Chung, C. 2015, *MNRAS*, 453, 3906
- Lee, Y.-W. & Jang, S., 2016, *ApJ*, 833, 236
- Leep, E. M. Wallerstein, G. & Oke, J. B., 1986, *AJ*, 91, 1117
- López-Corredoira, M., Cabrera-Lavers, A., Mahoney, T. J., Hammersley, P. L., Garzón, F., González-Fernández, C. 2007, *AJ*, 133, 154

- López-Corredoira, M. 2017, *ApJ*, 836, 218
- Lunnan, R., Vogelsberger, M., Frebel, A., et al. 2012, *ApJ*, 746, 109
- Luković, V. V., D’Agostino, R. & Vittorio, N. 2016, *A&A*, 595, 109
- Mackey, A. D., & Gilmore, G. F. 2004, *MNRAS*, 345, 747
- Mackey, A. D., & Gilmore, G. F. 2004, *MNRAS*, 355, 504
- Maeder, A. & Meynet, G. 2000, *ARA&A* 38 143
- Marconi, M., Coppola, G., Bono, G., et al. 2015, *ApJ*, 808, 50
- Marín-Franch, A. Aparicio, A. & Piotto, G., et al. 2009, *ApJ*, 694, 1498
- Marta, M. Formicola, A. Gyürky, G. et al. 2008, *Phys. Rev. C*, 78, 2
- Martínez-Valpuesta, I., Gerhard, O. 2011, *ApJL*, 734, L20
- Martínez-Vázquez, C. E., Monelli, M., Gallart, C., et al. 2016a, *MNRAS*, 461, L41
- Martínez-Vázquez, C. E., Stetson, P. B., Monelli, M., et al. 2016b, *MNRAS*, 462, 4349
- Mashonkina, L. Christlieb, N. Eriksson, K. 2014, *A&A*, 569, 43
- Massari, D., Bellini, A., Ferraro, F. R. et al. 2013, *ApJ*, 779, 81
- Massari, D., Fiorentino, G., McConnachie, A. et al. 2016a, *A&A*, 586, 51
- Massari, D., Fiorentino, G., McConnachie, A. et al. 2016b, *A&A*, 595, L2
- Matsumoto, T., Hayakawa, S., Koizumi, H., Murakami, H., Uyama, K., Yamagami, T., Thomas, J. A. 1982, eds Riegler, G.R. & Blandford, R.D., *AIP Conf. Proc.*, 83, 48
- Matsunaga, N., Feast, M. W., Kawadu, T., Nishiyama, S., Nagayama, T., Nagata, T., Tamura, M., Bono, G., Kobayashi, N. 2013, *MNRAS*, 429, 385
- Matteucci, F., Romano, D., Molaro, P. 1999, *A&A*, 341, 458
- McConnachie, A. W. 2012, *AJ*, 144, 4
- McWilliam, A. & Rich, R. M. 1994, *ApJS*, 91, 749
- McWilliam, A. 1997, *Annual review of astronomy and astrophysics*, 35, 503
- McWilliam, A., Fulbright, J., & Rich, R. M. 2010, *Chemical Abundances in the Universe: Connecting First Stars to Planets (IAU Sym. 265)*, ed. K. Cunha, M. Spite, & B. Barbuy (Cambridge: Cambridge Univ. Press), 279
- McWilliam, A., & Zoccali, M., 2010, *ApJ*, 724, 1491
- McWilliam, A. 2016, *PASA*, 33, 40
- McWilliam, A. & Zoccali, M. 2010, *ApJ*, 724, 1491
- Meléndez, J., Asplund, M., Alves-Brito, A., Cunha, K., Barbuy, B., Bessell, M. S., Chiappini, C., Freeman, K. C., Ramírez, I., Smith, V. V., Yong, D. 2008, *A&A*, 484, 21
- Merritt, D., Sellwood, J. A. 1994, *ApJ*, 425, 551
- Miceli, A., Rest, A., Stubbs, C. W., et al. 2008, *ApJ*, 678, 865
- Michaud, G. Richard, O. Richer, J. & Vandenberg, D. A. 2004, *ApJ*, 606, 452
- Milone, A., Marino, A.F., Cassisi, S., et al. 2012, *arXiv:1206.5529*
- Milone, A., Marino, A.F., Piotto, G., et al. 2013, *ApJ*, 767, 120
- Milone, A., Marino, A.F., Bedin, L. R., et al. 2014, *MNRAS*, 439, 1588
- Minniti, D., Olszewski, E. W., Liebert, J., White, S. D. M., Hill, J. M., Irwin, M. J. 1995, *MNRAS*, 277, 1293
- Minniti, D. 1994, *PASP*, 106, 813

- Minniti, D., Alcock, C., Alves, D., Cook, K., Marshall, S. et al., MACHO RR Lyrae stars in the Galactic bulge: the spatial distribution, in IAU Symp. 184, The central regions of the Galaxy and galaxies, ed. Y. Sofue, 123 (1998)
- Minniti, D., Lucas, P. W., Emerson, J. P., et al. 2010, *NewA*, 15, 433
- Minniti, D., Contreras Ramos, R., Zoccali, M., Rejkuba, M., Gonzalez, O. A., Valenti, E., Gran, F., 2016, *ApJ*, 830, L14
- Mizerski, T., 2003, *Acta Astronomica*, 53, 307
- Moehler, S. & Bono, G. 2008, arXiv:0806.4456
- Monelli, M., Testa, V. and Bono, G et al. 2015, *ApJ*, 812, 25
- Moore, B., Ghigna, S., Governato, F., et al. 1999, *ApJL*, 524, L19
- Moretti, M. I., Dall’Ora, M., Ripepi, V., et al. 2009, *ApJL*, 699, L125
- Müller, O., Jerjen, H., Pawlowski, M. S., & Binggeli, B. 2016, *A&A*, 595, A119
- Müller, O., Pawlowski, M.S., Jerjen, H. & Lelli, F. et al. 2018, *Sci*, 359, 534
- Musella, I., Ripepi, V., Clementini, G., et al. 2009, *ApJL*, 695, L83
- Musella, I., Ripepi, V., Marconi, M., et al. 2012, *ApJ*, 756, 121
- Nataf, D. M., Udalski, A., Gould, A., Fouqué, P., Stanek, K. Z., 2010, *ApJL*, 721, 28
- Nataf, D. M., Udalski, A., Gould, A., Pinsonneault, M. H. 2011, *ApJ*, 730, 228
- Nataf, D. M., Gould, A., Fouqué, P., Gonzalez, O. A., Johnson, J. A. et al., 2013, *ApJ*, 769, 88
- Neeley, J. R. Marengo, M. Bono, G. et al., 2017, *ApJ*, 841, 84
- Ness, M., Freeman, K., & Athanassoula, E. Wylie-De-Boer, E., Bland-Hawthorn, J., Lewis, G. F., Yong, D., Asplund, M., Lane, R. R., Kiss, L. L., Ibata, R. 2012, *ApJ*, 756, 22
- Ness, M., Freeman, K., & Athanassoula, E. et al. 2013b, *MNRAS*, 432, 2092
- Ness, M., Freeman, K., & Athanassoula, E. et al. 2013b, *MNRAS*, 430, 836
- Ness, M. & Lang, D. 2016, *AJ*, 152, 14
- Nishiyama, S., Nagata, T., Baba, D., Haba, Y., Kadowaki, R., Kato, D., Kurita, M., Nagashima, C., Nagayama, T., Murai, Y., Nakajima, Y., Tamura, M., Nakaya, H., Sugitani, K., Naoi, T., Matsunaga, N., Tanabé, T., Kusakabe, N., Sato, S. 2005, *ApJL*, 621, 105
- Nishiyama, S., Nagata, T., Kusakabe, N. et al. 2006, *ApJ*, 638, 839
- Nishiyama, S., Nagata, T., Tamura, M. et al. 2008, *ApJ*, 680, 1174
- Nishiyama, S., Tamura, M. Hatano, H. et al. 2009, *ApJ*, 696, 1407
- Niu, Z., Sun, B., & Meng, J. et al. 2009, *Phys. Rev. C*, 80, 6
- Nomoto, K., Thielemann, F.-K. & Wheeler, J. C. 1984, *ApJL*, 279, 23
- O’Connell, D. J. K. 1958, *Ricerche Astronomiche*, 5
- O’Malley, E. M. von Hippel, T. & van Dyk, D. A., 2013, *ApJ*, 775, 1
- Ortolani, S., Renzini, A., Gilmozzi, R., Marconi, G., Barbuy, B., Bica, E., Rich, R. M. 1995, *Nature*, 377, 701
- Osborn, W. H. 1971, Yale University PhDT, Positions of Globular Cluster Stars in the Physical H-R Diagram
- Pagel, B. E. J. & Portinari, L. 1998, *MNRAS*, 298, 747
- Patsis, P. A., Skokos, C., Athanassoula, E. 2002, *MNRAS*, 337, 578
- Peimbert, M. Peimbert, A. Carigi, L. & Luridiana, V. 2010, IAUS 268 eds: Charbonnel, C. Tosi, M. Primas, F. & Chiappini, C. 91

- Pawlowski, M. S., & Kroupa, P. 2013, *MNRAS*, 435, 2116
- Pawlowski, M. S., & Kroupa, P. 2014, *ApJ*, 790, 74
- Pérez-Villegas, A., Portail, M. & Gerhard, O. 2017, *MNRAS*, 464, 80
- Pérez-Villegas, A., Portail, M. & Gerhard, O. 2017, *MNRAS*, 464, 80
- Picaud, S. & Robin, A. C. 2004, *A&A*, 428, 891
- Pietrinferni, A., Cassisi, S., Salaris, M., & Castelli, F. 2004, *ApJ*, 612, 168
- Pietrinferni, A., Cassisi, S., Salaris, M., Percival, S. & Ferguson, J. W. 2009 *ApJ*, 697, 275
- Pietrukowicz, P., Udalski, A., Soszyński, I., Nataf, D. M., Wyrzykowski, L. et al., 2012, *ApJ*, 750, 169
- Pietrukowicz, P., Kozłowski, S., Skowron, J., Soszyński, I., Udalski, A., Poleski, R., Wyrzykowski, L., Szymański, M. K., Pietrzyński, G., Ulaczyk, K., Mróz, P., Skowron, D. M., Kubiak, M. 2015, *ApJ*, 811, 113
- Pietrukowicz, P., 2016, in *IAU Symp. 317, The General Assembly of Galaxy Halos: Structure, Origin and Evolution*, 116
- Pilachowski, C. A. Sneden, C. & Wallerstein, G., 1983, *ApJS*, 52, 241
- Piotto, G. Villanova, S. Bedin, L. R., et al. 2005, *ApJ*, 621, 777
- Piotto, G. Bedin, L. R., Anderson, J. et al. 2007, *ApJL*, 661, 53
- Planck Collaboration 2015, *A&A*, 580, 22
- Plez, B., Hill, V., Cayrel, R., et al. 2004, *A&A*, 428, 9
- Pritzl, B. J. Smith, H. A. Stetson, P. B. et al. 2003, *AJ*, 126, 1381
- Proffitt, C. R. & Vandenberg, D. A. 1991, *ApJS*, 77, 473
- Portail, M., Wegg, C., Gerhard, O., Martinez-Valpuesta, I. 2015, *MNRAS*, 448, 713
- Pulone, L., De Marchi, G., Paresce, F. & Allard, F. 1998, *ApJL*, 492, 41
- Pulone, L., De Marchi, G. & Paresce, F. 1999, *A&A*, 342, 440
- Raha, N., Sellwood, J. A., James, R. A., Kahn, F. D. 1991, *Nature*, 352, 411
- Rattenbury, N.J., Mao, S., Sumi, T., Smith, M.C., 2007, *MNRAS* 378, 1064
- Renzini, A. & Fusi Pecci, F. 1988, *Annual review of astronomy and astrophysics*, 26, 199
- Reylé, C., Robin, A. C., Schultheis, M., & Picaud, S. 2005, "The Three-Dimensional Universe with Gaia", *ESASP*, 576, 143 Eds: C. Turon, K.S. O'Flaherty, M.A.C. Perryman
- Rich, R. M. & Origlia, L. 2005, *ApJ*, 634, 1293
- Rich, R. M., 1988 *AJ*, 95, 828
- Rich, R. M., Reitzel, D. B., Howard, C. D. & Zhao, H. 2007, *ApJ*, 658, 29
- Rich, R. M., Origlia, L., Valenti, E. 2012, *ApJ*, 746, 59,
- Richer, H. B. Anderson, J. Brewer, J., et al. 2006, *Science*, 313, 936
- Richer, H. B. Goldsbury, R. Heyl, J. et al. 2013, *ApJ*, 778, 104
- Riess A. G., Macri L., Casertano S. et al 2011 *ApJ* 730 119
- Riess, A. G. et al. 2016, *ApJ*, 826, 56
- Robin, A. C., Marshall, D. J., Schultheis, M., Reylé, C. 2012, *A&A*, 538, 106
- Roederer, I. U. Kratz, K.-L. Frebel, A. et al. 2009, *ApJ*, 698, 1963
- Rojas-Arriagada, A., Recio-Blanco, A., Hill, V. et al., 2014, 569, 103,
- Romero-Gómez, M., Athanassoula, E., Antoja, T., Figueras, F., 2011, *MNRAS*, 418, 1176

- Rosenberg, A., Saviane, I., Piotto, G., & Aparicio, A. 1999, *AJ*, 118, 2306
- Rosenfield, P., Girardi, L., Williams, B. F., 2017, *ApJ*, 841, 69
- Saito, R. K., Zoccali, M., McWilliam, A., Minniti, D., Gonzalez, O. A., Hill, V. 2011, *AJ*, 142, 76
- Saito, R. K., Hempel, M., Minniti, D., Lucas, P. W., Rejkuba, M. et al., 2012, *A&A*, 537, A107
- Salaris, M. & Weiss, A. 1997, *A&A*, 327, 107
- Salaris, M. & Girardi, L. 2002, *MNRAS*, 337, 332
- Salaris, M. & Cassisi, S. 2005, *Evolution of Stars and Stellar Populations*, publisher: Chichester: John Wiley & Sons, Ltd
- Salaris, M. & Cassisi, S. 2008, *A&A*, 487 1075
- Salaris, M. Cassisi, S. Pietrinferni, A. Kowalski, P. M. Isern, J. 2010, *ApJ*, 716, 1241
- Salaris, M. 2016, *AN*, 337, 805
- Sales, L. V., Vogelsberger, M., Genel, S., et al. 2015, *MNRAS*, 447, L6
- Sandage, A. 1958, *Ricerche Astronomiche*, 5, 41
- Sarajedini, A. Bedin, L. R. Chaboyer, B. et al. 2015, *AJ*, 133, 1658
- Sarajedini, A. Dotter, A., & Kirkpatrick, A. 2009a, *ApJ*, 698, 1872
- Sarajedini, A. Mancone, C. L., Lauer, T. R. et al. 2009b, *AJ*, 138, 184
- Saumon, D., Bergeron, P., Lunine, J. I., Hubbard, W. B. & Burrows, A. 1994, *ApJ*, 424, 333
- Saumon, D. & Marley, M. S. 2008, *ApJ*, 689, 1327
- Sbordone, L. Salaris, M. Weiss, A. & Cassisi, S. 2011, *A&A*, 534, 9
- Schatz, H., Toenjes, R., Pfeiffer, B. et al. 1993, *ApJ*, 579, 626
- Schechter, P. L., Mateo, M. & Saha, A. 1993, *PASP*, 105, 1342
- Schlafly, E. F., & Finkbeiner, D. P. 2011, *ApJ*, 737, 103
- Schlaufman, K.C. & Casey, A.R. 2014, *ApJ*, 797, 13
- Schultheis, M., Zasowski, G. Allende Prieto, C. et al. 2014, *AJ*, 148, 24
- Schultheis, M., Cunha, K. Zasowski, G. et al. 2015, *A&A*, 584, 45
- Schwarzschild, M. 1970, *QJRAS*, 11, 12
- Searle, L., & Zinn, R. 1978, *ApJ*, 225, 357
- Sesar, B., Banholzer, S. R., Cohen, J. G., et al. 2014, *ApJ*, 793, 135
- Shen, J., Rich, R. M., Kormendy, J., et al. 2010, *ApJ*, 720, L72
- Sellwood, J. A., Sanders, R. H. 1988, *MNRAS* 233, 611
- Siegel, M. H. 2006, *ApJL*, 649, L83
- Siqueira Mello, C. Spite, M. Barbuy, B., et al. 2013, *A&A*, 550, 122
- Sneden, C., Preston, G. W., McWilliam, A. & Searle, L. 2003, *ApJL*, 431, 27
- Sneden, C. Cowan, J. J. Lawler, J. E. et al. 2003, *ApJ*, 591, 936
- Sneden, C. Cowan, J. J. Gallino, R. 2008, *ARA&A*, 46, 241
- Sneden, C., Lawler, J.E., Cowan, J. J., Ivans, I., & Den Harton, E.A. 2009, *ApJS*, 182, 80
- Stanek, K. Z., Mateo, M., Udalski, A., Szymanski, M., Kaluzny, J., Kubiak, M. 1994, *ApJL*, 429, 73
- Stanek, K. Z., Udalski, A., Szymanski, M., Kaluzny, J., Kubiak, Z. M., Mateo, M., Krzeminski, W. 1997, *ApJ*, 477, 163
- Stetson, P. B. 2000, *PASP*, 112, 925

- Smolec, R., 2005, *Acta Astronomica*, 55, 59
- Snedden, C. Cowan, J. J. & Gallino, R., 2008, *ARA&A*, 46, 241
- Sofue, Y. 1990, *ApJL*, 459, 69
- Sofue, Y., Honma, M. & Omodaka, T. 2009, *PASJ*, 61, 227
- Sofue, Y. 2013, *PASJ*, 65, 118
- Soszyński, I., Dziembowski, W. A., Udalski, A., Poleski, R., Szymański, M. K. et al., 2011, *Acta Astronomica*, 61, 1
- Soszyński, I., Udalski, A., Szymański, M. K., Pietrukowicz, P., Mróz, P. et al., 2014, *Acta Astronomica*, 64, 177
- Stanek, K. Z., Mateo, M., Udalski, A., Szymański, M., Kaluzny, J., & Kubiak, M., 1994, *ApJ*, 429, L73
- Stetson, P. B., Braga, V. F., Dall’Ora, M. et al., 1994, *ApJ*, 429, L73
- Sweigart, A. V., Greggio, L., Renzini, A., 1990, *ApJ*, 364, 527
- Sweigart, A. V., Lanz, T., Brown, T. M., 2004, *Ap&SS*, 291, 367
- Suntzeff, N. B., Kinman, T. D., Kraft, R. P. 1991, *ApJ*, 367, 528
- Suyu S. H., Auger M. W., Hilbert S. et al 2013 *ApJ* 766 70
- Terndrup, D. M. 1988, *AJ*, 96, 884
- Thompson, I. B. Kaluzny, J. Pych, W. et al. 2001, *AJ*, 121, 3089
- Turri, P., McConnachie, A. W., Stetson, P. B. 2016, *SPIE*, 9909, 990907
- Tumlinson, J. 2010, *ApJ*, 708, 1398
- Tognelli, E., Prada Moroni, P. G. & Degl’Innocenti, S. 2015, *MNRAS*, 454, 4037
- Udalski, A., Szymanski, M., Kaluzny, J., Kubiak, M., Mateo, M. 1992, *Acta Astron.* 42, 253
- Udalski, A., Zebrun, K., Szymanski, M., Kubiak, M., Pietrzynski, G., Soszynski, I., Wozniak, P. 2000, *Acta Astron.* 50, 1
- Udalski, A., Szymański, M., & Szymański, G., 2015, *Acta Astronomica*, 65, 1
- Uttenthaler, S., Schultheis, M., & Nataf, D. M. et al. 2012, *A&A*, 546, 57
- Valle, G., Dell’Omodarme, M., Prada Moroni, P. G. & Degl’Innocenti, S. 2013, *A&A*, 554, 68
- Valcarce, A. A. R., Catelan, M. & Sweigart, A. V. 2012, *A&A*, 547, 5
- Vallenari, A., Ragaini, S., Bertelli, G. 2008, *Formation and Evolution of Galaxy Bulges* (IAU Sym. 245), ed. M. Bureau, E. Athanassoula, E., B. Barbuy, 371
- Valenti, E., Ferraro, F. R., Origlia, L. 2010, *MNRAS*, 402, 1729
- Valenti, E., Zoccali, M., Renzini, A., Brown, T. M., Gonzalez, O. A., Minniti, D., Debattista, V. P., Mayer, L., 2013, *A&A*, 559, 98
- Valenti, E., Zoccali, M., Gonzalez, O. A., Minniti, D., Alonso-García, J., Marchetti, E., Hempel, M., Renzini, A., Rejkuba, M. 2016, *A&A*, 587, L6
- van den Bergh, S. & Herbst, E. 1974 *AJ*, 79, 603
- VandenBerg, D. A. Brogaard, K. Leaman, R. & Casagrande, L. 2013, *ApJ*, 775, 134
- VandenBerg, D. A. Bond, H. E. Nelan, E. P. Nissen, P. E. Schaefer, G. H. & Harmer, D. 2014a, *ApJ*, 792, 110
- VandenBerg, D. A. Bergbusch, P. A. Ferguson, J. W. & Edvardsson, B. 2014b, *ApJ*, 794, 72
- van Gent, H., 1993, 6, 163

- van Gent, H., 1993, 7, 21
- Ventura, P., D’Antona, F., Mazzitelli, I., & Gratton, R., 2001, 550, 65
- Vivas, A. K., Olsen, K., Blum, R., et al. 2016, AJ, 151, 118
- Walker, A.R. & Terndrup, D.M. 1991, ApJ, 378, 119
- Wegg, C. & Gerhard, O. 2013, MNRAS, 450, 4050
- Wegg, C., Gerhard, O. & Portail, M. 2015, MNRAS, 435, 1874
- Weiland, J. L., Arendt, R. G., Berriman, G. B., Dwek, E., Freudenreich, H. T., Hauser, M. G., Kelsall, T., Lisse, C. M., Mitra, M., Moseley, S. H., Odegard, N. P., Silverberg, R. F., Sodroski, T. J., Spiesman, W. J., Stemwedel, S. W. 1994, ApJL, 425, 81
- Westin, J., Sneden, C., Gustafsson, B., & Cowan, J. J. 2000, ApJ, 530, 783
- Wetzell, A. R., Hopkins, P. F., Kim, J.-h., et al. 2016, ApJL, 827, L23
- Woolley, S. E. & Weaver, T. A. 1995, NASA STI/Recon Technical Report N, Black Holes (Astronomy), Stellar Evolution, Stellar Mass, Implosions, Thermonuclear Explosions, Nuclear Fusion, Stellar Activity, Supernovae, Supernova Remnants, 96
- Wyman M., Rudd D. H., Vanderveld R. A. and Hu W. 2014 PhRvL 112 051302
- Wyse, R. F. G. 2000 Liege International Astrophysical Colloquia (eds Noels, A., Magain, P., Caro, D., Jehin, E., Parmentier, G., Thoul, A. A.), 35, 305
- Yoshino, A., Ichikawa, T., 2008, PASJ, 60, 493
- Zacharias, N., Finch, C. & Frouard, J. 2017, arXiv:1702.05621
- Zasowski, G., Ness, M. K., García Pérez, A. E., Martínez-Valpuesta, I., Johnson, J. A. & Majewski, S. R. 2016, 832, 132
- Zhao, H., Spergel, D. N., Rich, R. M. 1994, AJ, 108, 2154
- Zinn, R. 1993, The Globular Cluster-Galaxy Connection, 48, 38
- Zinn, R., Horowitz, B., Vivas, A. K., et al. 2014, ApJ, 781, 22
- Zinn, R., & West, M. J., 1984, ApJS, 55, 45
- Zoccali, M., Piotto, G., Zaggia, S. R., Capaccioli, M., A&A, 331, 541
- Zoccali, M., Cassisi, S., Frogel, J. A., Gould, A., Ortolani, S., Renzini, A., Rich, R. M., Stephens, A. W. 2000, ApJ, 530, 418
- Zoccali, M., Renzini, A., Ortolani, S., Bica, E., Barbuy, B. 2001a, AJ, 121, 2638
- Zoccali, M., Renzini, A., Ortolani, S., et al. 2001b, ApJ, 553, 733
- Zoccali, M., Renzini, A., Ortolani, S., Greggio, L., Saviane, I., Cassisi, S., Rejkuba, M., Barbuy, B., Rich, R. M., Bica, E. 2003, A&A, 399, 931
- Zoccali, M., Lecœur, A., Barbuy, B., et al. 2006, A&A, 457, 1
- Zoccali, M., Hill, V., Lecœur, A., Barbuy, B., Renzini, A., Minniti, D., Gómez, A., Ortolani, S. 2008, A&A, 486, 177
- Zoccali, M. 2010, Chemical Abundances in the Universe: Connecting First Stars to Planets (IAU Sym. 265), ed. K. Cunha, M. Spite, & B. Barbuy (Cambridge: Cambridge Univ. Press), 265
- Zoccali, M., Gonzalez, O. A., & Vasquez, S. et al. 2014, A&A, 562, 66
- Zoccali, M., Vasquez, S., Gonzalez, et al. 2017, A&A, 599, 12
- Zoccali, M., Valenti, E. 2016, PASA, 33, 25
- Zorotovic, M., Catelan, M., Smith, H. A., et al. 2010, AJ, 139, 357